6-9-2006

The Timing and Causes of Illite Formation in the Cretaceous Marias River Shale, Disturbed Belt, Montana

Stephen Gerard Osborn

THE TIMING AND CAUSES OF ILLITE FORMATION IN THE CRETACEOUS MARIAS RIVER SHALE, DISTURBED BELT, MONTANA

by

Stephen Gerard Osborn

Under the direction of W. Crawford Elliott

ABSTRACT

The clay mineralogy data and K-Ar ages of I/S measured in this study agree with previous work conducted within the Disturbed Belt (Hoffman, 1976) and show that diagenetic I/S formed quickly at several different places in response to thrust sheet burial during the Laramide orogeny. The averages of concordant age values for clay sub-fractions separated from three bentonites of Cretaceous and Jurassic depositional age increase from southeast (53.6 Ma) to northwest (56.7 Ma) along the trend of the Disturbed Belt. This northwestward increase of mean ages of I/S is consistent with a thrust sheet emplacement model for the Disturbed Belt (Mudge and Earhart, 1980). The rate of the eastward advancement of the Lewis Thrust Sheet derived from the concordant K-Ar dates of I/S was about 1 cm/year in the Marias River area. The absence of the $2M_1$ illite polytype in most bentonitic shales does not permit the derivation of the age of diagenetic I/S by Illite Age Analysis and yet constrains the estimate of maximum burial temperature to 250°C.

INDEX WORDS: K-Ar, illite, Chemical remanent magnetization, Disturbed Belt, Montana

THE TIMING AND CAUSES OF ILLITE FORMATION IN THE CRETACEOUS MARIAS RIVER SHALE, DISTURBED BELT, MONTANA

by

Stephen Gerard Osborn

A Thesis Submitted in Partial Fulfillment of the Requirements for the Degree of

Master of Science

In the College of Arts and Sciences

Georgia State University

2006

THE TIMING AND CAUSES OF ILLITE FORMATION IN THE CRETACEOUS MARIAS RIVER SHALE, DISTURBED BELT, MONTANA

by

Stephen Gerard Osborn

Major Professor:	W. Crawford Elliott
Committee:	J. Marion Wampler
	Seth Rose
	R. Douglas Elmore

Electronic Version Approved:

Office of Graduate Studies
College of Arts and Sciences
Georgia State University
May 2006

ACKNOWLEDGEMENTS

This study was funded by a grant provided by the Department of Energy (DOE) to Dr. Elliott. I am grateful to Dr. Elliott for the opportunity to work on this project. I am also thankful for all of his support and guidance as my advisor. I am thankful Dr. Wampler (Georgia Institute of Technology) for being on my committee and his invaluable direction with the K-Ar analyses. I thank Dr. Rose (Georgia State University) and Dr. Elmore (University of Oklahoma) for being on my committee and for their guidance during the completion of this project.

TABLE OF CONTENTS

LIST OF TABLES

LIST OF FIGURES

LIST OF ABBREVIATIONS AND SYMBOLS

α	Alpha
Al	Aluminum
Å	Ångstrom unit
Ar	Argon
β	Beta
CEC	cation exchange capacity
CBD	Sodium citrate, sodium bicarbonate, and sodium? dithionate
Cl	Chlorine
CRM	chemical remanent magnetization
cm	Centimeter
ºC	degree celsius
Cu	Copper
DI	deionized
EG	ethylene glycol
FEP	fluorinated ethylene propylene
Fe	Iron
GNP	Glacier National Park
g	Gram
>	Greater than
IAA	illite age analysis
I/S	illite/smectite
I	illite
K	Potassium
K-Ar	Potassium-argon
Km	Kilometer
<	Less than
LT	Lewis Thrust
M	molarity
Ma	million years
Mg	Magnesium
m	Meter
mm	millimeter
ml	Milliliter
mg	milligram
μm	Micrometer
mg	Milligram
MT	Montana
N	normal
Na	Sodium
NaOAc	sodium acetate

O	Oxygen
%	Percent
pmol	picomole
RPM	rotations per minute
R	Reichweite
S	smectite
Δs	difference in specific gravity
Si	Silicon
SST	solid State Transformation
TEM	transmission electron microscopy
θ	Theta
η	viscosity in Poises
λ	wavelength of X-Rays (Angstrom)
XRD	X-ray diffraction

CHAPTER 1.0 - INTRODUCTION

Phyllosilicate minerals are good indicators of maximum diagenetic temperatures (i.e., below 300^{o}C). For example, the stacking order of illite layers in illite/smectite (I/S) is a well-known semi-quantitative geothermometer (Hoffman and Hower, 1979; Velde et al., 1986). An intermediate mixed layer phase I/S is formed during the transformation of smectite to illite (i.e., illitization) in response to increases to temperature, to time, and to potassium concentration (Hower and Mowatt, 1966; Hower et al., 1976; Boles and Franks, 1979; Moore and Reynolds, 1997). This thesis presents the results of a study on the timing and causes of diagenetic illite formation in Cretaceous and Jurassic bentonites in the Disturbed Belt of northwestern Montana. Furthermore, a relation between the acquisition of chemical remanent magnetization (CRM) and the timing of illitization as measured by K-Ar isotopic methods is mentioned as a possible outcome of illitization, but the idea is not tested rigorously in this study. Potassium-argon (K-Ar) isotopic dating and X-ray diffraction (XRD) are widely known procedures for characterizing the apparent age and mineralogy of I/S, respectively. In addition to K-Ar age of I/S, paleomagnetic dating techniques, which have been broadly accepted for dating the formation of igneous rock and metamorphic events, can be used to determine the timing of diagenetic processes in sedimentary rocks. The ages of diagenetic I/S and CRM are useful for understanding the thermal histories of sedimentary basins.

Many of the early studies on the formation of I/S were done in geologic settings where shales had been buried progressively, reaching temperatures corresponding up to low-grade metamorphism. Diagenetic I/S has formed in sedimentary rocks buried by thrust sheets, as in the Disturbed Belt of Montana (Hoffman and Hower, 1979). I/S can also form by reaction with hydrothermal fluids and potassic basinal fluids (e.g., Moore and Reynolds, 1997; Elliott and Haynes, 2002). Illitization occurs at approximately the same temperature (~100^{o}C) as the conversion (cracking) of organic matter to form crude oil and natural gas (Velde and Lanson, 1993; Pevear, 1999). Therefore, assessing the extent of illitization by XRD and timing of illitization by way of isotopic age analysis and/or paleomagnetic age analysis is important for determining the formation of crude oil and natural gas as well as investigating the geologic history of a region (Pevear, 1999).

1.1 MEASURMENT OF THE TIMING OF ILLITIZATION

The apparent age determination of sediments utilizing K-Ar isotopic methods has been used extensively to constrain the timing of diagenetic events on basin-wide scales or at particular locations within sedimentary basins (e.g., Weaver and Wampler, 1970; Hower and Aronson, 1976; Elliott and Haynes, 2002). The K-Ar method for dating diagenetic I/S is complicated by the presence in most argillaceous rocks of detrital illite that formed prior to deposition as well as illite that formed during diagenetic events. Three polytypes of illite ($2M_1$, 1M, and $1M_d$) are present in many sedimentary rocks. Hower and Mowatt (1966) recognized the importance and difficulty of distinguishing between diagenetic illite and detrital illite. Therefore, the K-Ar method for determining the apparent age of a

clay fraction containing mixed sources of illite provides a weighted average reflecting the presence of both detrital and diagenetic illite. I/S in bentonites and K-bentonites is assuredly diagenetic, while in shales the clay fraction contains both detrital and diagenetic illite.

Illite age analysis (IAA) is a method that has been developed to estimate the age of diagenetic illite in mixed polytype source rocks (shales) (Figure 1.1). IAA assumes a linear relationship between the apparent age of I/S and the percentage of $2M_1$ illite

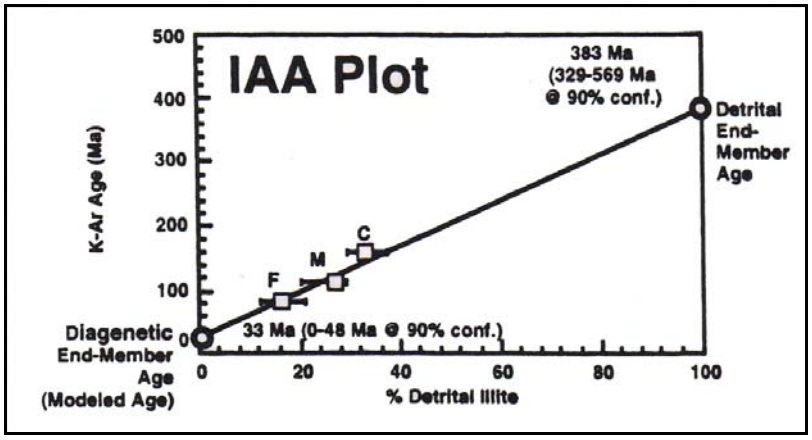

Figure 1.1: Illite age analysis plot. Plot of percentage of detrital illite ($2M_1$ polytype) versus K-Ar age of I/S (Pevear, 1999).

polytype measured in the fine, medium, and coarse clay size fractions that result in a modeled age of diagenetic illite (Pevear, 1999). Środoń (1999, 2000) pointed out that a linear relationship is not likely to exist in most cases and argued that the application of IAA results in an overestimation of the age of diagenetic illite. Ylagan et al. (2000), however, argued that IAA is a useful tool for obtaining an estimate of the age of diagenetic illite if the difference in age between the diagenetic and detrital illite end members is less than 500 million years (Ma). In addition to the K-Ar ages of diagenetic

illite, paleomagnetic age analysis can possibly be employed as an alternative or complimentary method for determining the age of diagenetic events in sedimentary rocks (Katz et al., 2000; Gill et al., 2002).

Paleomagnetic techniques have been widely recognized for determining the ages of igneous rocks and for determining when metamorphic events occurred. Minerals containing transition elements, primarily iron (Fe), can acquire a magnetic field that is oriented parallel to the applied geomagnetic field and subsequently preserved as magma/lava cools below the Curie temperature during rock formation (Butler, 1992). Chemical remanent magnetization (CRM) occurs when Fe-oxides, formed from chemical reactions during diagenesis, acquire a magnetization parallel to the applied geomagnetic field below the Curie temperature (Butler, 1992). CRM's are common in sedimentary rocks and can occur by the alteration of preexisting minerals or the precipitation of ferromagnetic minerals, such as magnetite, from solution associated with or due to diagenetic processes involving the release of Fe to form Fe-oxides (McCabe and Elmore, 1989; Butler, 1992). For example, sandstones that have undergone diagenesis can contain cements and concretions precipitated from solution that have appreciable amounts of Fe and magnesium (Boles and Franks, 1979). Although, there have been recent studies that suggest a relationship between illitization and the acquisition of CRM during progressive burial diagenesis, the subject has not been extensively studied (Katz et al., 2000; Woods et al., 2002; Basu, 2004).

1.2 REVIEW OF PREVIOUS WORK ON I/S

Smectite and illite, along with vermiculite, chlorite, and glauconite are 2:1 layer phyllosilicate minerals with a layer charge less than one based on eleven oxygen atoms per formula unit (Moore and Reynolds, 1997). The determination of the unit formula comes from Moore and Reynolds (1997) where by the eleven oxygens are from the tetrahedral sheets (8 oxygens) and the octahedral sheet (3 oxygens) with the oxygen from water not considered. Illite is a dioctahedral phyllosilicate with a layer charge of approximately 0.8 equivalents per eleven oxygens. There are dioctahedral or trioctahedral smectites in rocks whose layer charge is between 0.2 equivalents and 0.4 equivalents per eleven oxygens (Moore and Reynolds, 1997; Brindley and Brown, 1984). The relatively high layer charge of illite prevents it from expanding like smectite. Since smectite is expandable, the detection of expandable smectite layers in association with mixed layered I/S is a characteristic of I/S. The diffraction peak positions for I/S are intermediate between diffraction peaks for pure smectite and pure illite (Moore and Reynolds, 1997).

Although early studies thought illite was crystal mica in structure, it was later determined to lie between muscovite mica and smectite compositionally (Hower and Mowatt, 1966; Nadeau and Bain, 1986; Moore and Reynolds, 1997). Illite has more silica (Si), magnesium (Mg), and water, but less aluminum (Al) in the tetrahedral layer and less K in the interlayer than muscovite (Nadeau and Bain, 1986; Moore and Reynolds, 1997). Illite is stable or metastable at the earth's surface and is created as a result of weathering processes, soil formation, and diagenesis (Moore and Reynolds, 1997). Therefore, the processes that govern illite formation reflect its environment and

are manifested by the presence of different polytypes ($1M_d$, 1M, and $2M_1$). Hower and Mowatt (1966) noted that diagenetic illite ($1M_d$ polytype) dominated the smallest grain size separations, and that a proportional relationship exists between the cation exchange capacity (CEC) and the percentage of expandable layers (smectite). Furthermore, they concluded that illite represents an end member of interstratified clay layers with smectite in a continuous series that is distinct from micas based on the lower K content. Detrital illite in shales typically exhibits the $2M_1$ polytype. It can also exhibit the $1M_d$ polytype where maximum burial temperature does not exceed approximately 250ºC (Hoffman and Hower, 1979).

Weaver and Wampler (1970) studied the variation of K and Ar isotopic content and apparent age of sediment samples collected from the Gulf Coast, USA as a function of burial depth and grain size. They noted a decrease in the apparent age of the bulk rock sample and the finest clay size fraction (<0.2 μm) with depth. The fine grain size fraction had an apparent age less than the time elapsed since deposition, while the bulk rock sample was older than the depositional age. The largest grain size fraction (>2 μm) had the largest age value at approximately 400 Ma and varied little with depth. The apparent age of the intermediate grain size fraction (2 μm to 0.2 μm) varied between 202 Ma and 245 Ma with depth. A decreased K content in the >2 μm grain size fraction and an increased K content in the <0.2 μm fraction was noted. Therefore, they concluded that the observed K content trend resulted from the release of K from the decomposition of K-feldspar and some mica accompanied with the fixation of K in the interlayer position of illite in I/S. They further concluded that the decomposition of K-feldspar and mica is driven by increased temperature associated with burial depth.

Hower et al. (1976), and Hower and Aronson (1976) confirmed the observations of Weaver and Wampler (1970) by concluding that the increased K in the fine grain size fraction with depth resulted from the formation of diagenetic illite. They further noted an increased amount of radiogenic ^{40}Ar upon the formation of I/S. Hower et al. (1976) observed that the Al and Si content increases, as does K, with depth in the clay size fraction composed of I/S. They posed that the mechanism of illite formation is the decomposition of feldspars and micas in the presence of smectite to form illite, quartz, and chlorite through an interstratified series of illite and smectite layers (reactions provided below).

$$\text{K-feldspar} + \text{mica} + \text{smectite} \rightarrow \text{illite} + \text{quartz} + \text{chlorite}$$

$$K^{+} + Al^{+3} + \text{smectite} \rightarrow \text{illite} + Si^{+4}$$

Hower et al. (1976) noted that illitization ceased at approximately 80% illite layers in I/S in their study with little change at increased depth and concluded that all the available K-bearing minerals (e.g., K-feldspar) had been consumed by diagenetic reactions in these shales. Altaner (1986) concluded that between 50ºC and 200ºC the rate of K release by the decomposition of feldspars is much greater than the rate of consumption of K by illitization. Therefore, the Gulf Coast data show the importance of both temperature and the availability of K in the conversion of smectite to illite. Later, Altaner (1989) noted the importance of knowing the diffusion characteristics of K along with temperature as factors regulating the extent of illitization in thick bentonites.

Although, the extent of illitization is controlled in large part by temperature and the availability K and Al, the duration of the reaction (kinetics) is also a factor controlling the extent of illitization (e.g., Elliott and Matisoff, 1996). As in all chemical reactions, the time required for illitization is inversely related to temperature. This implies that illite may form over a long period of time at relatively low temperatures (shallow burial). Morton (1985) showed that a sudden change in pore water chemistry favoring high K content accompanied with rapid burial of sediments resulted in rapid illitization at relatively shallow depths (2133 m to 2438 m) in the Gulf Coast. This conclusion was termed "punctuated diagenesis" and is contrary to the progressive burial model proposed by many Gulf Coast researchers. Thus, the geologic mechanisms that favor illitization are complex, and time, temperature, and availability of K are important parameters in the study of illitization.

1.3 MECHANISM OF ILLITE FORMATION

The observation of a depth-dependent (i.e., temperature-dependent) increase in the percentage of illite layers in I/S in Gulf Coast sediments (Hower et al., 1976) led to recognition that the extent of illitization could be used as a geothermometer for interpreting the maximum temperature ($<300^{o}C$) experienced by sedimentary rocks during diagenetic events. This semi-quantitative geothermometer (i.e., percentage of illite layers in I/S) provides a useful tool, when coupled with K-Ar age analysis, for determining the time-temperature (burial) history of a region. Thus, the percentage of illite layers in I/S and the stacking order of illite and smectite layers in I/S can be used to

understand the geologic history of sedimentary basins and to predict the thermal maturity of organic matter contained in sediments (Hoffman and Hower, 1979; Moore and Reynolds, 1997; Pevear, 1999). The Reichweite (R) is a measure of stacking order of illite layers in I/S that represents the probability of finding an illite layer(s) following a smectite layer in a two-component system such as I/S (e.g. Moore and Reynolds, 1997). With some variance, it has been observed that as temperature increases with progressive burial, the proportion of illite layers increases and the stacking order of I/S proceeds from a random arrangement (R=0) to short range ordering (SISISI…, R=1), followed by long range ordering (SIIISIII…, R=3) of smectite and illite layers (Hoffman and Hower, 1979). Short-range and long-range ordering are also known as Rectorite and Kalkberg ordering, respectively. The stacking order of illite layers in I/S is useful as an indicator of maximum diagenetic temperatures between 100ºC and 200ºC (Hoffman and Hower, 1979).

The stacking order and percentage of illite layers in I/S are conveniently measured using XRD. A solid-state transformation (SST) model has been traditionally employed by many Gulf Coast researchers to describe the mechanism of illitization by progressive burial. According to this model, the conversion of smectite to illite via I/S intermediates occurs through a solid-state transformation involving isomorphous substitutions (e.g., Al for Si, Mg for Al) within intact layers during diagenesis (e.g., Altaner and Ylagan, 1997; Moore and Reynolds, 1997), no changes in polytype or morphology occur during the formation of I/S, smectite interlayers may grade laterally into illite interlayers, and radiogenic Ar is retained in the illite interlayers (Weaver and Wampler, 1970; Aronson and Hower, 1976).

Contrary to the SST model, Nadeau et al. (1984) concluded that illite is formed by dissolution of smectite layers and the direct precipitation of illite layers in a process that does not produce mixed-layer intermediate forms. From transmission electron microscopy (TEM) examination, smectite particles are 10-angstrom (Å) "fundamental" particles and illite particles range in thickness from 20-50 Å thick. Rotliegendes illites are 50 Å thick, while Tioga bentonite illites (R=3 I/S) are 30-40 Å thick. These particles are stacked parallel to the C axis to produce larger crystallites (Altaner and Ylagan, 1997; Moore and Reynolds, 1997). Abrupt chemical and structural changes are characteristic of the fundamental particle model (Altaner and Ylagan, 1997). The term "fundamental particle" in the Nadeau sense is not carried much further into the literature. For example, Ahn and Peacor (1986) showed that packets of illite layers known as megacrystals or domains form sub-parallel smectite domains and show the reaction of smectite to form illite. SST and dissolution-precipitation are two end member hypotheses that attempt to explain the formation of diagenetic illite. By XRD, the conversion of smectite to illite occurs via I/S. By TEM, smectite is reacted to form illite without I/S intermediates.

1.4 GEOLOGIC BACKGROUND

The study area is the Disturbed Belt, which is located in northwest Montana, southeast of Glacier National Park (GNP) and lies within the northeastern portion of the Cordillera physiographic province. The Cordillera in this region is a northwestward trending zone, which is subdivided from east to west into three regions called the Foothills, the Front Ranges, and the Main Ranges (Mudge, 1970). The Disturbed Belt as defined by Mudge

(1970) comprises the Foothills and Front Ranges which trend northwest into the Laramide thrust belt of southern Alberta, Canada. The Sawtooth and Lewis and Clark Ranges comprise the Front Ranges (Mudge, 1970). The Sweetgrass Arch abuts the Disturbed Belt to the east, while the Main Ranges are at the western boundary (Mudge, 1977). The Disturbed Belt contains a complex assemblage of closely spaced westward dipping thrust faults and normal faults and associated folds resulting from large-scale eastward displacement that occurred early in the Tertiary period during the Laramide orogeny (Mudge, 1970; Mudge, 1977; Mudge and Earhart, 1980; Mudge and Earhart, 1991). The intensity of thrusting decreases from the Front Ranges in the west to the eastern boundary of the Foothills. Figure 1.2 depicts the Disturbed Belt and regional geologic features (Mudge, 1970).

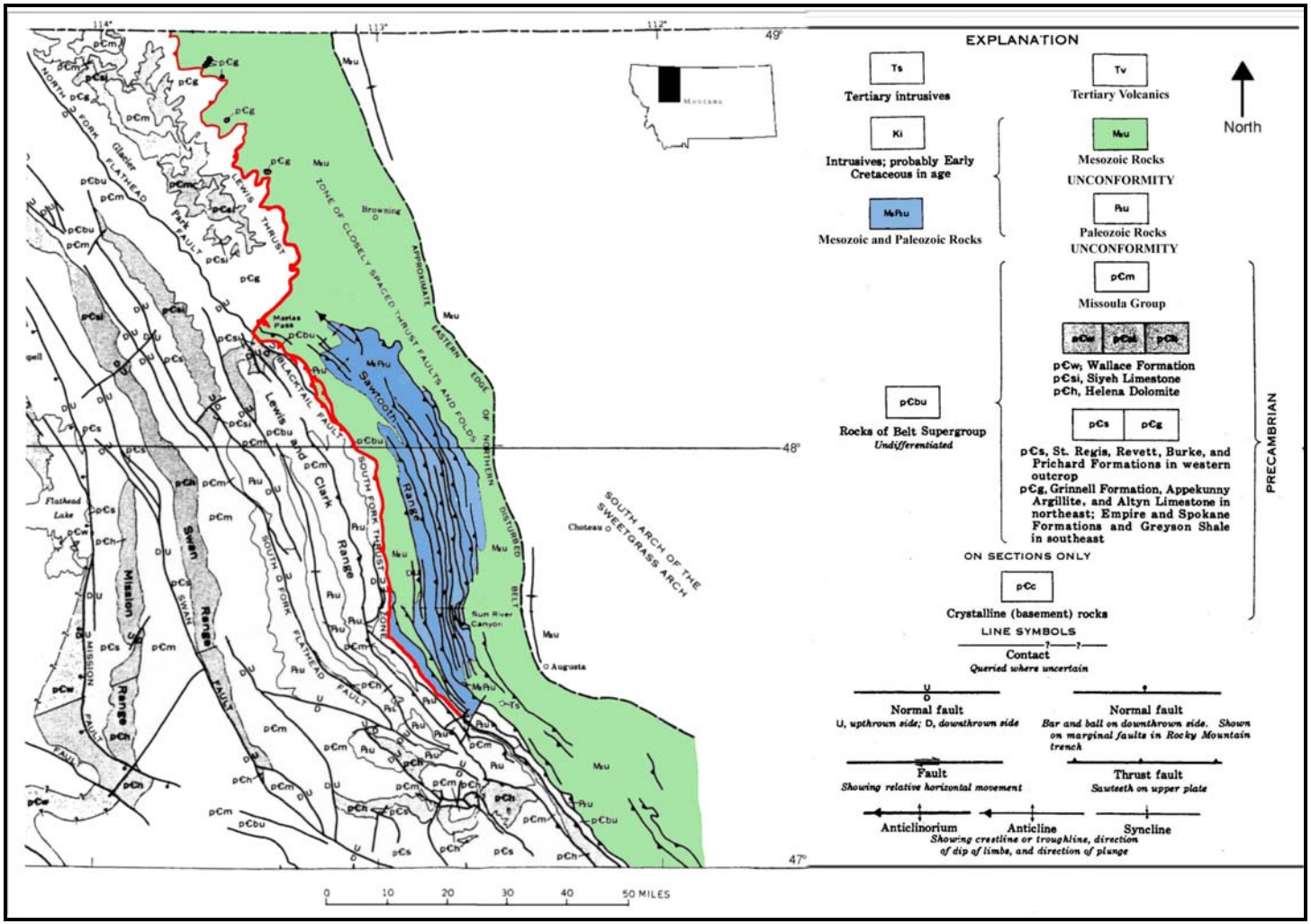

Figure 1.2: Map of the Disturbed Belt (base map after Mudge, 1970). The red line denotes the Lewis Thrust.

The Lewis Thrust (LT) is a major feature of the Disturbed Belt; it trends northwest-southeast and dips to the west at a low angle (Figure 1.2). The LT forms the western boundary of the northern Disturbed Belt with GNP to the east (Mudge, 1977; Mudge and Earhart, 1983). The western boundary of the southern Disturbed Belt (south of Steamboat Mountain) is formed by the Hoadley Thrust fault, which is west of the LT (Mudge and Earhart, 1980; Mudge and Earhart, 1983). Mudge (1980) estimated that in the Disturbed Belt the amount of eastward horizontal displacement increases along a transect trending to the northwest from no displacement at Steamboat Mountain (where the LT outcrops) to approximately 65 kilometers (km) at Marias Pass. Clockwise rotation occurred about a hinge point near the west fork of the Sun River. At a larger, regional scale, Sears (2001) estimated that eastward horizontal displacement of the major thrust slab comprising the Lewis, Hoadley, and Eldorado thrust sheets is approximately 40 km at Rogers Pass (approximately 25 km southeast of Steamboat Mountain). The horizontal displacement increases progressively to the northwest to 140 km at the U.S.-Canadian border resulting from clockwise rotation about a pole near Helena, MT (Sears, 2001).

Mudge (1970) proposed gravitational gliding following uplift as the main mechanism for the displacement creating the Disturbed Belt (Figure 1.3). Thick sediments accumulated in a subsiding basin to the west from the Middle Proterozoic Era through the Paleozoic Era (Figure 1.3, Event A). Sediments thinned eastward toward the Sweetgrass Arch, which was a structural high. Carbonate sedimentation from shallow seas was pervasive in the Paleozoic. During the late Jurassic, volcanism and plutonism occurring to the west uplifted western Montana (Figure 1.3, Event B). The uplift caused erosion of

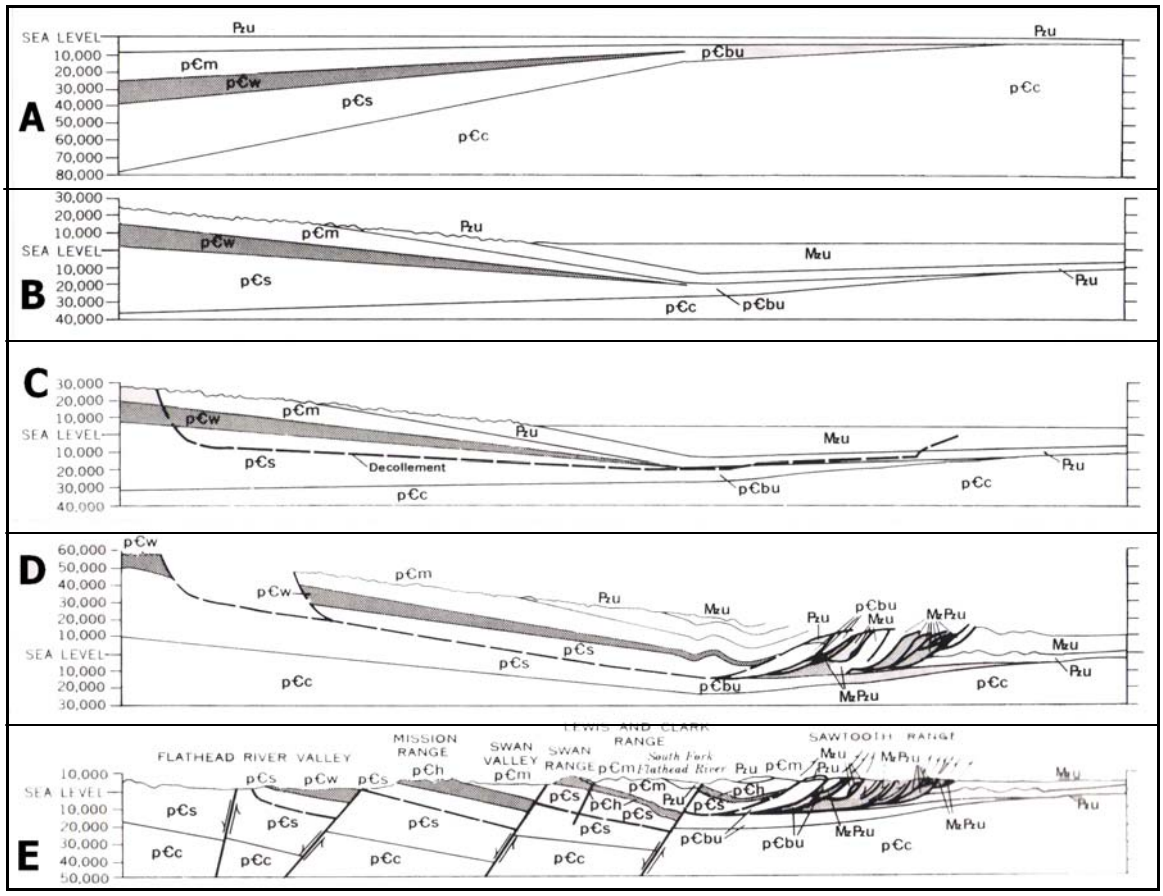

Figure 1.3: Figure depicting the development of the Disturbed Belt (after Mudge, 1970). The elevation (y-axis) is in feet relative to sea level.

the Paleozoic and Precambrian sediments and deposition in a foreland basin to the east. The uplift, erosion, and deposition continued until the early Tertiary. Mudge (1970) postulated that as uplift continued in the west during the late Cretaceous, a large mass of sedimentary rocks detached (Figure 1.3, Event C) in a zone with very high fluid pressure. The mass moved eastward (down slope) under the influence of gravity toward the Sweetgrass Arch to the east (Figure 1.3, Event D). As a result, the rocks to the east of the gliding mass were intensely folded and thrust faulted in an imbricate fashion, after which longitudinal normal faults and grabens formed to the west in response to extension.

Continued erosion through the Tertiary and Quaternary Periods lowered the topography (Figure 1.3, Event E) to its present configuration.

1.5 STRATIGRAPHY

Rocks exposed within the Disturbed Belt generally increase in age from east to west. The Disturbed Belt south of GNP contains an assemblage of Cambrian, Paleozoic, and Mesozoic age rocks with the location and geometry of exposures being controlled by the northwest-southeast striking, closely spaced thrust faults (Mudge, 1977; Mudge and Earhart, 1983; Mudge and Earhart, 1991). Paleozoic and Mesozoic rocks of the Madison and Ellis Groups, respectively, outcrop southeast of GNP and trend northwest-southeast (Mudge and Earhart, 1983). The exposures of the Madison and Ellis Groups alternate from west to east and are bounded by the closely spaced thrust faults within the Disturbed Belt. The Madison Group consists of dolomite, calcitic dolomite, dolomitic limestone, limestone, and shale with light gray and dark gray chert nodules. The Ellis Group consists of the Swift, Rierdon, and Morrison Formations. The Swift Formation is upper and middle Jurassic rock that ranges in thickness from 30 meters (m) to 60 m within the Disturbed Belt (Mudge and Earhart, 1983). The upper member of the Swift Formation consists of thin bedded, fine- to very fine-grained sandstone, while the lower member consists of dark gray shale with thin beds of sandstone (Mudge and Earhart, 1983). The Madison and Ellis Groups were sampled for this study.

The Kootenai Formation is lower Cretaceous and was deposited unconformably on top of upper Jurassic rocks of the Ellis Group (Rice and Cobban, 1977). The Kootenai

Formation is an approximately 1,000 m thick deposit of mudstone, siltstone, and sandstone of non-marine origin (Rice and Cobban, 1977). Exposures of the Kootenai Formation occur at the southern tip of GNP and strike northwest-southeast, alternating from west to east with exposures of the Cretaceous Blackleaf Formation (Mudge and Earhart, 1983). The Blackleaf Formation, consisting of the Vaughn, Taft Hill, and Flood Members, is lower Cretaceous and was deposited unconformably above the Kootenai Formation. The Blackleaf Formation is a marine deposit consisting of dark gray fissile shale with quartzose sandstone at the base (Rice and Cobban, 1977). The Vaughn Member is the upper member of the Blackleaf Formation and consists of gray to olive mudstone and bentonitic mudstone with thin beds of light gray, fine- to coarse-grained sandstone (Mudge and Earhart, 1983; Mudge and Earhart, 1991). Some thin beds of bentonite were observed by Rice and Cobban (1977). A sample of one bentonite for this study was collected from the Vaughn Member outside (east of) the Disturbed Belt.

The area east of GNP within the northern Disturbed Belt also contains many closely spaced thrust faults and folds that trend to the northwest-southeast and are covered by Quaternary deposits (Mudge, 1977; Mudge and Earhart, 1983; Mudge and Earhart, 1991). Exposures in the northern Disturbed Belt consist predominately of upper Cretaceous rocks. The Marias River Shale is an upper Cretaceous deposit that is thick (366 m to 396 m) in the area of GNP, and it was deposited unconformably on top of the Blackleaf Formation. The Marias River Shale consists of the Floweree, Cone, Ferdig, and Kevin Members (Rice and Cobban, 1977). The Marias River Shale Formation consists of dark gray mudstone with thin beds of bentonite and of limestone, sandstone, siltstone, and calcareous and ferruginous concretions (Rice and Cobban, 1977; Mudge

and Earhart, 1983; Mudge and Earhart, 1991). Northwest-southeast trending exposures of the Marias River Shale Formation exist predominately at the western boundary of the northern Disturbed Belt with GNP, but they cross over to the eastern Disturbed Belt boundary south of GNP (Mudge and Earhart, 1983). The Marias River Shale was sampled extensively for this study. Other upper Cretaceous rocks deposited above the Marias River Shale in sequence from oldest to youngest are the Telegraph Creek Formation, Virgelle Sandstone, Two Medicine Formation, Bearpaw Shale, Horsethief Sandstone, and Willow Creek Formation. Exposures of these formations trend northwest-southeast and these outcrops alternate with the next younger formation eastward through the Disturbed Belt (Rice and Cobban, 1977; Mudge and Earhart, 1983; Mudge and Earhart, 1991). The exposures of the Two Medicine Formation alternate with those of the Virgelle and Telegraph Creek Formations in a northwest-southeast trending zone, east of the exposures of the Marias River Shale. The Two Medicine Formation consists of mudstone with some calcareous nodules and of sandstone that is fine- to very coarse-grained (Mudge and Earhart, 1983).

1.6 PURPOSE OF THIS STUDY

Hoffman and Hower (1979) and Hoffman et al., (1976) noted that shales and bentonites from the Disturbed Belt had not been buried deeply enough by overlying sediments to induce the extent of illitization that has been observed. The diagenetic mineralogical changes they observed are similar to those observed in the deepest Gulf Coast sediments resulting from burial diagenesis. Hoffman (1976) noted that low-grade

metamorphism of the Cretaceous sedimentary rocks was extensive throughout the Disturbed Belt. From K-Ar ages of I/S and from characterization of the stacking order and percentage of illite layers in I/S, Hoffman et al. (1976) and Hoffman and Hower (1979) concluded that the observed diagenetic changes are illitization that was a result of thrust fault burial. Furthermore, Hoffman determined a range of K-Ar ages for diagenetic illite from 56 Ma to 72 Ma that was interpreted to result from the Laramide orogeny. The K-Ar ages measured by Hoffman (1976) do not exhibit a trend with regard to location within the Disturbed Belt.

Recent studies by Katz et al. (2000), Woods et al. (2002), and Basu (2004) have suggested a relation between the acquisition of CRM and the transformation of smectite to illite under diagenetic conditions. Support for this hypothesis may be observed by comparison of K-Ar age of diagenetic illite and the age of CRM by paleomagnetic analysis. Although, K-Ar dating methods have traditionally been employed in I/S research to determine the timing of illitization, alternative methods such as paleomagnetic techniques may provide the age determination of diagenetic illite formation where mixtures of polytypes make it difficult to determine K-Ar age of I/S.

In this study, we investigate the diagenesis of upper Cretaceous sediments in the Disturbed Belt via the K-Ar age of I/S whose data will be combined with paleomagnetic data measured by V. O'Brien and Dr. R. Douglas Elmore. The main contribution of this study is to provide a description of the clay mineralogy and K-Ar ages of I/S in close proximity to concretions sampled for paleomagnetic analyses that will test the relationship between illitization and formation of CRM.

CHAPTER 2.0 - METHODS

2.1 SAMPLING

Samples were collected for this study from various rock exposures of the Ellis Group, Madison Group, Marias River Shale, and Vaughn Member of the Blackleaf Formation. Eleven sets of bentonite and concretion samples were collected during the summers of 2004 and 2005. The concretions were collected by Dr. Douglas Elmore and Vanessa O'Brien (graduate student) from the University of Oklahoma. Concurrently, Dr. Crawford Elliott and the author of this thesis from Georgia State University collected the bentonite samples. The samples were field identified as BC-3 (Badger Creek), VQ (Vaughn Quadrangle), SR-04 (Sun River), Cl Coulee (Cleary Coulee), TM (Two Medicine), SD-03 (Swift Damn), BC-01, BC-05, BC-06, MP-01 (Marias Pass), and TMCE-01 (Two Medicine, collected by C. Elliott). Sample location information is provided in Table 2.1 and depicted on Figure 2.1. Bentonite sample identification for the remainder of this text will utilize the map symbol name listed in Table 2.1, except that the several samples from BC must be distinguished from one another by the sample numbers that follow "BC."

The concretion sample of each sample set was collected by drill core in the field by Dr. Elmore and O'Brien, and subsequently tested for acquired CRM by paleomagnetic methods (Elliott et al., in press). The bentonites of each sample set were carefully sampled in the field by Dr. Elliott and the author so as to collect bentonite or bentonitic

Table 2.1: Sample location information.

Sample Identification	Map Symbol	Location Latitude	Location Longitude	Period	Stratigraphic Unit
05-BC-01	BC	N 48° 19.56'	W 112° 58.38'	Cretaceous	Marias River Shale
BC-3	BC	N 48° 19.36'	W 112° 57.98'	Cretaceous	Marias River Shale
05-BC-05	BC	N 48° 19.35'	W 112° 57.99'	Cretaceous	Marias River Shale
05-BC-06	BC	N 48° 19.34'	W 112° 58.12'	Cretaceous	Marias River Shale
Cl Coulee	CCL	N 47° 53.18'	W 112° 42.47'	Mississippian	Madison Group
05-MP-01	MP	N 48° 19.77'	W 113° 20.33'	Cretaceous	Marias River Shale
05-SD-03	SD	N 48° 9.95'	W 112° 52.34'	Jurassic	Ellis Group
SR-04	SR	N 47° 38.17'	W 112° 38.62'	Cretaceous	Marias River Shale
TM	TM	N 48° 22.64'	W 113° 5.14'	Cretaceous	Marias River Shale
05TMCE-01 (a)	TMCE	N 48° 24.37'	W 113° 8.96'	Cretaceous	Marias River Shale
VQ	VQ	N 47° 34.99'	W 111° 42.19'	Cretaceous	Vaughn Member (b)

a = Sample collected approximately 0.5 mile south of latitude/longitude shown
b = Vaughn Member of the Blackleaf Formation

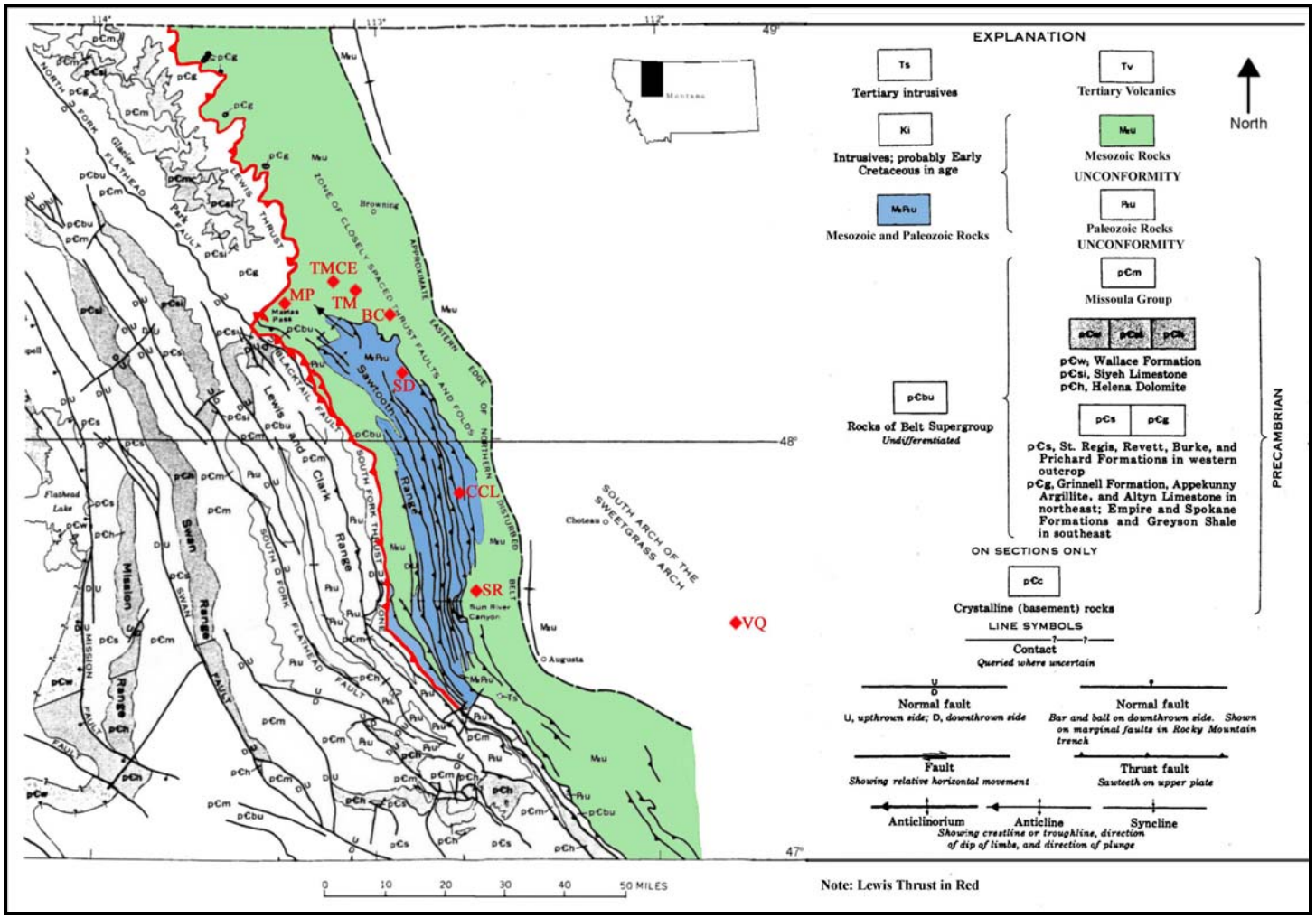

Figure 2.1: Sample location map (base map after Mudge, 1970).

shale samples while minimizing sample contamination by the enclosing shale or soil. Figures 2.2 and 2.3 show white to yellow-white bentonites that are relatively thick (>2 cm) and have a soft spongy/clayey texture for samples SD and BC-01, respectively. Figure 2.4 (sample BC-05) shows a yellowish-white bentonitic shale that is relatively thin (<2cm) and brittle. These pictures also show that the enclosing shales and soil are strikingly darker than the bentonite and bentonitic shales with a relatively sharp boundary that made targeted field sampling easier. It should also be noted that prior to any sample treatments, all samples were observed under a magnifying lense in the lab to remove any of the darker enclosing shale or soil that may have mixed with the lighter colored bentonite/bentonitic shale sample. Each bentonite sample was separated into fractions by grain size, and the mineralogy and apparent age of each fraction were determined by XRD methods and K-Ar isotopic analyses, respectively. In addition to K-Ar and ordinary XRD measurements, selected bentonite samples whose clay sub-fraction ages are discordant were analyzed for the presence of different illite polytypes.

2.2 GRAIN SIZE SEPERATIONS AND SAMPLE TREATMENTS

Approximately 20 to 30 g of the bulk rock (after removing shale and soil particles) for each sample detailed above is placed in a cleaned and labeled beaker with deionized (DI) water to soak for one to two days. The samples were then gently crushed using a mortar and pestle to disaggregate the bulk sample. The disaggregation of the bulk samples was necessary to increase surface area for the chemical pre-treatments (described below) to be effective as well as to obtain representative size fractions for analysis. No

Figure 2.2: Sample location SD. The bentonite sample was collected from the white to yellow-white section.

Figure 2.3: Sample location BC-01. The bentonite sample was collected from the white to yellow-white section.

Figure 2.4: Sample location BC-05. The bentonitic shale sample was collected from the yellow-white section.

organic materials were observed in the bulk samples collected for this study. Chemical treatments to remove organic materials were performed on samples collected from the summer of 2005 only in accordance to procedures outlined by Jackson (1979). Calcium carbonates and Fe-oxides, which act as cements, were removed from the disaggregated shale samples by chemical treatment as specified by Jackson (1979). Carbonate cements were dissolved with a 1 normal (N) sodium acetate-acetic acid buffer of pH 5.0 (NaOAc buffer). Following carbonate removal, Fe-oxide cements were removed by reaction with a mixture of sodium citrate, sodium bicarbonate, and sodium hydrosulfite (CBD Method). Hassanipak and Wampler (1996) found that the <2 μm fraction of illite lost nearly 1% of its radiogenic argon when heated at 250ºC for 24 hours. Therefore, all chemical and physical treatments were performed at or below a conservative temperature of 50ºC to prevent damage to clay particles and loss of Ar (e.g., Elliott et al., 1991). Salts and exchangeable ions were removed after each chemical pre-treatment by washing the samples with NaOAc buffer solution. Samples were preserved in DI water and methanol between procedures to prevent the growth of bacteria in the samples. The DI water-methanol solution was decanted at the beginning of each procedure.

The samples were then separated according to grain size. Grain size separations between 50 μm and 2 μm were performed in accordance with Stoke's Law and methods detailed by Jackson (1979). One to two ml of 5% sodium metaphosphate (Na-phosphate), a dispersant, and DI water are added to the beaker and the sample was stirred into suspension with a cleaned stirring rod. The stirring rod was removed at time zero. Particles were allowed to settle for 10 seconds per inch of water column in the beaker to separate the >50 μm from the dispersed suspension (Jackson, 1979). The supernatant

suspension (<50 μm) was then carefully decanted into a separate, labeled, and clean beaker, making sure to leave the >50 μm size fraction behind in the first beaker. DI water only was then added to the first beaker with the >50 μm fraction, which was stirred into suspension again. The procedure was repeated at least 3 times to remove any <50 μm material. The separations of the <20 μm and <2 μm size fractions were completed in the same manner, with settling times of five minutes per four inches of water column and eight hours per four inches of water column, respectively (Jackson, 1979).

A representative portion of the suspension of the <2 μm fraction of each sample was placed aside for mineralogical analysis and dating by K-Ar techniques (described in the following sections). The remainder of the <2 μm size was further divided by timed centrifugation into coarse (2 μm – 1 μm), medium (1 μm – 0.25 μm), and fine (<0.25 μm) clay size fractions in accordance with methods detailed by Jackson (1979). For the remainder of this text, coarse, medium, and fine will refer to 2 μm – 1 μm, 1 μm – 0.25 μm, <0.25 μm grain sizes fraction, respectively. DI water was then added to the beaker containing the <2 μm grain size fraction and the sample was thoroughly stirred into suspension. The sample was immediately and completely transferred to a 250 ml centrifuge bottle where 1-2 ml of 1 M calcium chloride, a flocculant, was added. The sample was then balanced to the nearest 0.1 g on an Ohaus Trip Balance with the other centrifuge bottles and placed into the centrifuge. The resulting suspensions were then centrifuged at 1,200 rotations per minute (RPM) for 10 minutes. The supernatant was decanted and DI water only was added to the centrifuge bottle. The sample was stirred into suspension and the procedure repeated with DI water until the clay started to re-suspend which signifies the removal of the calcium chloride flocculent. The coarse,

medium, and fine size separations were completed by repeated centrifugation according to the following equation provided by Jackson (1979):

$$t_{(minutes)} = [63.0 \times 10^8 \, \eta \, \log_{10}(R/S)]/[(N_m)^2(D_{\mu m})^2(\Delta s)]$$

where R is the rotational radius, S is the height of the suspension in the centrifuge bottle, η is viscosity, N_m is rotation rate in RPM, $D_{\mu m}$ is particle diameter in μm, and Δs is the difference in specific gravity between the solvated particle and the suspension liquid. Once the calcium chloride was sufficiently washed from the sample, DI water was added to a measured height and centrifuged for a calculated time interval and rotational rate in accordance with the above equation. The procedure was repeated several times to insure as complete a separation as possible for each of the coarse, medium, and fine clay fractions.

The separated size fractions were completely transferred to dialysis bags and washed in DI water for three days at room temperature. A large dessicator is used as a dialysis tank. The dialysis bags hang from an acrylic disk attached to a low speed motor, which turned at approximately one rotation per minute. The dialysis bags, typically used in the medical industry, have pores small enough to allow water and dissolved materials to pass across the bag boundary, but not clay size particles. The dialysis with DI water was to remove any soluble salts that may have been present in the solution. The DI water was changed several times per day throughout the dialysis period. Any cloudiness that might have indicated a ruptured or leaky dialysis bag would have been noted. No such leaks were observed. Following dialysis, the clay slurries were poured on to plastic wrap lined

drying dishes. A representative portion of each dialyzed sample was then taken up in a clean disposable pipette and dropped onto a clean and labeled glass slide in a manner such that the suspension covered the entire slide without spilling over the sides. The slurries remaining on plastic wrap were then placed in an oven set at 50ºC to dry over night while those on the glass slides were left to dry in air over night to produce oriented mounts for XRD study. The glass slides with the air-dried samples were placed in a storage container for later analysis by XRD. The oven-dried samples were carefully removed from the plastic wrap and gently crushed with a mortar and pestle to disaggregate the clay. The resulting powders were then placed in cleaned and labeled containers for K-Ar analyses. XRD analysis and K-Ar isotopic age analysis were conducted on the <2 μm fraction of the 2004 samples only and on the coarse, medium, and fine clay size fractions of all samples.

2.3 POTASSIUM – ARGON ANALYSES

The K-Ar dating method is based on the decay of ^{40}K, a long-lived radioactive isotope of potassium. An atom of ^{40}K can decay to an atom of ^{40}Ar, by electron capture, with or without the emission of a gamma ray, or by positron emission (Dalrymple and Lanphere, 1969). Furthermore, such an atom ^{40}K can decay to an atom of ^{40}Ca by beta emission (Dalrymple and Lanphere, 1969). Therefore, the decay of ^{40}K, which obeys the radioactive decay law, produces two daughter isotopes (^{40}Ar and ^{40}Ca). Argon is a gas, but the daughter atoms of ^{40}Ar are physically trapped in the crystal lattice of I/S.

The K-Ar method assumes that the decay of non-exchangeable K in the interlayer lattice of I/S and illite is constant; the ratio of ^{40}K to total K is consistent in all materials (at time zero); all Ar in a rock sample is either radiogenic (coming from the decay of ^{40}K) or atmospheric; and there is no loss of the parent isotope (^{40}K) or the daughter isotope (^{40}Ar) (Dalrymple and Lanphere, 1969). The amount of ^{40}Ar accumulated in the crystal lattice is measured along with the amount of ^{40}K. The apparent age (t) is determined by the K-Ar age equation (Dalrymple and Lanphere, 1969) as follows:

$$t = (1/(\lambda_\varepsilon+\lambda_\beta))\log_e[(^{40}Ar_{(radiogenic)}/\ ^{40}K)((\lambda_\varepsilon+\lambda_\beta)/\lambda_\varepsilon) + 1]$$

where λ_ε and λ_β are decay constants and the symbols for the nuclides stand for their amounts. It should be noted that the ^{40}Ar in the above equation is the radiogenic argon and does not include any atmospheric argon that may have been in a sample. A blank measurement was performed. The fraction of radiogenic ^{40}Ar is the relative excess of ^{40}Ar in the argon from the sample relative to the isotopic composition of argon in air (Dalrymple and Lanphere, 1969).

The K-Ar measurements were performed with the assistance of Dr. J. Marion Wampler of the Georgia Institute of Technology. The specific procedures used are described with his permission as Appendix A. A portion, usually between 20 mg and 30 mg, of the oven-dried sample to be used for argon isotopic analysis was carefully transferred to a pre-weighed copper-foil capsule and weighed on a microbalance to the nearest 0.01 mg. A comparable but usually smaller amount of sample was weighed in a similar manner and transferred to a fluorinated ethylene propylene (FEP) container with a

screw-on cap for K determination. The latter sample was then digested in the FEP container with approximately 1 ml of 10:1 HF-$HClO_4$. The resultant liquid was evaporated under a hood, leaving perchlorate salts in the FEP container. The salts were then dissolved with a diluting solution 0.1 M in HNO_3 and 0.01 M in cesium chloride and completely transferred to a pre-weighed 125 ml polyethylene bottle. The cesium-bearing diluting solution was then added to the top of the bottle and the mass of the solution was determined by weighing. As necessary, solutions were further diluted, to a degree determined gravimetrically, with the cesium-bearing solution. The K content of each solution was measured with a flame atomic absorption spectrophotometer using reference solutions prepared from a potassium chloride standard. The potassium hollow-cathode lamp was operated at 6 mA. Absorption within the flame was measured at a wavelength of 766.5 nm. Absorbance by potassium atoms from aspirated sample solutions within the flame is compared to the absorbance during aspiration of the prepared standard solutions, for which there is a linear relationship between absorbance and K content. Readings were taken in one-second increments for ten readings and averaged. The average value of absorbance was recorded for use in calculation of the K in a sample.

The apparatus for the argon isotopic analyses was appropriately calibrated and tested in accordance with the procedures provided by Dr. Wampler (2005). The copper-foil capsules containing the samples prepared for the Ar analyses were placed in the Ar extraction glass tubing in a specific and noted order. After evacuation of the argon extraction line for at least 16 hours, argon was extracted from the samples one by one and isotopically analyzed. In this process, an individual sample is dropped into an electrical resistance furnace where it is heated in slow progressive steps to melting and beyond.

Occasional blank fusions (i.e., heating the furnace with no sample) were run to show that argon was completely extracted from the melted samples. Concurrently, an ^{38}Ar spike (i.e., a known amount of highly enriched ^{38}Ar) is prepared and discharged to mix with the argon released from the sample. Condensable gasses, in particular CO_2 and water, are removed by condensation on a glass cold finger cooled at the closed end by liquid nitrogen. Any remaining reactive gasses are removed by reaction with heated titanium strips or by reaction with the titanium as it is later allowed to cool, leaving only Ar and other inert gasses, if any, in the gas phase just before entry into the mass spectrometer. The argon gas is then allowed to expand into the mass spectrometer, where the amounts of atoms with mass numbers 36, 38, and 40 are measured. In this work, the signals corresponding to these mass numbers were due only to ^{36}Ar, ^{38}Ar, and ^{40}Ar, respectively. Background signals at these mass numbers due to other species were negligible. The radiogenic ^{40}Ar was subsequently determined from the mass spectrometer output. Corrections for slight mass discrimination by the mass spectrometer were based on occasional isotopic analyses of atmospheric argon. Potassium and argon in the reference material LP-6 Bio were measured and compared to accepted values to gauge the accuracy of the K and Ar measurements of the samples. Duplicate analyses of selected samples were conducted to test precision.

2.4 ACCURACY AND PRECISION

The estimated error of the K measurement is less than 2% of the measured amount in most cases. The K error ranged from 0.01 to 0.13 percent by mass (Table 3.1). Several

samples were run in duplicate to test precision. The K-Ar apparent age was measured on duplicate BC-3 samples of the fine, medium, and coarse grain size fractions. The fine grain size fraction of sample TM and the coarse grain size of sample BC-01 have duplicate K-Ar apparent age measurements as well. The K measurements of the duplicate fine, medium, and coarse samples of BC-3 were the same, within the estimated errors, as the original measurements. The difference between the original and duplicate K measurements is less than 2.9 % of the original amount in all cases. With the exception of sample TM (<0.25 μm) the difference in calculated amount of radiogenic Ar (pmol/g) between the original and the duplicate determinations is less than 0.8% of the original amount. That difference in the case of sample TM (<0.25 μm) is approximately 6.7% of the original amount.

The K-Ar measurements were done in groups of 5 to 15 samples, and a sample of the interlaboratory reference material LP-6 Bio was concurrently measured with each group of I/S clay samples. Five LP-6 measurements were completed during this study (Table 2.2). With the exception of the measurement on 12-20-04, the difference between the

Table 2.2: Analytical results for LP-6 Bio.

Date	Potassium in Sample as K (% by mass)	RADIOGENIC ARGON (% of ^{40}Ar)	RADIOGENIC ARGON (pmol/g)	Apparent Age (Ma)
12-20-04	8.12 ± 0.12	96	1943	132.9 ± 2.7
3-11-05	8.34 ± 0.08	97	1935	129.1 ± 1.9
6-02-05	8.25 ± 0.08	97	1921	129.4 ± 1.9
8-29-05	8.37 ± 0.09	97	1918	127.5 ± 1.9
10-13-05	8.23 ± 0.08	97	1943	131.2 ± 1.9
Accepted Values	8.33 ± 0.03		1930	127.7 ± 1.4

(a) = Sample solution for potassium content was rediluted from the original solution and measured on 10-14-05. Sample result is shown.

measured K content of LP-6 Bio and the accepted value is less than 1.15% of the accepted value. That difference is 2.48% of the accepted value for the measurement on 12-20-04. The difference between the measured radiogenic Ar and the accepted radiogenic Ar value is less than 0.67 % of the accepted value in all LP-6 measurements.

2.5 X-RAY DIFFRACTION ANALYSES

Clay minerals (or any crystalline material) can be identified by the unique positions of the 00*l* peaks on an XRD pattern (Moore and Reynolds, 1997). Scattering occurs as electrons in atoms that make up the crystal lattice absorb energy from the incoming X-rays and re-emit it in all directions with the same wavelength as the incident X-rays (Moore and Reynolds, 1997). The scattered X-rays will be out of phase with each other (destructive interference), except at specific angles (θ) between the incident beam and the planes of the crystal lattice where the waves will be in phase (constructive interference) (Moore and Reynolds, 1997). Bragg's law (provided below), relates the wavelength (λ)

$$2d \sin\theta = n\lambda,$$

of incident and diffracted X-rays to the distance between atoms in a crystal lattice (d), where n is an integer denoting the difference in distance traversed by constructively interfering beams as an integral number of wavelengths (order) (Moore and Reynolds, 1997). Angles of constructive interference (2θ) are identified by the positions of peaks

on an XRD pattern. The 00*l* peaks correspond to apparent lattice spacing obtained by using whole numbers as divisors of the actual 001 spacing (d/n, where n = 1,2,3,…,n).

Basal reflections of d (001) = 10 Å on the XRD pattern from untreated oriented clay show the presence of illite (Brown and Brindley, 1984). A basal reflection of 12.4 Å to 15 Å from such clay, which shifts to 17 Å upon solvation with ethylene glycol (EG), shows the presence of smectite. The illite 001 reflection (a 10 Å peak) occurs at 8.8° 2θ when Cu K_α radiation is used. This peak does not shift upon solvation with EG (Brindley and Brown, 1984). Three slides per grain size separation were prepared as described above. Each of the three slides represents the untreated (air dry), heated (at 550 °C), or solvated by EG treatments, respectively prior to XRD analyses. The percentage of illite layers in I/S was determined by the position of the $002_{10}/003_{17}$ reflection from EG treated oriented clay between approximately 15.8° and 17.39° 2θ (Moore and Reynolds, 1997). The stacking order was determined by the position of the 001 peak upon EG solvation (Hower, 1981). Illite polytypes were determined by XRD on randomly oriented clay samples, by scanning from 28° to 36° 2θ (Cu K_α) in steps of 0.02° at 10 seconds per step, measuring the area under the 3.00 Å peak ($2M_1$ polytype) and the 2.58 Å peaks (all polytypes). Samples that contain kaolinite were heated to 550ºC for one hour prior to XRD analyses for polytype identification. The percentage of the $2M_1$ polytype is determined by the following equation (Grathoff, 1996):

$$\%2M_1 = 3.25 + 335\ [2M_1 \text{ polytype-peak area / total polytype peak area}].$$

The percentage of $2M_1$ illite polytype was measured in an attempt to determine the age of diagenetic illite through IAA as outlined by Pevear (1999).

CHAPTER 3.0 – RESULTS

3.1 CLAY FRACTION MINERALOGY

The results of the XRD analyses and K-Ar dating conducted on samples collected from the Disturbed Belt are summarized in Table 3.1 and depicted in Figures 3.1 and 3.2. The XRD patterns for air-dried, EG-treated, and heated clays are attached as Appendix B. All samples contain I/S as determined by XRD analyses. Kaolinite (d_{001}=7.15 Å) is present in all samples except CCL and the smallest grain size fractions (<0.25 μm) of samples SR and VQ. In all cases, the I/S crystal lattice collapses to d-spacings that match the d-spacings for pure illite upon heating to 550ºC for one hour.

Samples collected from within the Disturbed Belt contain more than 60% percent illite layers in I/S, indicative of Rectorite stacking order (R≥1) and Kalkberg stacking order (R≥3) of illite and smectite layers. Samples SR, TM, SD, BC-01, BC-06, and MP all have Rectorite stacking order and contain 60% to 90% illite layers in I/S. Samples BC-3, CCL, BC-05, and TMCE exhibited long range Kalkberg stacking order and contain greater than 90% illite layers in I/S. Sample VQ, collected east of the Disturbed Belt, contains between 20% and 30% illite in I/S and the stacking order is random (R=0).

Table 3.1: Sample K-Ar apparent age and mineralogy

Sample	Clay Mineralogy	Potassium in Sample as K (% by mass)	RADIOGENIC ARGON (% of ^{40}Ar)	(pmol/g)	Apparent Age (Ma)
BC-3 <0.25 micrometer	Illite-Smectite (~ >90% I), Kaolinite	3.01 ± 0.05	78	658	121.9 ± 2.3
BC-3 <0.25 micrometer (a)	Illite-Smectite (~ >90% I), Kaolinite	2.97 ± 0.06	74	662	124.1 ± 2.9
BC-3 0.25-1.0 micrometer	Illite-Smectite (~ >90% I), Kaolinite	3.09 ± 0.03	94	1008	178.9 ± 2.6
BC-3 0.25-1.0 micrometer (a)	Illite-Smectite (~ >90% I), Kaolinite	3.08 ± 0.03	95	1004	179.1 ± 2.6
BC-3 1.0-2.0 micrometer	Illite-Smectite (~ >90% I), Kaolinite	2.47 ± 0.03	95	1046	228.6 ± 3.9
BC-3 1.0-2.0 micrometer (a)	Illite-Smectite (~ >90% I), Kaolinite	2.42 ± 0.02	95	1042	232.5 ± 3.3
BC-3 <2.0 micrometer	Illite-Smectite (~ >90% I), Kaolinite	3.18 ± 0.07	89	851	148.2 ± 3.7
SR <0.25 micrometer	Illite-Smectite (~ 70%-80% I)	4.14 ± 0.04	81	389	53.3 ± 0.8
SR 0.25-1.0 micrometer	Illite-Smectite (~ 70%-80% I), Kaolinite	4.15 ± 0.08	92	390	53.4 ± 1.1
SR 1.0-2.0 micrometer	Illite-Smectite (~ 70%-80% I), Kaolinite	4.14 ± 0.07	88	395	54.1 ± 1.1
SR <2.0 micrometer	Illite-Smectite (~ 70%-80% I), Kaolinite	3.98 ± 0.11	84	363	51.9 ± 1.6
TM <0.25 micrometer	Illite-Smectite (~ 70%-80% I), Kaolinite	2.63 ± 0.03	84	401	86.0 ± 1.4
TM <0.25 micrometer (a)	Illite-Smectite (~ 70%-80% I), Kaolinite	2.69 ± 0.13	74	374	78.4 ± 3.8
TM 0.25-1.0 micrometer	Illite-Smectite (~ 70%-80% I), Kaolinite	2.16 ± 0.03	79	323	84.1 ± 1.5
TM 1.0-2.0 micrometer	Illite-Smectite (~ 70%-80% I), Kaolinite	1.80 ± 0.02	91	238	74.6 ± 1.3
TM <2.0 micrometer	Illite-Smectite (~ 70%-80% I), Kaolinite	2.59 ± 0.06	90	382	83.0 ± 2.2
CCL <0.25 micrometer	Illite-Smectite (~ >90% I)	4.55 ± 0.05	92	1382	167.2 ± 2.4
CCL 0.25-1.0 micrometer	Illite-Smectite (~ >90% I)	6.87 ± 0.07	96	2423	192.7 ± 2.8
CCL 1.0-2.0 micrometer	Illite-Smectite (~ >90% I)	6.89 ± 0.07	97	2955	231.7 ± 3.3
CCL <2.0 micrometer	Illite-Smectite (~ >90% I)	6.30 ± 0.09	94	1956	170.8 ± 3.4
VQ <0.25 micrometer	Illite-Smectite (~ 20%-30% I)	0.89 ± 0.02	60	79	50.6 ± 1.2
VQ 0.25-1.0 micrometer	Illite-Smectite (~ 20%-30% I), Kaolinite	0.95 ± 0.01	66	86	51.7 ± 0.8
VQ 1.0-2.0 micrometer	Illite-Smectite (~ 20%-30% I), Kaolinite	1.04 ± 0.01	65	95	51.8 ± 0.9
VQ <2.0 micrometer	Illite-Smectite (~ 10%-20% I), Kaolinite	1.18 ± 0.02	54	100	48.3 ± 1.2
SD <0.25 micrometer (b)	Illite-Smectite (~ 70%-80% I), Kaolinite	4.47 ± 0.05	88	436	55.3 ± 0.8
SD 0.25-1.0 micrometer (b)	Illite-Smectite (~ 80%-90% I), Kaolinite	3.65 ± 0.04	88	362	56.2 ± 1.0
SD 1.0-2.0 micrometer (b)	Illite-Smectite (~ 80%-90% I), Kaolinite	3.37 ± 0.03	86	330	55.7 ± 0.8
BC-01 <0.25 micrometer (b)	Illite-Smectite (~ 60%-70% I), Kaolinite	3.68 ± 0.04	87	367	56.6 ± 1.0
BC-01 0.25-1.0 micrometer (b)	Illite-Smectite (~ 60%-70% I), Kaolinite	3.71 ± 0.04	89	375	57.4 ± 0.9
BC-01 1.0-2.0 micrometer (b)	Illite-Smectite (~ 60%-70% I), Kaolinite	3.75 ± 0.04	88	368	55.8 ± 0.8
BC-01 1.0-2.0 micrometer (a)	Illite-Smectite (~ 60%-70% I), Kaolinite	3.64 ± 0.04	88	365	56.9 ± 0.9
BC-05 <0.25 micrometer (b)	Illite-Smectite (~ >90% I), Kaolinite	3.78 ± 0.04	94	883	129.8 ± 1.9
BC-05 0.25-1.0 micrometer (b)	Illite-Smectite (~ >90% I), Kaolinite	3.24 ± 0.03	95	1193	200.9 ± 2.9
BC-05 1.0-2.0 micrometer (b)	Illite-Smectite (~ >90% I), Kaolinite	3.34 ± 0.03	95	1107	181.9 ± 2.6
BC-06 <0.25 micrometer (b)	Illite-Smectite (~ 70%-80% I), Kaolinite	3.34 ± 0.03	85	354	60.2 ± 0.9
BC-06 0.25-1.0 micrometer (b)	Illite-Smectite (~ 70%-80% I), Kaolinite	3.09 ± 0.03	87	340	62.3 ± 1.1
BC-06 1.0-2.0 micrometer (b)	Illite-Smectite (~ 60%-70% I), Kaolinite	2.80 ± 0.03	89	343	69.3 ± 1.2
MP-01 <0.25 micrometer (b)	Illite-Smectite (~ 70%-80% I), Kaolinite	3.79 ± 0.04	93	700	103.3 ± 1.5
MP-01 0.25-1.0 micrometer (b)	Illite-Smectite (~ 70%-80% I), Kaolinite	3.10 ± 0.03	92	783	140.2 ± 2.1
MP-01 1.0-2.0 micrometer (b)	Illite-Smectite (~ 70%-80% I), Kaolinite	2.65 ± 0.03	93	2043	397.0 ± 5.5
TMCE-01 <0.25 micrometer (b)	Illite-Smectite (~ >90% I), Kaolinite	2.51 ± 0.03	89	470	104.8 ± 1.7
TMCE-01 0.25-1.0 micrometer (b)	Illite-Smectite (~ >90% I), Kaolinite	2.55 ± 0.04	95	602	131.3 ± 2.3
TMCE-01 1.0-2.0 micrometer (b)	Illite-Smectite (~ >90% I), Kaolinite	2.44 ± 0.03	94	660	149.3 ± 2.2

(a) = Duplicate Sample

(b) = Sample potassium content was remeasured on 10/14/05. Results are shown.

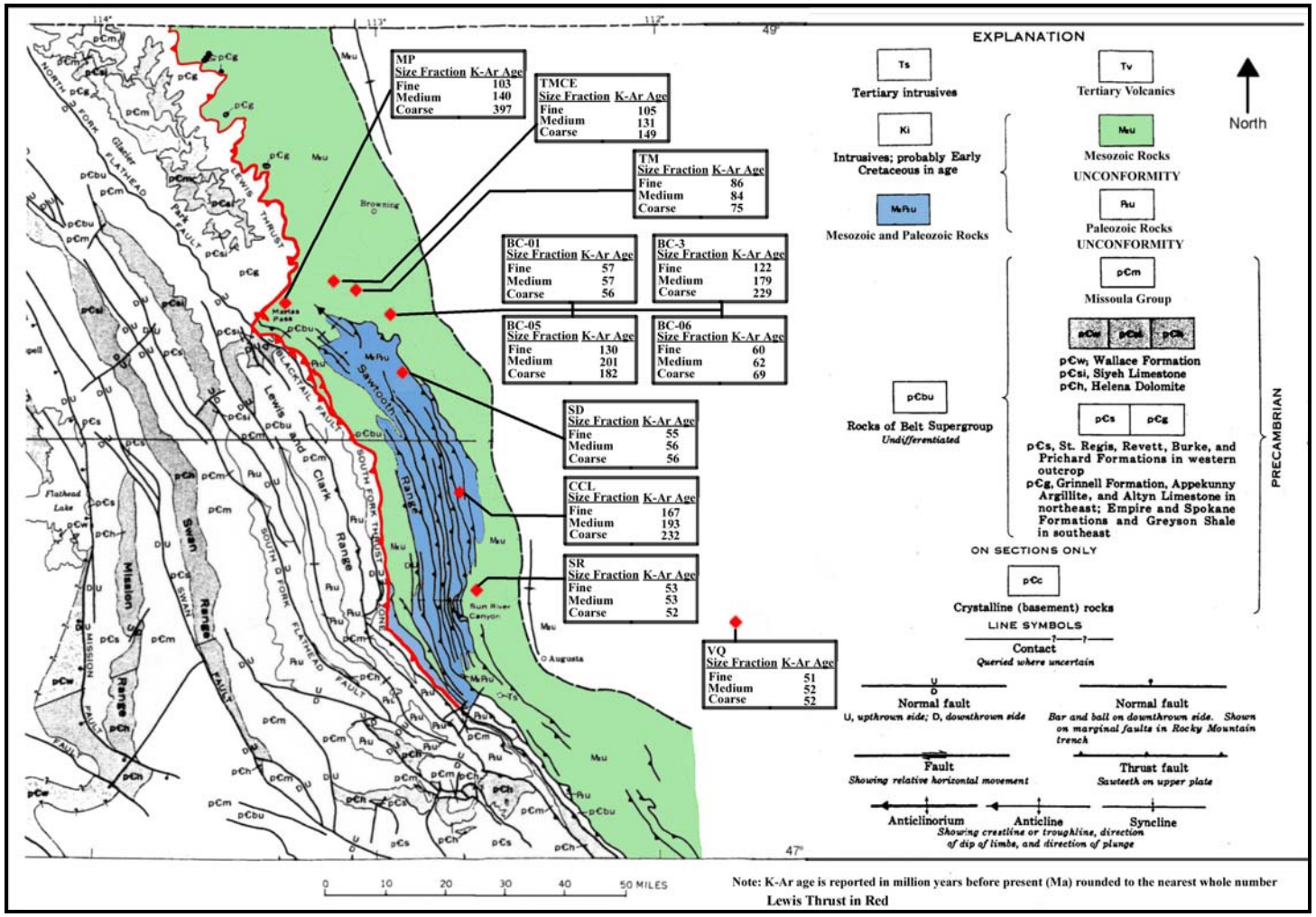

Figure 3.1: K-Ar apparent age map (base map after Mudge, 1970).

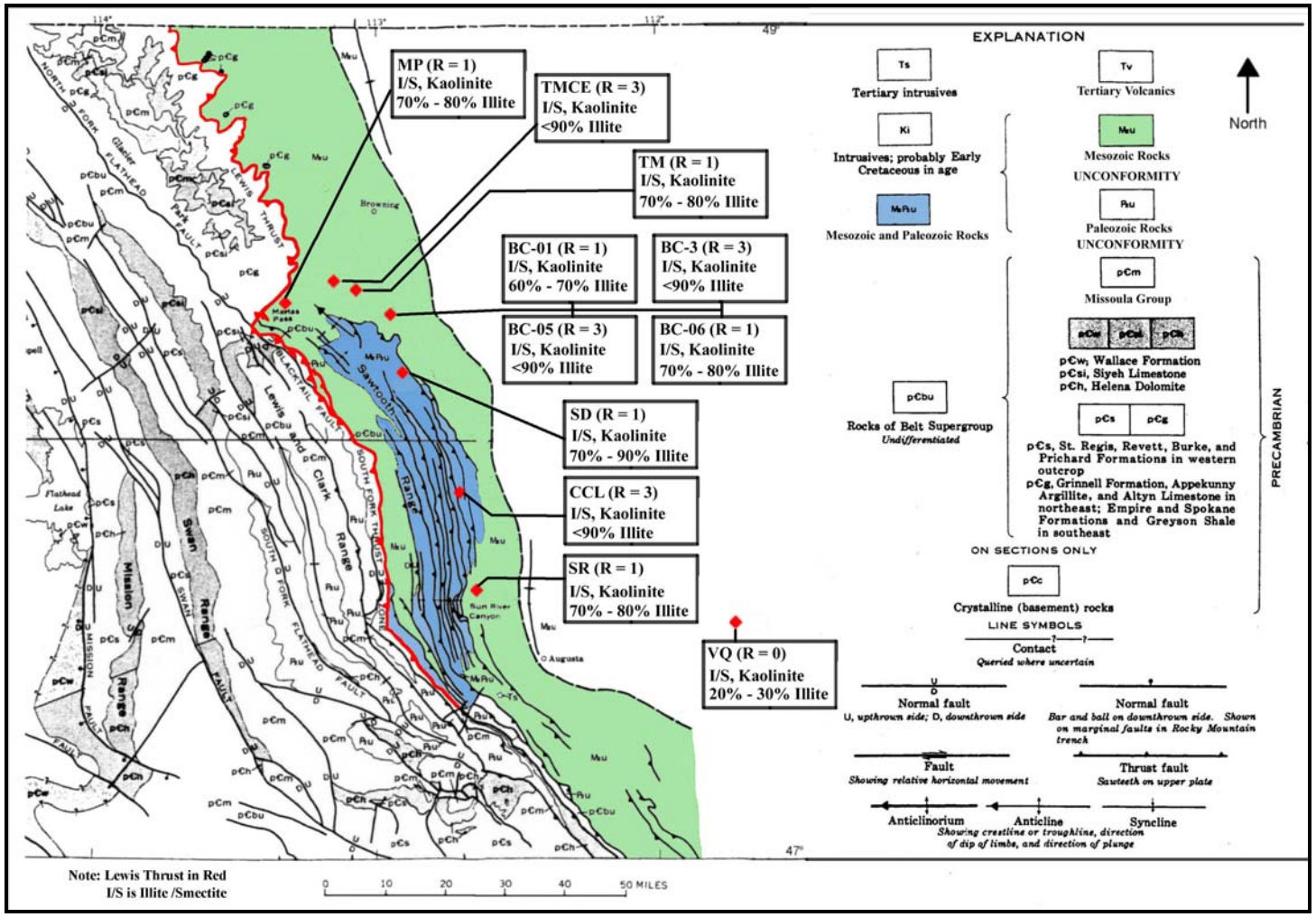

Figure 3.2: Mineralogy map (base map after Mudge, 1970).

Little or no $2M_1$ illite was observed in samples BC-05, BC-06, CCL, MP, and SD based on the absence of a 3.0 Å reflection after XRD scanning of a randomly oriented mount. The XRD pattern for a randomly oriented mount of sample BC-3 exhibits a reflection at 3.0 Å that is much larger than expected relative to the 2.58 Å peak that is common to all illite polytypes. Therefore, an unreasonable percentage of the $2M_1$ polytype is calculated as per Grathoff (1996). The 3.0 Å peak in all likelihood reflects the presence of calcite as well as the $2M_1$ illite polytype. XRD patterns used for polytype determination are attached as Appendix C.

3.2 K-Ar RESULTS

The K-Ar apparent ages of all samples, across all grain size fractions, are between 48.3 Ma and 397 Ma, with estimated errors (2σ) ranging between 1.4% and 4.8% of the apparent K-Ar age. Most samples, however, have an associated error of less than 2% of the apparent age (Table 3.1). The <2.0 μm grain size fraction of samples collected in 2004 (BC-3, SR, TM, CCL, and VQ) was analyzed for K-Ar apparent age and mineralogy, but that fraction of samples collected in 2005 was not. The apparent ages of samples VQ and SR are concordant across the coarse, medium, and fine grain size fractions. VQ has apparent ages of 50.6 Ma, 51.7 Ma, and 51.8 Ma from fine to coarse grain sizes, respectively, and the corresponding values for SR are 53.3 Ma, 53.4 Ma, and 54.1 Ma. The average apparent ages of VQ and SR are 51.4 Ma and 53.6 Ma, respectively. In both samples, the <2.0 μm grain size fraction has an apparent age slightly less than the average apparent age of the clay subfractions, 48.3 Ma and 51.9 Ma,

respectively. Samples BC-3 and CCL exhibit increasing apparent age with increasing grain size. The <2.0 grain size separates are intermediate in apparent age relative to the clay subfractions. The apparent age of sample BC-3 increased from 122 Ma in the finest grain size fraction to 179 Ma and 229 Ma in the intermediate and coarse grain size fractions, respectively, while for sample CCL the corresponding values are 167 Ma, 193 Ma, and 232 Ma. Sample TM does not exhibit a trend with respect to K-Ar apparent ages that is similar to the other samples.

The samples SD and BC-01, collected in 2005, have concordant apparent ages a little greater than those of SR and VQ. The apparent ages of sample SD, from fine to coarse grain size, are 55.3 Ma, 56.2 Ma, and 55.7 Ma, respectively. The average apparent age is 55.7 Ma. Sample BC-01 has concordant ages from fine to coarse grained of 56.6 Ma, 57.4 Ma, and 55.8 Ma, respectively and the average apparent age is 56.7 Ma. Of the three samples with concordant apparent ages and within the Disturbed Belt, the average apparent age increases from southeast to northwest along the trend of the Disturbed Belt (Figure 3.1). Samples BC-06, MP, and TMCE show increasing apparent age from fine to coarse grain size (Table 3.1). The fine fraction of sample BC-05 has an apparent age comparable to those of the fine fractions of several other samples with discordant apparent ages, but the apparent ages of the medium and coarse fractions of BC-05 are not in the usual order.

CHAPTER 4.0 - DISCUSSION

4.1 CLAY MINERALOGY AND K-AR AGES OF I/S

The clay fraction of the bentonite from the Sweetgrass Arch (VQ) contains I/S with random stacking order (R=0) with ~ 20% illite layers in I-S, while the bentonites from the Disturbed Belt contain I/S with Rectorite (R≥1) or Kalkberg (R≥3) stacking order with > 60% illite layers in I/S (Table 3.1). The observed stacking order indicates the burial temperature of the VQ bentonite in the Sweetgrass Arch was not more than 100ºC (Hoffman and Hower, 1979). Conversely, the stacking orders of I/S from bentonites collected from the Disturbed Belt indicates that these strata were buried sufficiently to produce temperatures from 100ºC to 200ºC (Hoffman and Hower, 1979). It should be noted that samples collected for this study with greater than 90% illite in I/S (e.g. CC, BC-3, BC-05, and TMCE) all have a substantial amount of detrital illite whose source is unrelated to thrust sheet burial during the Laramide orogeny. The percentages of illite in I/S and stacking order data in this study are consistent with results from earlier studies (Hoffman, 1976; Hoffman et al., 1976; Hoffman and Hower, 1979). Kaolinite in the clay fractions is considered a dilutant with respect to K-Ar analyses .

A mean age calculated from the K-Ar ages of the three subfractions from concordant K-bentonites as discussed in a following paragraph (SD, SR, and BC-01) ranged from 54

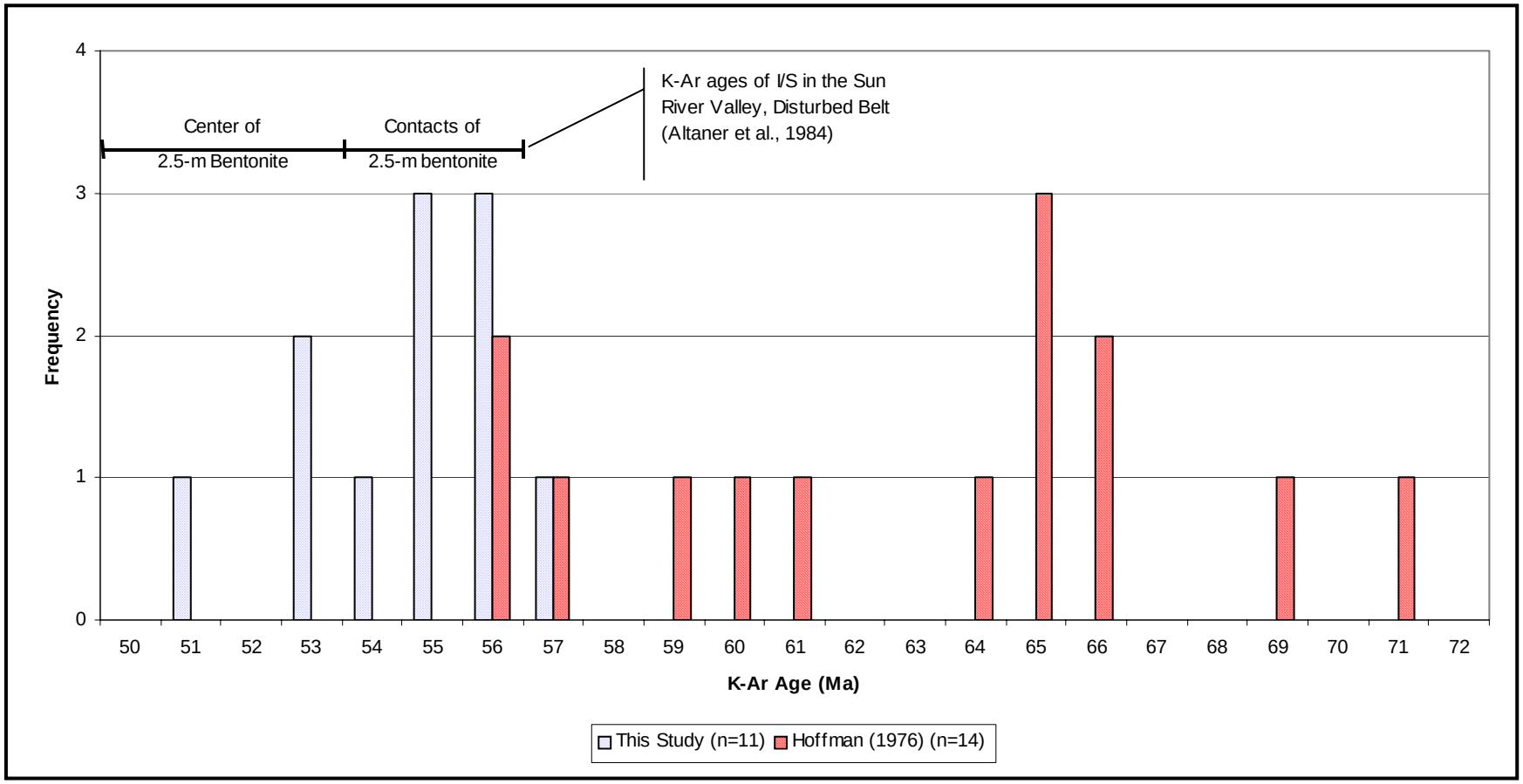

Figure 4.1: Frequency of K-Ar ages measured in the Disturbed Belt between Marias Pass and the Sun River.

Ma to 57 Ma. The range of the mean ages is virtually coincident with the lower end of the range of ages (56-72 Ma) reported by Hoffman (1976) and Hoffman et al. (1976) (Figure 4.1). However, the interpretation of the K-Ar ages of I/S measured in this study are in agreement with the interpretation of Hoffman (1976) that diagenetic I/S was formed as a result of thrust sheet burial during the Laramide Orogeny. The samples collected by Hoffman could not be found for duplicate measurements in this work. It is difficult to identify the reason(s) for the range of K-Ar ages measured by Hoffman. Altaner et al. (1984) measured a range of ages (51-56 Ma) from a thick (2.5 m) potassium bentonite in the Sun River Valley in the Disturbed Belt. Altaner (1989) argued that the range of K-Ar ages resulted from slow diffusion of potassium from the edges to the center in that thick K-bentonite. Based on the observed age pattern, they derived a diffusion-kinetic model to describe the diffusion of potassium and its reaction to form illite in thick bentonites. The K-Ar ages determined by Altaner et al. for samples from the edges of the thick bentonite ranged from 54 Ma to 56 Ma and were interpreted to correspond to the time of maximum temperature owing to the Laramide thrusting (Figure 4.1). These ages are also similar to the mean ages of the concordant K-bentonites measured in this study. The bentonites sampled in this study were thin (< 30 cm) and diffusion of potassium was not thought to be significant.

Considering all samples, the K-Ar ages of I/S collected in this study exhibited considerable range (Table 3.1). The K-Ar ages of I/S of some of the clay fractions are internally concordant (e.g., VQ, SR, SD, BC-01) while the K-Ar ages of the other bentonites are discordant to varying degrees (TM, TMCE, MP, BC-3, BC-05, BC-06, CCL). The concordant ages samples are noted to come from bentonites that are relatively

thick (>15 cm), yellowish white to white in color, and have massive clayey lithology (see figures 2.2 and 2.3). The discordant ages are noted to come from samples that in the field might be considered either bentonites or mixed bentonite-shale, and that are relatively thin (<5 cm) with a yellowish white to yellow color and brittle (see Figure 2.4).

Where concordant age values were measured, the K-Ar ages exhibit an extremely high degree of concordance relative to other some other studies (e.g., Elliott and Aronson, 1987; Elliott et al., 1991; Elliott and Haynes, 2002). Elliott et al. (1991) showed that as burial depth increases (i.e., increasing temperature), the duration of illitization decreases at the contacts of 30-cm thick bentonites collected from the Denver basin. Elliott and Matisoff (1996) showed that a significant proportion if illite in I/S formed over a relatively short (20,000-year) period due to burial at the Salton Sea Geothermal field (elevated geothermal gradient approximately 76^{o}C/km). Therefore, the concordance of the K-Ar age of I/S of the subfractions of both the Cretaceous (SR and BC-01) and Jurassic (SD) K-bentonites reflect rapid formation of diagenetic I/S formed from a short-lived event such as thrust sheet burial. As mentioned earlier, thrust sheet emplacement during the Laramide orogeny is the likely cause for the formation of diagnetic illite in I./S based on the measured K-Ar ages of I/S.

The K-Ar ages of I/S at VQ are also internally concordant. This bentonite is believed to have had a different burial history. It is located on the Sweetgrass Arch and was not buried to great depths by thrust sheets during the Laramide Orogeny. The shallow burial is also seen in this bentonite by the low percentage of illite layers in I/S (~20%). Consequently, the K-Ar ages of I/S are believed to have resulted from a more protracted illitization. It is interesting that the measured K-Ar ages are concordant in this bentonite,

but this concordance of K-Ar ages of I/S may not be related to protracted burial. Alternatively, warm fluids expelled from the Disturbed Belt during thrusting may have reached the VQ sample location or small amounts of burial occurred due to a limited amount of thrust sheet burial. These two reasons may also account for the internal concordance with respect to K-Ar age in VQ. The fluids by that time may have been cooler and reduced in potassium content as a result of illitization occurring along the flow path, which would have resulted in the low percentage of illite observed in VQ. Oliver (1992) postulated that fluids expelled into a foreland basin during orogenic events might travel hundreds of kilometers from their source. Sears (2001) suggested that material was rapidly eroded from the thrust sheet for some ten million years after the thrusting ended. This sediment may have buried the Sweetgrass Arch bentonite far enough to induce minor illitization in the early Eocene.

The mineralogy of the clay fractions showing discordant K-Ar ages was studied further to see the kinds of polytypes present in them. In particular, the clay fractions from bentonites that have discordant K-Ar apparent age values were analyzed for the percentage of $2M_1$ illite (detrital) in an attempt to model the diagenetic illite age by IAA (Pevear, 1999). XRD patterns from the polytype analyses are attached as Appendix C. The absence of the 3.0 Å reflection, one of the diagnostic reflections for the $2M_1$ polytype, shows that there is no $2M_1$ illite present in most bentonites collected in this study. The reflection at 3.0 Å was observed in the CCL (Madison Group) and BC-3 bentonites. The reflection at 3.0 Å in the BC-3 polytype analysis was determined to be very intense relative to the peak at 2.58 Å (all polytypes) per Grathoff (1996). The intense peak at 3.0 Å is likely due to an impurity (calcite). The absence of the $2M_1$ illite

polytype observed in the clay fractions with discordant K-Ar ages (MP, BC-05, and BC-06) is additional evidence that the Cretaceous rocks were not buried deeply enough to reach temperatures above 250ºC (Hoffman and Hower, 1979). Therefore, detrital illite obviously present in some of the bentontites collected in this study based on discordant ages has detrital 1M illite or possibly detrital$1M_d$ illite whose source is likely Paleozoic or early Mesozoic deposits that covered the Belt Supergroup rocks during the late Jurassic.

4.2 THRUST SHEET EMPLACEMENT

The mean age was calculated from the subfractions of each K-bentonite with concordant K-Ar ages collected from within the Disturbed Belt (BC-01, SD, and SR) as mentioned in the previous section. The average age increases from southeast to northwest (Figures 4.2 and 4.3). This observation is consistent with the mechanism of thrust sheet emplacement as proposed by Mudge and Earhart (1980) whereby the Lewis thrust rotates clockwise about a hinge point located at the west fork of the Sun River. It is also consistent with the alternative hypothesis that the Disturbed Belt was created by a west to east displacement direction without rotation. The increase in the mean ages from southeast to northwest assumes that there is a significant difference between the three samples with respect to the K-Ar apparent ages, which may or may not be valid. The validity of this assumption is difficult to test statistically without multiple samples measurements. However, the errors for the samples furthest apart (BC-01 and SR) do not

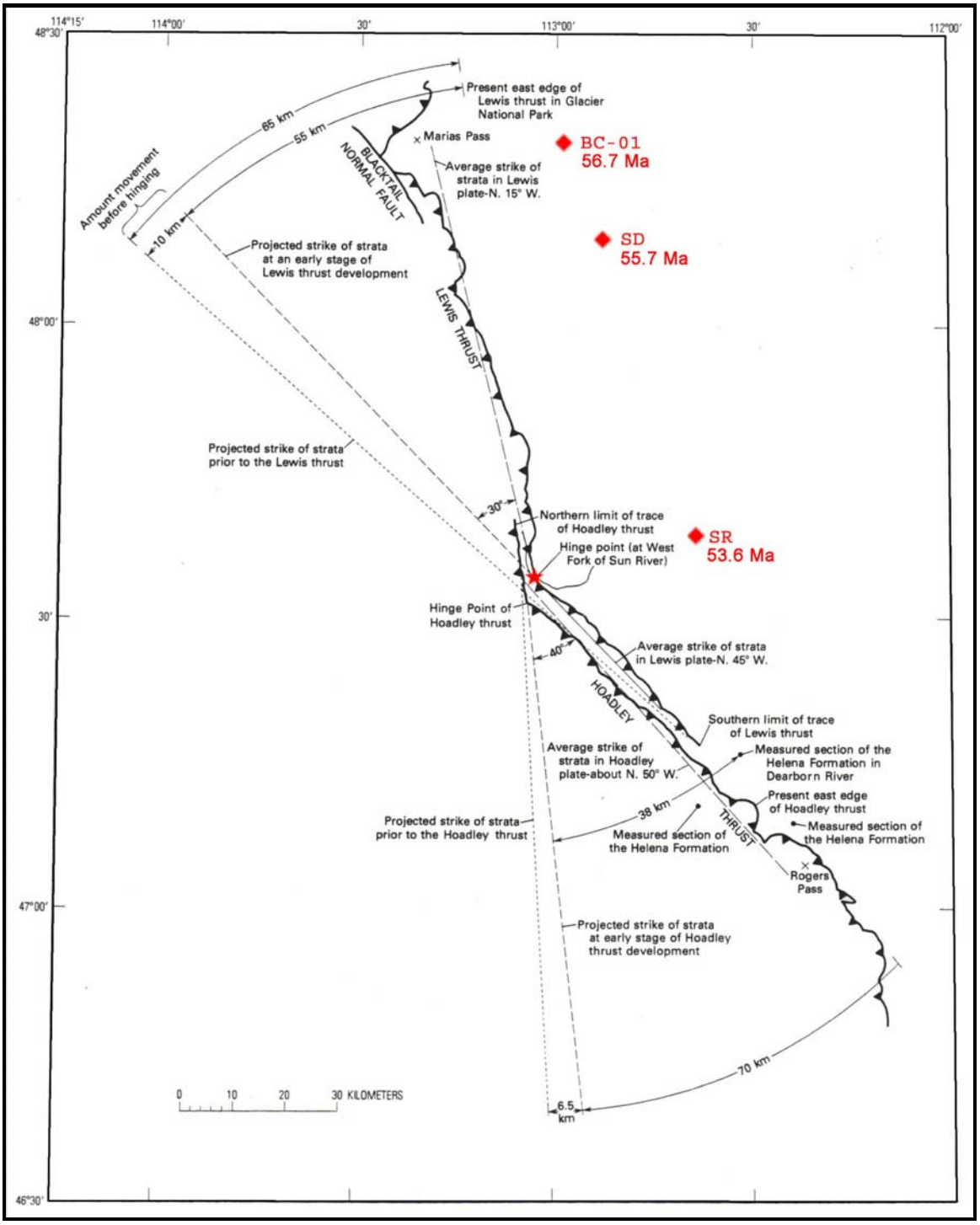

Figure 4.2: Projected displacement along the Lewis Thrust Fault (modified from Mudge, 1980).

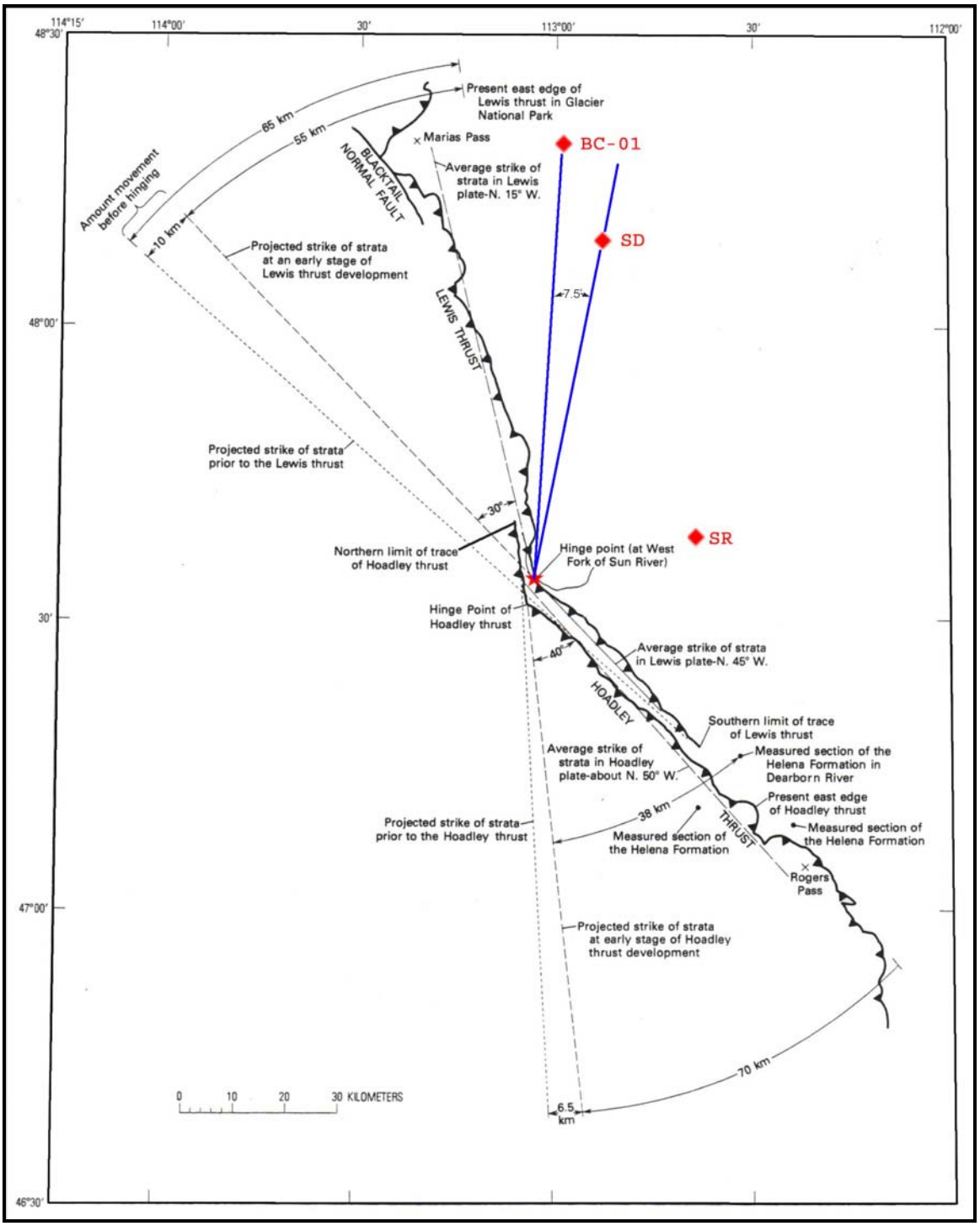

Figure 4.3: Map of the Lewis Thrust Fault depicting the angle traversed between BC-01 and SD (modified from Mudge, 1980).

overlap with the stated K-Ar apparent ages of the other sample. Furthermore, the strong concordance of K-Ar ages across the grain size fractions within each sample, as stated above, suggest a relatively short duration of diagenetic illite formation, which may support that a difference is possible. Within this context, the average of K-Ar ages of the subfractions may be useful to estimate a rate of thrust sheet emplacement.

Mudge and Earhart (1980) postulated that the Lewis Thrust Sheet rotated clockwise about a hinge point near the west fork of the Sun River (Figures 4.2 and 4.3). As a result, the horizontal displacement increases to the northwest from the hinge point. Assuming that the conditions for illitization to occur were the same (i.e., temperature, availability of K, burial depth, the horizontal displacement of a thrust sheet on top of a given bentonite) at the time illitization occurred at different places, and assuming that the front of the thrust sheet was straight from the hinge point northwestward, the sample furthest to the northwest would have experienced illitization first (greater K-Ar apparent age) because the thrust sheet would have covered that sample location first.

The arc length that the Lewis thrust sheet traveled between samples BC-01 and SD subtends an angle of approximately 7.5°. As the average age difference is 1 Ma, with an uncertainty that may be as small as 0.5 Ma, the angular velocity would have been roughly 7° per Ma with an uncertainty that may be as small as 50%. The arc length at a given distance from the hinge point is determined by

$$S = r\theta,$$

where S is the arc length, r is the radius (distance from the hinge point), and θ is the angle in radians that the arc length subtends. At a distance of approximately 84 km, the arc

length that the Lewis thrust sheet traveled in rotating 7.5° from the BC-01 sample location would have been approximately 11 km. This translates to a horizontal displacement of approximately 11 mm/yr through that 7.5° angle along the arc on which sample BC-01 is located (Table 4.1). At a distance of approximately 66 km, the arc length that the Lewis thrust sheet traveled in the same period toward the SD sample location would have been approximately 9 km. This is approximately 9 mm/year of horizontal displacement along that arc (Table 4.1). It should be noted that Sears (2001) reported that the thrust slab composed of the Lewis, Hoadley, and Eldorado thrusts

Table 4.1: Inferred rates of horizontal displacement at samples BC-01 and SD locations with rotation (Mudge and Earhart Model, 1980).

Sample ID	Angle Traveled		Radius (Km)	Arc Length (Km)	Age of I/S (Ma)	Travel Time (Ma)	Rate	
	Degrees	Radians					(Km/Ma)	(mm/yr)
BC1	7.5	0.13	84.1	11	56.7	1	11	11
SD	7.5	0.13	66.4	9	55.7	1	9	9

Radius is the straight line distance from the hinge point to the sample location
Travel time is the difference between the age of illitization of BC-01 and SD

displaced approximately 3 mm/yr at Rogers Pass (south of the sample area for this study) and 9 mm/yr at the U.S.-Canada border (north of the sample area for this study). The estimated rates presented here match well, although slightly higher than those of Sears (2001) at a larger scale.

Sample SR was not used to calculate a rate of horizontal displacement as it is almost due east from the hinge point and is unlikely the Lewis thrust sheet traveled an angle of approximately 120^{o} from the start of hinging within the approximately 16 Ma year period that the thrust sheet emplacement is estimated to occur. The younger apparent age of diagenetic illite formation at SR reflects a relatively later time of thrusting further south. As an alternative hypothesis, the conversion of ashes to potassium bentonites and the

formation of diagenetic illite in I/S may also be due to the migration of heated fluids eastward as thrusting is proceeding (Oliver 1986). In this model, heated fluids are squeezed from the pore spaces of sediments and hydrated minerals exposed to increased temperatures and pressures due to thrust sheet burial (Oliver, 1986; Oliver, 1992). The "hot" potassium rich fluids move into the foreland basin ahead of the advancing thrust sheet causing diagenetic alternation to form diagenetic I/S in these potassium bentonites. It is possible to test this hypothesis by observing the presence of saline fluid inclusions, and presence of external potassium (K/Rb) in diagenetic illite (e.g. Elliott and Haynes, 2002).

Alternative to the model proposed by Mudge, eastward displacement of the trust sheet without rotation may also account for the geographic trend of concordant bentonite samples collected within the Disturbed Belt. Given the assumptions stated above with regard to the timing of diagenetic illite formation during thrust sheet emplacement and that leading edge of the thrust slab strikes north/south BC-01 would still be the first sample to experience illitization as it is the sample that is furthest to the west. Samples SD (east of BC-01) and SR (east of SD) would follow in series as the thrust sheet progressed to the east. Table 4.2 shows the estimated rate rounded to the nearest whole number assuming eastward displacement without rotation from the BC-01 sample location to the SR sample location. The estimate of between 7 mm/yr and 9 mm/yr is slightly less than the proposed estimate stated above for the Mudge and Earhart (1980) model and match well with the estimate of displacement proposed by Sears (2001).

Table 4.2: Inferred rates of horizontal displacement (eastward displacement with no rotation).

East-West Segment	East-West Distance Between Samples (km)	Travel Time (Ma)	Rate (mm/yr)
BC-01 to SD	7	1	7
SD to SR	18	2.1	9
BC-01 to SR	25	3.1	8

CHAPTER 5.0 – CONCLUSIONS

The following conclusions are derived from the results of this study:

1. Potassium bentonites collected from within the Disturbed Belt have a high percentage of illite layers that exhibit Rectorite and Kalkberg stacking orders of illite layers in I/S that agrees with previous I/S work conducted in the Disturbed Belt (Hoffman, 1976). The stacking orders and the absences of the $2M_1$ illite polytype in the bentonitic shale (e.g. BC-3, BC-05, BC-06, MP) and bentonite at SD) indicate that the maximum burial temperature did not exceed 250^{o}C and the source of the detrital minerals is further west in the Western Interior Basin as opposed to the nearby Belt Supergroup.
2. Samples BC-01, SD, and SR have concordant K-Ar apparent ages across the coarse, medium, and fine clay size fractions. The average apparent age of these samples is 56.7 Ma, 55.7 Ma, and 53.6 Ma, respectively. The concordance of K-Ar ages from bentonites of Jurassic and Cretaceous ages further supports the previous argument (Hoffman, 1976) that diagenetic illite formed as a result of thrust sheet burial during the Laramide Orogeny.
3. The clay fractions having concordant K-Ar ages of I/S were separated from bentonites that were thick (>2 cm), light yellow-white or white, and had massive spongy/clayey appearance. Discordant K-Ar ages were collected from thinner (< 2 cm) yellow-white clayey bentonites or bentonitic shales. These thinner beds were more brittle.

4. The mean of the concordant K-Ar ages of diagenetic I/S from samples BC-01, SD, and SR increase from southeast to northwest along strike of the Disturbed Belt. This northwestward increase in the mean K-Ar ages of I/S is consistent with a model of thrust sheet emplacement proposed for the Disturbed Belt by Mudge (1980) whereby the increase of K-Ar ages of I/S from concordant samples SR to SD and BC-01 records the clockwise rotation of the Lewis Thrust relative to the hinge point near Sun River during its eastward emplacement. More data is needed to test this idea.
5. A rate of thrusting at a distance between 66 km and 84 km from the hinge point is estimated between 9 and 11 mm/yr, respectively along the arc length subtending the angle between BC-01 and SD (Figure 4.3).
6. Employing a west-east thrust model, the rates of thrusting derived are 7-9 mm/yr, and more data are needed to evaluate this conclusion.

5.1 FUTURE DIRECTIONS

The clay mineralogy and K-Ar ages determined from this study will be combined with paleomagnetic data to investigate the hypothesis that chemical remanent magnetization (collaboration with University of Oklahoma) is related to the formation of diagenetic illite. The estimation of thrust sheet emplacement rate should be investigated more rigorously as well as the question of "hot" potassium enriched fluids expelled by thrusting into the foreland basin and onto the Sweetgrass Arch. This may be done by sampling K- bentonites (concordant type) along transects between BC-01 and SR, BC-01

and VQ, and SR and VQ, if possible. In addition, more sampling of the concordant type bentonites should be conducted in other areas of the Disturbed Belt and areas east on the Sweetgrass Arch, thought to be outside the Disturbed Belt. Furthermore, measurement of the rubidium (Rb) for calculation of K/Rb ratios and comparison of these ratios to a crustal average may provide a test that warm potassium enriched fluids helped form diagenetic illite in sample VQ (or other areas on the Sweetgrass Arch), whose fine, medium, and coarse grain size fractions have a K-Ar concordant age that is slightly younger than the concordant samples collected from within the Disturbed Belt.

REFERENCES

Ahn, J.H. and Peacor, D.R.(1986) Transmission and Analytical Electron Microscopy of the Smectite to Illite Transition. Clays and Clay Minerals, v. 34, no. 2, p. 165-179.

Altaner, S.P., Hower, J., Whitney, G., and Aronson, J.L. (1984) Model for K-Bentonite Formation: Evidence from Zoned K-Bentonites in the disturbed Belt, Montana. Geology, v. 12, p. 412-415.

Altaner, S.P. (1986) Comparison of Rates of Smectite Illitization with Rates of K-Feldspar Dissolution. Clays and Clay Minerals, v. 34, no. 5, p. 608-611.

Altaner, S.P. (1989) Calculation of K Diffusional Rates in Bentonite Beds. Geochemica et Cosmochimica Acta, v. 53, p. 923-931.

Altaner, S.P. and Ylagan, R.F. (1997) Comparison of Structural Models of Mixed-Layer Illite/Smectite and Reaction Mechanisms of Smectite Illitization. Clays and Clay Minerals, v. 45, p. 517-533.

Basu, A. (2004) A Comparison of K-Ar Ages of Illite to the Age of Chemical Remnant Magnetization. M.S. Thesis, Department of Geology, Georgia State University.

Brindley, G.W. and Brown, G. (1980) Crystal Structures of Clay Minerals and their X-Ray Identification. Mineralogical Society, London, England.

Boles, J.R. and Franks, S.G. (1979) Clay Diagenesis in Wilcox Sandstones of Southwest Texas: Implications of Smectite Diagenesis on Sandstone Cementation. Journal of Sedimentary Petrology, v. 49, no. 1, p. 55-70.

Butler, R.F. (1992) Paleomagnetism, Magnetic Domains to Geologic Terranes. Blackwell Scientific Publications, Boston, MA.

Dalrymple, G.B. and Lanphere, M.A. (1969) Potassium-Argon Dating, Principles, Techniques, and Applications to Geochronology. W.H. Freeman and Company, San Fransisco, CA.

Elliott, W.C., Aronson, J.L., Matisoff, G., and Gautier, D.L. (1991) Kinetics of the Smectite to Illite Transformation in the Denver Basin: Clay Mineral, K-Ar Data, and Mathematical Model Results. The American Association of Petroleum Geologists Bulletin, v. 75, no. 4, p. 436-462.

Elliott, W.C. and Matisoff, G. (1996) Evaluation of Kinetic Models for the Smectite to Illite Transformation. Clays and Clay Minerals, v. 44, no. 1, p. 77-87.

Elliott, W.C., Edenfield, A.M., Wampler, J.M., Matisoff, G., and Long, P.E. (1999) The Kinetics of the Smectite to Illite Transformation in Cretaceous Bentonites, Cerro Negro, New Mexico. Clays and Clay Minerals, Volume 47, No. 3, p. 286-296.

Elliott, W.C. and Haynes, J. (2002) The Chemical Character of Fluids Forming Diagenetic Illite in the Southern Appalachian Basin. American Mineralogist, v. 87, p. 1519-1527.

Elliott, W. C., Osborn, S.G., O'Brien, V.J., Elmore, R.D., Engel, M.H., and Wampler, J.M. (In Press) On the Timing and Causes of Illite Formation and Remagnetization in the Cretaceous Marias River Shale, Disturbed Belt, Montana. Journal of Geochemical Exploration.

Gill, J.D., Elmore, R.D., and Engel, M.H. (2002) Chemical Remagnetization and Clay Diagenesis: Testing the Hypothesis in the Cretaceous Sedimentary Rocks of Northwestern Montana. Physics and Chemistry of Earth, v. 27, p. 1131-1139.

Grathoff, G.H. (1996) Illite in the Lower Paleozoic of the Illinois Basin: Origin, Age, and Polytype Quantification. Doctoral Dissertation, Department of Geology, University of Illinois at Urbana-Champaign.

Hassanipak, A.A. and Wampler, J.M. (1996) Radiogenic Argon Released by Stepwise Heating of Glauconite and Illite: The Influence of Composition and Particle Size. Clays and Clay Minerals, v. 44, p. 717-726.

Hoffman, J. (1976) Regional Metamorphism and K-Ar Dating of Clay Minerals in Cretaceous Sediments of the Disturbed Belt of Montana. Doctoral Dissertation, Department of Geology, Case Western Reserve University.

Hoffman, J., Hower, J., and Aronson, J.L. (1976) Radiometric Dating of Time of Thrusting in the Disturbed Belt of Montana. Geology, v. 4, p. 16-20.

Hoffman, J. and Hower, J. (1979) Clay Mineral Assemblages as Low Grade Metamorphic Geothermometers: Application to the Thrust Faulted Disturbed Belt of Montana, U.S.A.. Society of Economic Paleontologists and Mineralogists, Special Publication no. 26, p. 55-79.

Hower, J.F. (1981) X-ray Diffraction Identification of Mixed-Layered Clay Minerals, In:F.J. Longstaffe (Ed.). Clays and the Resource Geologist, Mineralogical Society of Canada Short Course 7, p. 39-59.

Hower, J. and Mowatt, T.C. (1966) The Mineralogy of Illites and Mixed-Layer Illite/Montmorillinites. The American Mineralogist, v. 51, p. 825-850.

Hower, J., Eslinger, E.V., Hower, M., and Perry, E.A. (1976) Mechanism of Burial Metamorphism of Argillaceous Sediment: 1. Mineralogical and Chemical Evidence. Geological Society of America Bulletin, v. 87, p. 725-737.

Hower, J. and Aronson, J.L. (1976) Mechanism of Burial Metamorphism of Argillaceous Sediment: 2. Radiogenic Argon Evidence. Geological Society of America Bulletin, v. 87, p 738-74.

Jackson, M.L. (1979) Soil Chemical Analysis-Advanced Course, A Manual of Methods Useful for Instruction and Research in Soil Chemistry, Physical Chemistry of Soils, Soil Fertility, and Soil Genesis. Second Edition, Revised from original edition of 1956, Published by the Author.

Katz, B., Elmore, D.R., Cogoini, M; Engel, M.H., and Ferry, S (2000) Associations between Burial Diagenesis of Smectite, Chemical Remagnetization, and Magnetite Authigenesis in the Volcontian Trough, SE France. Journal of Geophysical Research, v. 105, no. B1, p. 851-868.

McCabe, C. and Elmore, R.D., 1989, The Occurrence and Origin of Late Paleozoic Remagnetization in the Sedimentary Rocks of North America, Reviews of Geophysics volume 27, no. 4, p. 471-494.

Moe, J.A., Ryan, P.C., Elliott, W.C., and Reynolds, R.C. Jr. (1996) Chemistry, and Clay Mineralogy of a K-Bentonite in the Proterozoic Belt Supergroup of Western Montana. Journal of Sedimentary Research, v. 66, no. 1, p. 95-99.

Moore, D.M. and Reynolds, R.C. Jr. (1997) X-ray Diffraction and the Identification and Analysis of Clay Minerals. Oxford University Press, Inc.; New York, New York.

Morton, J.P. (1985) Rb-Sr Evidence for punctuated Illite/Smectite Diagenesis in the Oligocene Frio Formation, Texas Gulf Coast. Geological Society of America Bulletin, v. 96, p. 114-122.

Mudge, M.R. (1970) Origin of the Disturbed Belt in Northwestern Montana. Geological Society of America bulletin, v. 81, p. 377-392.

Mudge, M.R. (1977) General Geology of Glacier National Park and Adjacent Areas, Montana. Bulletin of Canadian Petroleum Geology, v. 25, no. 4, p. 736-751.

Mudge, M.R. and Earhart, R.L. (1980) The Lewis Thrust Fault and Related Structures in the Disturbed Belt, Northwestern Montana. Geological Survey Professional Paper 1174, U.S. Department of the Interior, U.S. Government Printing Office.

Mudge, M.R. and Earhart, R.L. (1983) Bedrock Geologic Map of the Northern Disturbed Belt, Lewis and Clark, Teton, Pondera, Glacier, Flathead, Cascade, and Powell Counties, Montana. U.S. Geological Survey Miscellaneous Investigations Series Map I-1375, scale 1:125,000.

Mudge, M.R. and Earhart, R.L. (1991) Bedrock Geological Map of Part of the Disturbed Belt South and East of Glacier National Park, Montana, U.S. Geological Survey Miscellaneous Investigations Series Map I-2130, scale 1:48,000.

Nadeau, P.H., Wilson, M.J., McHardy, W.J., and Tait, J.M. (1984) Interstratified Clays as Fundamental Particles. Science, New Series, v. 225, no. 4665, p. 823-925.

Nadeau, P.H. and Bain, D.C. (1986) Composition of Some Smectites and Diagenetic Illitic Clays and Implications for their Origin. Clays and Clay Minerals, v. 34, no. 4, p. 455-464.

Odin, G.S. (1982) *Numerical Dating in Stratigraphy*. John Wiley & Sons, New York, 1040 pp.

Odin, G.S. and 35 collaborators (1982) Interlaboratory standards for dating purposes. Pp. 123-150 in: *Numerical Dating in Stratigraphy* (G.S. Odin, editor). John Wiley & Sons, New York, 1040 pp.

Oliver, J. (1986) Fluids Expelled Tectonically from Orogenic Belts: Their Role In Hydrocarbon Migration and Other Geologic Phenomena. Geology, v. 14, p. 99-102.

Oliver, J. (1992) The Spots and Stains of Plate Tectonics. Earth-Science Reviews, v. 32, p. 77-106.

Pevear, D.R. (1999) Illite and Hydrocarbon Exploration. Proceedings of the National Academy of Sciences, v. 96, p. 3440-3446.

Rice, D.D. and Cobban, W.A. (1977) Cretaceous Stratigraphy of the Glacier National Park Area, Northwest Montana, Cordilleran Geology of Southern Alberta and Adjacent Areas. Canadian Society of Petroleum Geologists, v 25, no. 4, p. 828-841.

Sears, J.W. (2001) Emplacement and Denudation History of the Lewis-Eldorado-Hoadley Thrust Slab in the Northern Montana Cordillera, USA: Implications for Steady-State Orogenic Processes. American Journal of Science, v. 301, p. 359-373.

Środoń, J. (1999) Extracting K-Ar Ages From Shales: A Theoretical Test. Clay Minerals, v. 33, p. 375-378.

Środoń, J. (2000) Reply to Discussion of "Extracting K-Ar Ages from Shales: A Theoretical Test". Clay Minerals, v. 35, p. 605-608.

Velde, B., Suzuki, T., and Nicot, E. (1986) Pressure-Temperature-Composition of Illite/Smectite Mixed Layer Minerals: Niger Delta Mudstones and Other Examples. Clays and Clay Minerals, v. 34, no. 4, p. 435-441.

Velde, B. and Lanson, B. (1993) Comparison of I/S Transformation and Maturity of Organic Matter at Elevated Temperatures. Clays and Clay Minerals, v. 41, no. 2, p. 178-183.

Weaver, C.E. and Wampler, J.M. (1970) K, Ar, Illite Burial. Geological Society of America Bulletin, v. 81, p. 3423-3430.

Woods, S.D., Elmore, R.D. and Engel, M.H. (2002) Paleomagnetic dating of the smectite-to-illite conversion: Testing the hypothesis in Jurassic sedimentary rocks, Skye, Scotland. *Journal of Geophysical Research*, 107, B5, 10.1029/2000JB000053

Ylagan, R.F., Pevear, D.R., and Vrolijk, P.J. (2000) Discussion of "Extracting K-Ar Ages From Shales: A Theoretical Test". Clay Minerals, v. 35, p. 599-604.

APPENDIX A: K-AR METHOD (J. MARION WAMPLER, 2005)

WEIGHING

Containers

1. Select or prepare a copper-foil capsule for each sample to be analyzed for argon isotopes.	*No special precautions are needed to avoid contamination in handling the copper capsules, but they must be kept free of extraneous rock or soil dust that would contain radiogenic argon.*
2. Place the set of capsules in a holder so that each capsule can be distinguished from the others by its position within the holder.	*It is not convenient to label the capsules, but it is convenient to associate each capsule with an identified position in the sample holder. The identifying letters and/or numbers may be used in forming the "serial sample numbers" needed to distinguish the weighed samples from one another (and from members of all other sets of weighed samples).*
3. Select a clean FEP container for each sample to be used for potassium determination.	*Containers should have been washed in detergent solution, then rinsed well with tap water, and then finally rinsed with de-ionized or distilled water. The containers should not be dry, so that static electric charges may be avoided.*
4. Label each FEP container so that it can be distinguished from the others in the set.	*It is convenient to use for each FEP container the identifier (letter, number, or combination) associated with the corresponding copper capsule.*

Weighing

5. Set an appropriate balance to zero.	*Taring cannot be used in this procedure. All mass values must be relative to a zero setting obtained with nothing on the balance pan. Frequent re-zeroing is good practice.*
6. Weigh an empty copper capsule. Record the mass as that of the "Empty capsule."	*It is good practice to check each mass value after it has been written down. It will not be possible to check any mass value after the analyst has gone on to the next step of the weighing procedure.*
7. Put in the capsule an amount of material appropriate for determining the potassium content of the material.	*It is essential that what is put in the capsule be an unbiased sample of the larger sample of material whose argon isotope and potassium contents are to be determined. For well-mixed clay, the amount weighed should be between 5 and 10 mg. More material may be needed to obtain an unbiased sample of coarser material.*
8. Weigh the capsule and its contents. Record the mass as that of the "Capsule plus K sample."	*In the end, the copper capsule will hold the sample for argon isotope determination, but here the same capsule is used temporarily for weighing the sample to be used for potassium determination.*
9. Holding the capsule with special self-closing forceps, empty the contents of the capsule into the appropriate FEP container.	*Be careful that static charge on the FEP container doesn't cause loss of fine particles during transfer. It isn't necessary that all of the material go into the FEP container. Any material that may cling to the inside of the copper capsule will become part of the sample for argon isotope determination.*
10. Weigh the capsule. Record the mass as	*This mass value will be greater than the originally*

that of the "Capsule (without K sample)."	*determined mass of the empty capsule if any particles remained inside the capsule after the transfer.*
11. Put in the capsule an amount of the sample appropriate for the argon isotope determination.	*It is essential that what is put in the capsule be an unbiased sample of the larger sample of material on which argon isotopes and potassium are to be determined.*
12. Weigh the capsule and its contents. Record the mass as that of the "Capsule plus Ar sample."	*This sample includes any material that remained in the capsule when the sample for potassium determination was transferred to FEP. Such material has become part of the sample for argon isotope determination.*
13. Close the capsule by flattening the open end and folding it over. Then crumple the capsule, with care to avoid loss of material, as necessary to reduce its size.	*No part of the closed capsule should be more than ¼ inch across.*
14. Reweigh the capsule.	*This is to be sure no material was lost when the capsule was crumpled (or to account for any that was lost).*

Repeat Steps 5 through 14 for each sample of material on which argon isotopes and potassium are to be determined.

Drying and re-weighing

15. Dry the set of samples for argon determination, each sample within its capsule and identified by the position of the capsule within the holder.	*The recommended method of drying is by vacuum, overnight. If time is short, a few hours in vacuum is usually sufficient.*
16. Re-weigh each capsule and its contents, so the mass fraction of water that had been adsorbed by the sample may be determined. Record the mass as that of the "dry Ar sample plus container."	*Re-weighing should be done soon after the drying operation has been terminated. Re-hydration may be significant if a capsule stands in normal air for more than a short time.* *The dry masses of both samples may be calculated from the recorded data.*

Approved by _____ *on* _____

DAILY STARTUP

1. Turn on chart recorder as follows: a. Put pen in place. b. Turn chart drive on (0.5 cm/min). c. Record date, time, analyst (initials), and chart speed.	*Use the chart to keep a written record of subsequent activity. If you are careful to record all changes in chart speed (preferably along the left side of the chart) the chart will be a useful time record of your work.*
2. Read and record the pressure shown by the Hastings gauge.	*This is the pressure in the "rough pump" line. It should be less than 75 millitorr.*
3. Read and record the water flow rate, and check that the diffusion pump is running.	*The water flow rate should be at least 2 GPH. Normally, the diffusion pump works adequately on the low power setting.*
4. Put liquid nitrogen on the trap DT-1.	*Any water in the small Dewar flask should be removed before the liquid nitrogen is put in it.*
5. Check that the valves T2, T4, and V1 are closed and that valve R1 is open.	*Valve R1 is sufficiently open when its knob has been turned counterclockwise a few turns. It should not be opened fully.*
6. Put liquid nitrogen on the trap DT-2.	*Any water in the small Dewar flask should be removed before the liquid nitrogen is put in it.*
7. Turn on the mass spectrometer as follows: a. Release the zero check button of the electrometer and set to the 10×10^{-11} A range. b. Check that the mass selector on the MS-10 is set to the $m/e = 40$ position. c. On the MS-10 control panel, turn the mains switch on. (The filament switch is always on.) d. Adjust the mass selector as necessary to the top of the $m/e = 40$ peak.	*The position where m/e=40 is near but not necessarily at the "Red 40" marker.* *A signal should appear in less than one-half minute. Argon invariably accumulates in the mass spectrometer overnight.*
8. Open valve D2.	*The driver should be turned counterclockwise three turns.*
9. Open valve T3.	*The signal at m/e = 40 should decrease.*
10. Turn power on to the titanium heaters (TF-1 and TF-2).	
11. Open the valves D1 (if closed) and T0 (if closed).	*It is good practice to note the response of the Hastings gauge and of the mass spectrometer to the opening of each of these valves. Turn off the mass spectrometer if there is a substantial response by the Hastings gauge to the opening of any of these valves.*
12. Open valve T1.	

13. Open any other valve appropriate for the work at hand.	*For example, valve F1 should be opened at this point (if it is not already open) if the fusion system is to be used for argon extraction. The operator must be mindful of situations that might let too much gas into the mass spectrometer. As before, watch the Hastings gauge.*
14. Check that valves S2 and A2 are closed.	*Do not open any of these valves in the process of checking that they are closed (fully turned clockwise).*
15. Open valve S0. Then open, as appropriate for the intended work, valves A1 and/or S1.	*It is good practice to note the response of the Hastings gauge and of the mass spectrometer to the opening of each of these valves.*

DAILY SHUTDOWN

1. Turn off the mass spectrometer as follows: a. On the MS-10 control panel, turn the mains switch off. b. Depress the zero check button of the electrometer.	*The shutdown procedures have been written for the typical situation in which a day's work ends with the completion of the isotopic analysis of a sample of argon in the mass spectrometer.*
2. See that valve T2 is closed. Close valve T3. Close valve D2 if it is not already closed. (Valve T4 is normally kept closed.)	*It is not necessary that the last argon sample be pumped out of the mass spectrometer before shutdown. There will be plenty of time for that on the next day.*
3. Close any of the valves A1 and S1 that may be open. Then close valve S0.	*Having these valves closed during periods of inactivity is important to the integrity of the reference gases.*
4. If valve T1 is open, close it.	
5. Turn off the recorder chart drive and remove the pen from its holder.	*The operator may choose to remove the chart paper having the record of the day's work, or not.* *Do not turn off power to the chart recorder.*
6. See that there is sufficient coolant on the cold traps below the table to last overnight.	*The large Dewar flask below the table should be at least half full of dry ice or liquid nitrogen.*

Approved by J. M. Wampler *on* 3/10/2005

DISSOLUTION OF SILICATE SAMPLES FOR POTASSIUM DETERMINATION

1. Pour into a clean fluorocarbon beaker enough of an acid mixture for digestion of all of the samples in the set to be analyzed for potassium.	*The solution to be used in most cases is a 10:1(molar ratio) mixture of concentrated HF and concentrated $HClO_4$. For samples containing organic matter, a mixture that contains these two acids and some HNO_3 as well may be used.*
2. Use a disposable squeeze pipette to add 0.5 ml of the acid mixture to each sample in its FEP container.	*If the mass of a sample is more than about 50 mg, use 1 ml of the acid mixture for each 100 mg of the sample.*
3. Close the FEP containers and heat them gently (not more than 100°C) until the material has been digested.	*An overnight period is sufficient for almost any ordinary silicate material to be completely digested. In some samples there may be minor amounts of certain accessory minerals that will not dissolve.*
4. In a fume hood, open the FEP containers and increase the heat to the open containers to drive off SiF_4 and remaining HF.	***Caution—concentrated HF solution condensed on the inside of the lids poses a hazard for skin and laboratory surfaces.***
5. Continue heating each container until fumes of perchloric acid appear.	*If HNO_3 was in the original acid mixture, it will evaporate before the perchloric acid fumes appear. In the process it should oxidize at least some of the organic matter present.* *Heating may continue until the residue is largely solid perchlorate salts of metallic elements. These salts are readily soluble.*
6. Take the residual material into solution by partially filling each container with a cesium-bearing diluting solution.	*The cesium-bearing diluting solution will be used for dissolving and diluting the digested samples and for preparing the reference solutions used in potassium determination.* *It is best to warm the containers gently after the diluting solution has been added. This helps the residue dissolve completely and allows an easy transfer of the solution in the next step.*
7. Transfer each solution to a pre-weighed and appropriately labeled polyethylene bottle. Rinse the FEP container at least once with the diluting solution, adding the rinse to the polyethylene bottle.	*The empty bottle is to have been weighed with its cap on, for the cap will be on the bottle when it is later weighed with solution inside it.* *One rinse is sufficient when the inner surface of the FEP container is clean enough that it is not wetted by the solution. Otherwise, rinse several times.*
8. Use the diluting solution to bring the material in each polyethylene bottle to an appropriate volume. Cap the bottle, shake it to homogenize the contents, and weigh the bottle and its contents.	*In most cases, the appropriate volume will be that of a nearly full bottle. In cases where the amount of potassium is expected to be much less than normal (a blank run, for example), a volume smaller than that of a full bottle would be appropriate.*

Approved by _____ *on* _____

ARGON EXTRACTION BY SAMPLE FUSION, ARGON CLEANUP, AND ARGON ISOTOPE MEASUREMENT BY STABLE ISOTOPE DILUTION AND MASS SPECTROMETRY

Setup Check ***This list is to be checked before the first sample is run, not thereafter.***	*This is a checklist for seeing that the extraction line and mass spectrometer are set up for argon extraction by fusion of samples and argon measurement by isotope dilution and mass spectrometry.*
1. Liquid nitrogen on traps DT-1 and DT-2.	
2. Valves R1, D1, D2, T0, T1, T3, F1, S0, and S1 open.	
3. Valves V1, C1, F2, T2, T4, A1, S2, and S3 closed.	*Certain other valves, in particular A2 and S4, will also be closed, but their status does not need to be checked.*
4. Titanium heaters TF-1 and TF-2 hot.	*The titanium heaters should have been hot for at least 20 minutes before proceeding. This is to ensure that they have been well degassed.*
5. Mass spectrometer on and set to $m/e = 40$.	*The signal at $m/e = 40$ should be low on the 0.1×10^{-11} A range, as it will be if the system is well degassed and there are no leaks.*
Argon Extraction and Cleanup	
1. Put liquid nitrogen in the cold finger of trap MT-1.	*When the liquid nitrogen is stable, the cold finger should be about one-third filled.*
2. Put liquid nitrogen around MT-1.	*The levels of liquid nitrogen in the cold finger and in the outer Dewar flask should be about the same.*
3. Prepare the spike by closing S1 and then opening S2.	*The underlining is to emphasize the importance of not having both S1 and S2 open at the same time.*
4. Close valve T0.	*This important step isolates the extraction line from the diffusion pump. The "Mass Spectrometer Setup" below may begin at any time after T0 has been closed.*
5. Drop the sample into the furnace.	*Be careful that the "sample pusher" doesn't fall into the furnace.*
6. Turn on power to the furnace.	*This is done by raising the variable transformer setting to 25. A magnet may be used to check that current is flowing.*
7. Release the spike by closing S2 and then opening S1.	*The underlining is to emphasize the importance of not having both S1 and S2 open at the same time. Record the spike number on the chart.*
8. Turn the fan on.	
9. At intervals of one minute or longer, raise the power to the furnace in steps of five units on the variable transformer.	*It is good practice to observe the interior of the furnace after each increase in power. It is useful to see when the capsule melts and to observe the behavior of the sample as it melts.*

10. After the sample has melted, set the variable transformer to the maximum power to be used and hold at that setting for at least three minutes.	*The maximum transformer setting is currently 50. The maximum power may be held for up to ten minutes, but three minutes is sufficient for most samples.*
11. Turn off power to the furnace.	*This is done by turning the variable transformer to zero.*
12. Turn the fan off.	
13. Wait one minute and then turn off power to the titanium heater TF-1.	
14. Wait another minute and then put liquid nitrogen in the cold finger of trap MT-2. Adjust the height of the liquid nitrogen to between 1 and 2 cm.	*Rapid boiling of the nitrogen should cease after a short time.* ***Continual rapid boiling indicates an unusually high gas pressure.***
15. Wait another minute and then put liquid nitrogen on the charcoal, CC-1.	*Make sure the liquid nitrogen level is above the glass wool above the charcoal.*
16. Wait another minute and then move the Dewar flask of liquid nitrogen that is on MT-1 to MT-2.	*Wash the outside of MT-1 with ethanol in order to see the ice ring(s) from the volatiles condensed on the cold finger.*
17. Remove any liquid nitrogen that is in the cold finger of MT-1.	*Use a large Teflon stirring rod to heat the liquid nitrogen so that it evaporates.*
18. Wait two minutes and then close valve T1.	*The wait allows ices to evaporate from the cold finger of MT-1, releasing any argon that may have been trapped in them. It also allows enough time for nearly all of the argon to be adsorbed by the charcoal.*
19. Remove the liquid nitrogen from CC-1.	*Be very careful not to break the glass.*
Extraction Line Setup, Part 1 ***This part of the extraction line setup may be postponed until after valve D2 has been closed to start "Argon Transfer" (below).***	*The extraction line setup may not be started if "Mass Spectrometer Setup" is in progress.*
1. Check that liquid nitrogen is on DT-1.	
2. Open valve T0.	*A small transient pulse of argon should be observed (if D2 and T3 are open). The pulse provides a crude measure of the argon from the sample that was <u>not</u> adsorbed on the charcoal.*
3. Remove the Dewar of liquid nitrogen from MT-2.	*Wash the outside of the trap with ethanol in order to see the ice ring(s) from the volatiles condensed on the cold finger.*
4. Remove the remaining liquid nitrogen from the MT-2 cold finger.	*Any pulse of argon seen (if D2 and T3 are open) as the cold finger warms represents argon that was trapped in ice. Wait for such a pulse to go away before proceeding.*

Argon Transfer	**Alternative Argon Transfer**
Follow only the steps in the left-hand column, below, unless there is a reason that less than the maximum amount of argon be transferred to the mass spectrometer.	***Follow the alternative steps in the right-hand column, below, if there is a reason that less than the maximum amount of argon be transferred to the mass spectrometer.***
1. Close valve D2.	1. Close valve D2.
2. Turn off power to TF-2.	2. Turn off power to TF-2.
3. Set the electrometer to the 10×10^{-11} A range.	2. Close valve T3 and open valve T2.
3. Open valve T2. Observe the signal at $m/e = 40$ and change the electrometer range as necessary.	3. Wait one minute, then close valve T2.
4. Wait two minutes and then close T2.	4. Set the electrometer to the 10×10^{-11} A range.
If there should be too much argon, special procedures, not written here, must be used to reduce the amount of argon without isotopic fractionation.	5. Open T3. Observe the signal at $m/e = 40$ and change the electrometer range as necessary.
	If there should be too much argon, special procedures, not written here, must be used to reduce the amount of argon without isotopic fractionation.
Extraction Line Setup, Part 2	*This part of the extraction line setup need be done only if another sample is to be run before shutdown. It may be done before, in parallel with, or after "Isotopic Analysis of Argon" (below).*
1. Turn on power to TF-1	*Do not do this step before "Argon Transfer" has been completed.* ***Valve T2 must have been closed.***
2. Open valve T1.	
Wait at least ten minutes for the extraction line to become fully evacuated and for TF-1 to become hot before beginning "Argon Extraction and Cleanup" (above) for the next sample.	
Isotopic Analysis of Argon	*This procedure may begin as soon as "Argon Transfer," above, has been completed. There is no need wait until "Extraction Line Setup, Part 2," has been completed.*
1. Set the mass selector to below $m/e = 36$, set the electrometer to the 0.1×10^{-11} A range, and scan over $m/e = 36$ one or more times to confirm that pressure is low enough for accurate measurement of the argon isotopes.	*When pressure is sufficiently low, the baseline for the $m/e = 36$ peak will be stable and will not be steeply sloped. Early on, it is normal for the baseline to decrease in level and in slope as the cooling titanium in TF-2 absorbs hydrogen (which scatters some CO_2 ions so that they go through the collector slit of the mass spectrometer).*

2. Take two sets of measurements of the argon isotopes, each set consisting of a scan upward through the mass range and then a scan of the peaks in reverse order.	*Choose the most sensitive electrometer range possible for each isotope. Be sure to get the baseline on each side of each 36 peak, and similarly for at least one of the 38 peaks and one of the 40 peaks in each of the two sets of measurements.*
3. When the isotopic measurements are done, go to "Mass Spectrometer Setup," above.	*"Mass Spectrometer Setup" may begin at any time after step 4 of "Argon Extraction and Cleanup" has been completed for the next sample. (It can be done earlier if the operator takes special care to see that argon coming out of the mass spectrometer does not get mixed with argon, from sample or spike, of the next run.) There is no need to do the setup if no further samples are to be run before shutdown.*
Mass Spectrometer Setup	*The mass spectrometer setup will have already been done for the first sample of the day. For other samples, it may be begun at any time after step 4 of "Argon Extraction and Cleanup" (above) has been done.*
1. Turn on power to titanium heater TF-2.	
2. Set the mass selector to $m/e = 40$.	*The electrometer should be set to a range appropriated for the signal.*
3. Check that liquid nitrogen is on trap DT-2.	*Do not proceed if a "Spike Preparation" is in progress or if an "Argon Extraction and Cleanup" is in progress but not beyond step 5.*
4. Open valve D2.	*T3 must also be open in order for the mass spectrometer to be evacuated.*
Wait at least three minutes for the argon in the mass spectrometer to be evacuated.	

Approved by _____ *on* _____

APPENDIX B: AIR DRY, EG, AND HEATED TREATMENT XRD PATTERNS

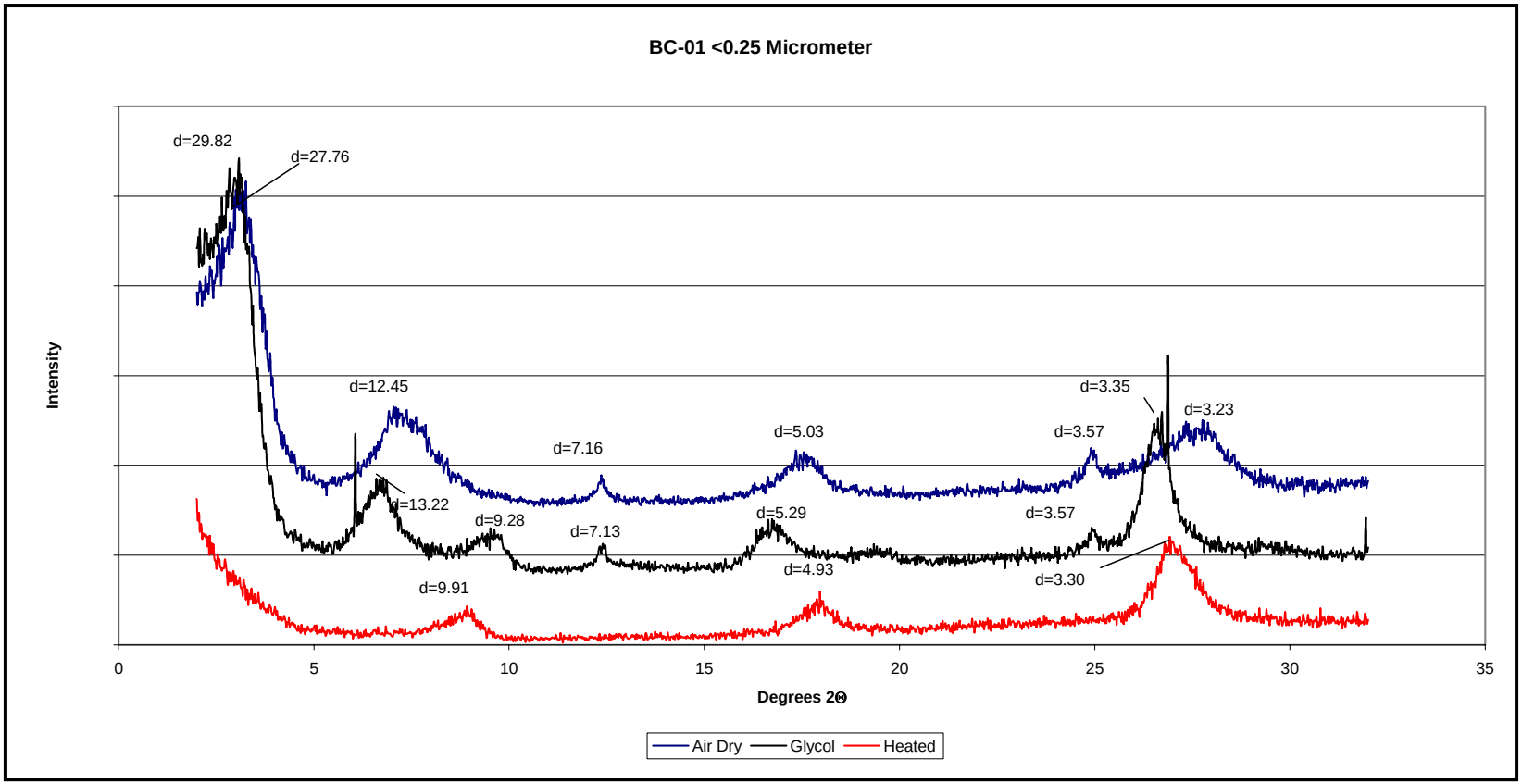
BC-01 <0.25 Micrometer
Intensity
d=29.82
d=27.76
d=12.45
d=13.22
d=9.28
d=9.91
d=7.16
d=7.13
d=5.03
d=5.29
d=4.93
d=3.57
d=3.57
d=3.35
d=3.23
d=3.30
0
5
10
15
20
25
30
35
Degrees 2Θ
Air Dry
Glycol
Heated

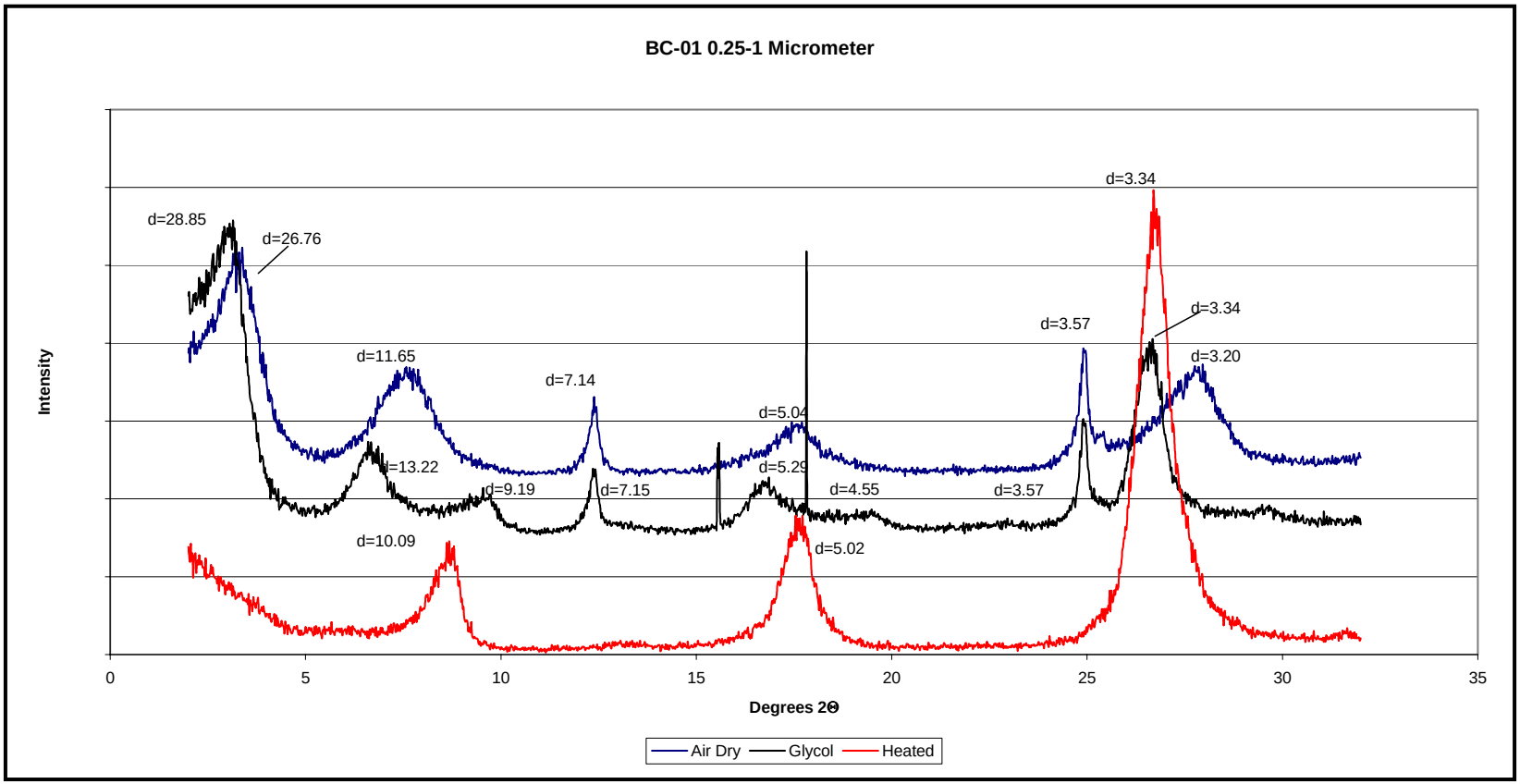
BC-01 0.25-1 Micrometer
Intensity
d=28.85
d=26.76
d=11.65
d=7.14
d=5.04
d=3.57
d=3.34
d=3.34
d=3.20
d=13.22
d=9.19
d=7.15
d=5.29
d=4.55
d=3.57
d=10.09
d=5.02
0
5
10
15
20
25
30
35
Degrees 2Θ
Air Dry
Glycol
Heated

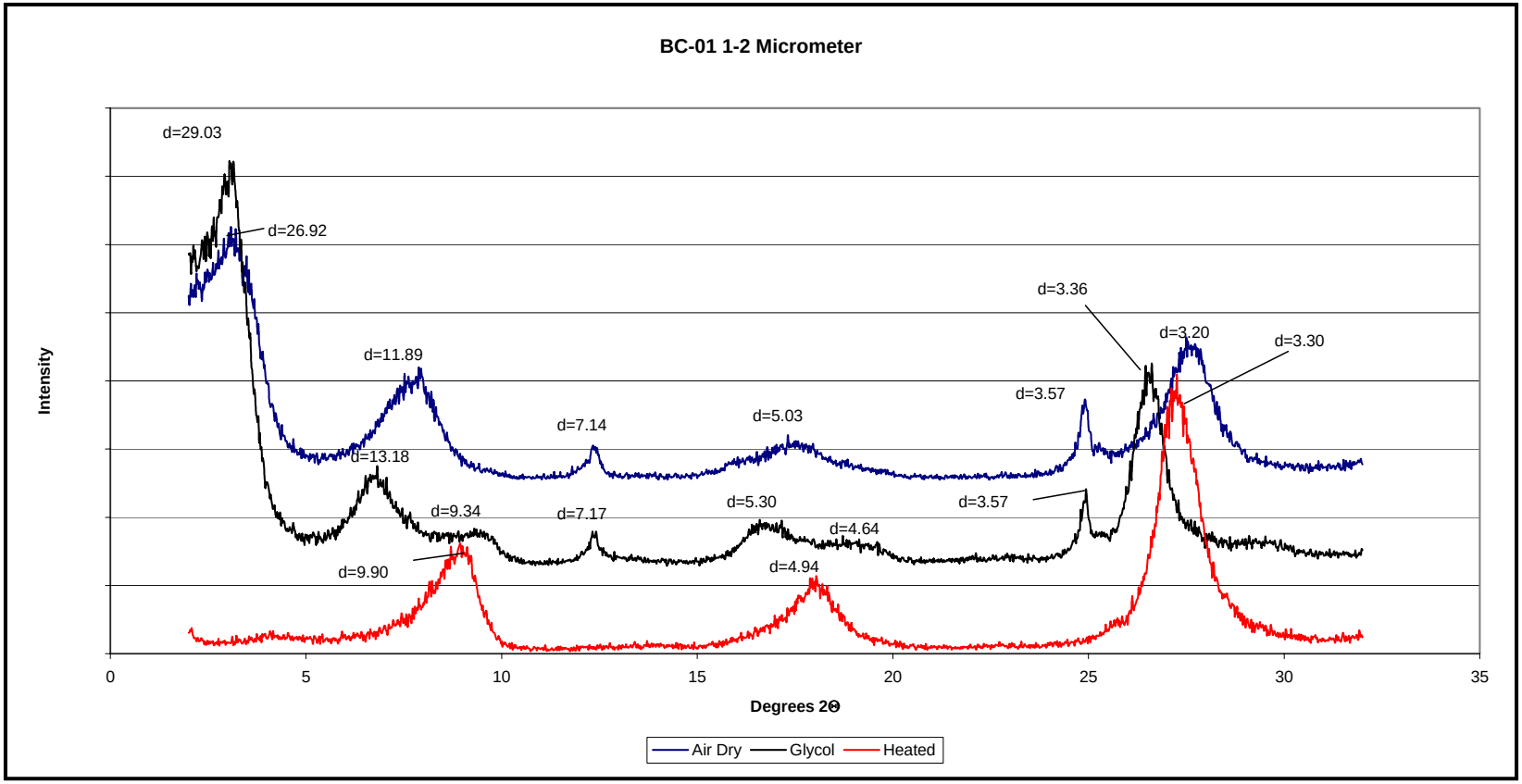
BC-01 1-2 Micrometer
Intensity
d=29.03
d=26.92
d=11.89
d=13.18
d=7.14
d=5.03
d=3.36
d=3.20
d=3.30
d=3.57
d=9.34
d=7.17
d=5.30
d=4.64
d=3.57
d=9.90
d=4.94
0
5
10
15
20
25
30
35
Degrees 2Θ
Air Dry
Glycol
Heated

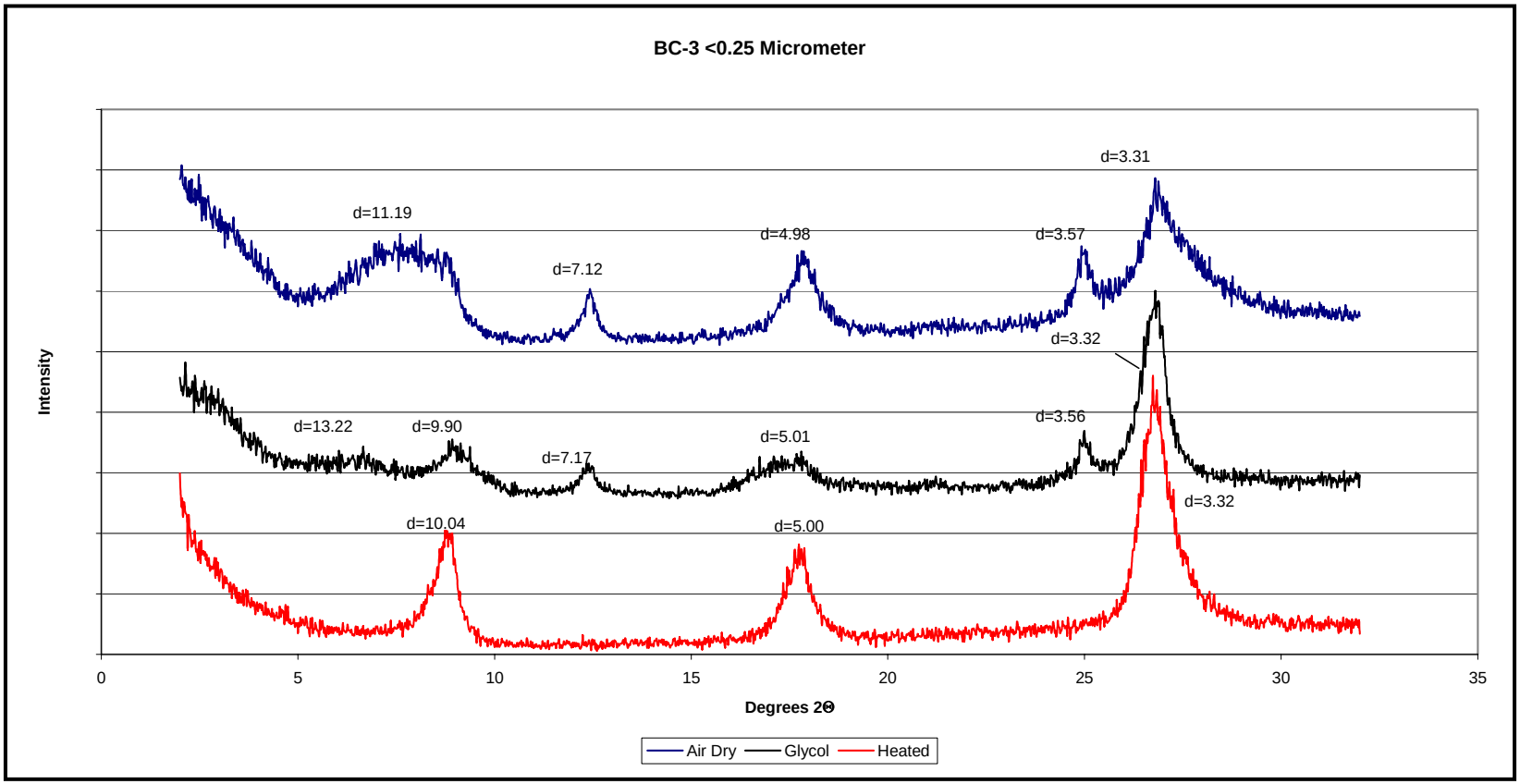
BC-3 <0.25 Micrometer
Intensity
d=11.19
d=7.12
d=4.98
d=3.57
d=3.31
d=3.32
d=13.22
d=9.90
d=7.17
d=5.01
d=3.56
d=3.32
d=10.04
d=5.00
0
5
10
15
20
25
30
35
Degrees 2Θ
Air Dry
Glycol
Heated

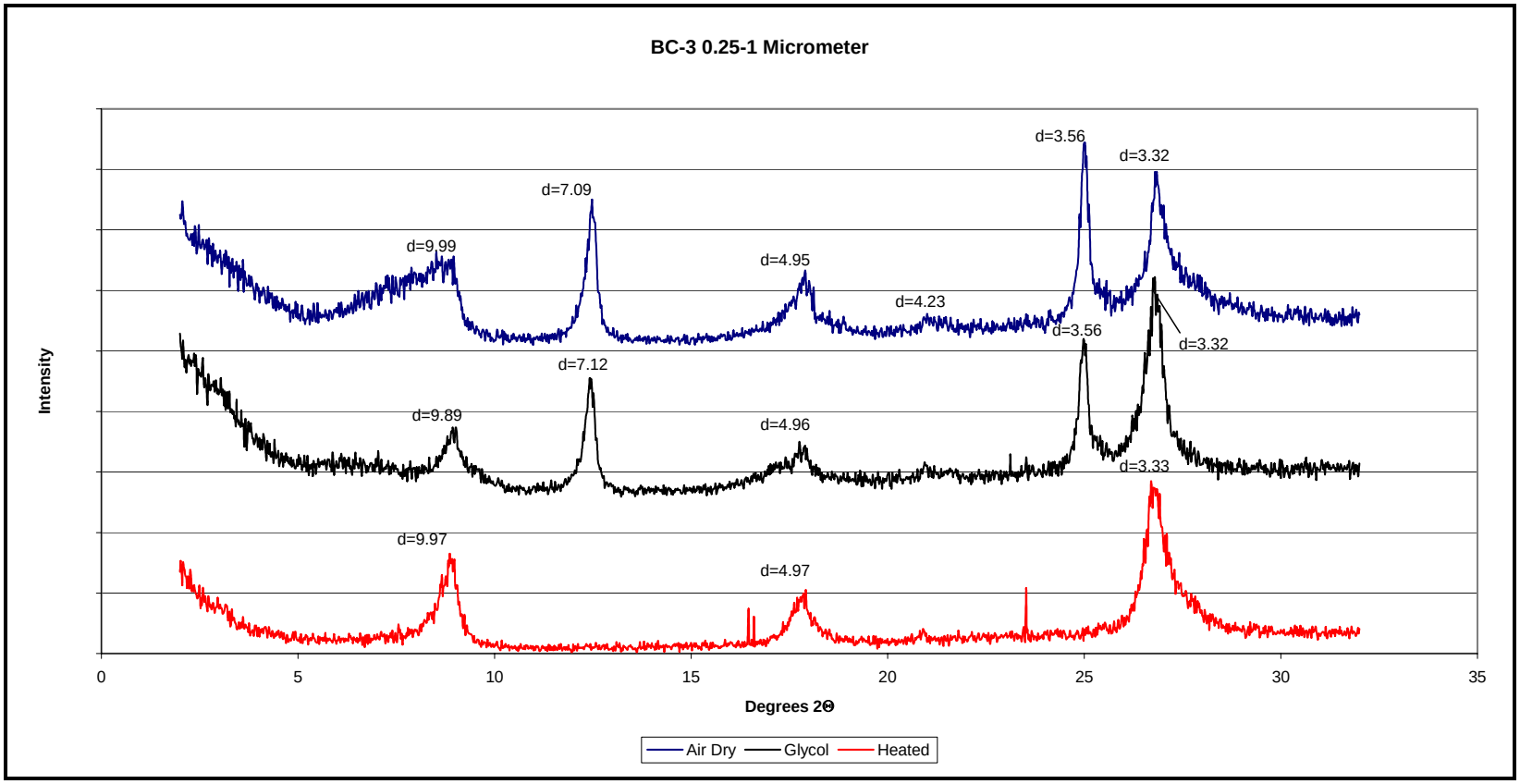
BC-3 0.25-1 Micrometer
Intensity
d=3.56
d=3.32
d=7.09
d=9.99
d=4.95
d=4.23
d=3.56
d=3.32
d=7.12
d=9.89
d=4.96
d=3.33
d=9.97
d=4.97
0
5
10
15
20
25
30
35
Degrees 2Θ
Air Dry
Glycol
Heated

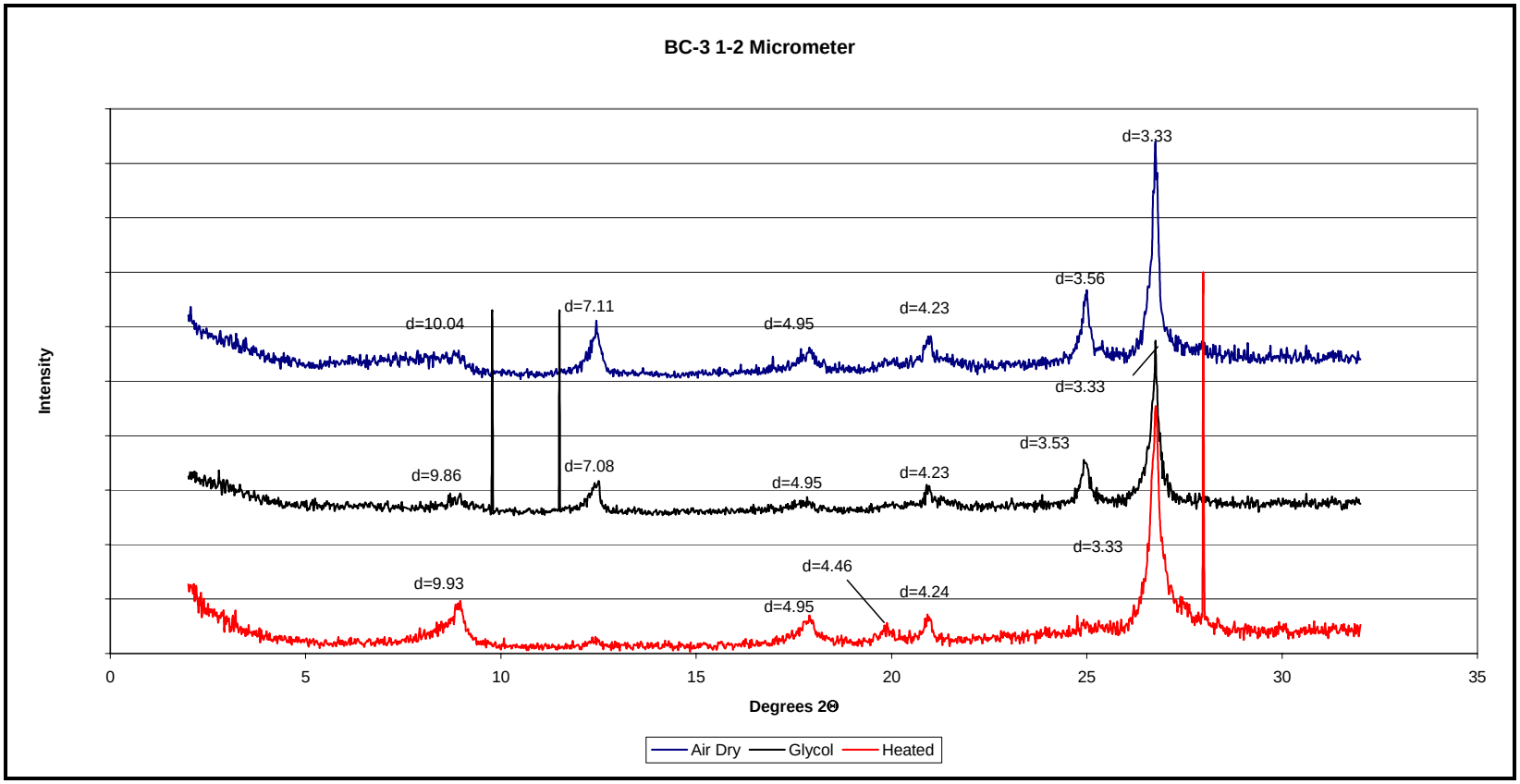
BC-3 1-2 Micrometer
Intensity
d=3.33
d=3.56
d=7.11
d=10.04
d=4.95
d=4.23
d=3.33
d=3.53
d=9.86
d=7.08
d=4.95
d=4.23
d=3.33
d=4.46
d=9.93
d=4.24
d=4.95
0
5
10
15
20
25
30
35
Degrees 2Θ
Air Dry
Glycol
Heated

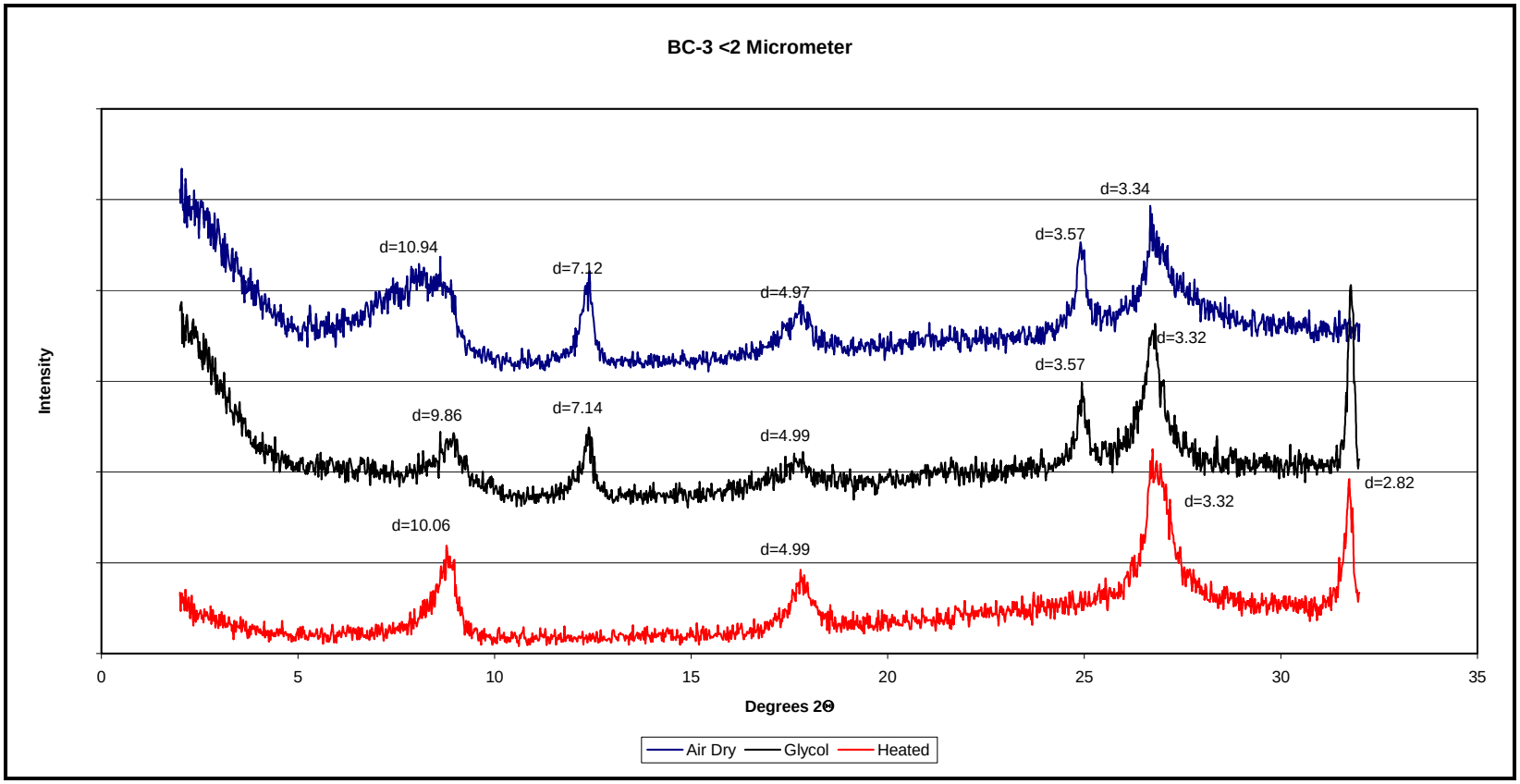
BC-3 <2 Micrometer
Intensity
d=10.94
d=7.12
d=4.97
d=3.57
d=3.34
d=9.86
d=7.14
d=4.99
d=3.57
d=3.32
d=2.82
d=10.06
d=4.99
d=3.32
0
5
10
15
20
25
30
35
Degrees 2Θ
Air Dry
Glycol
Heated

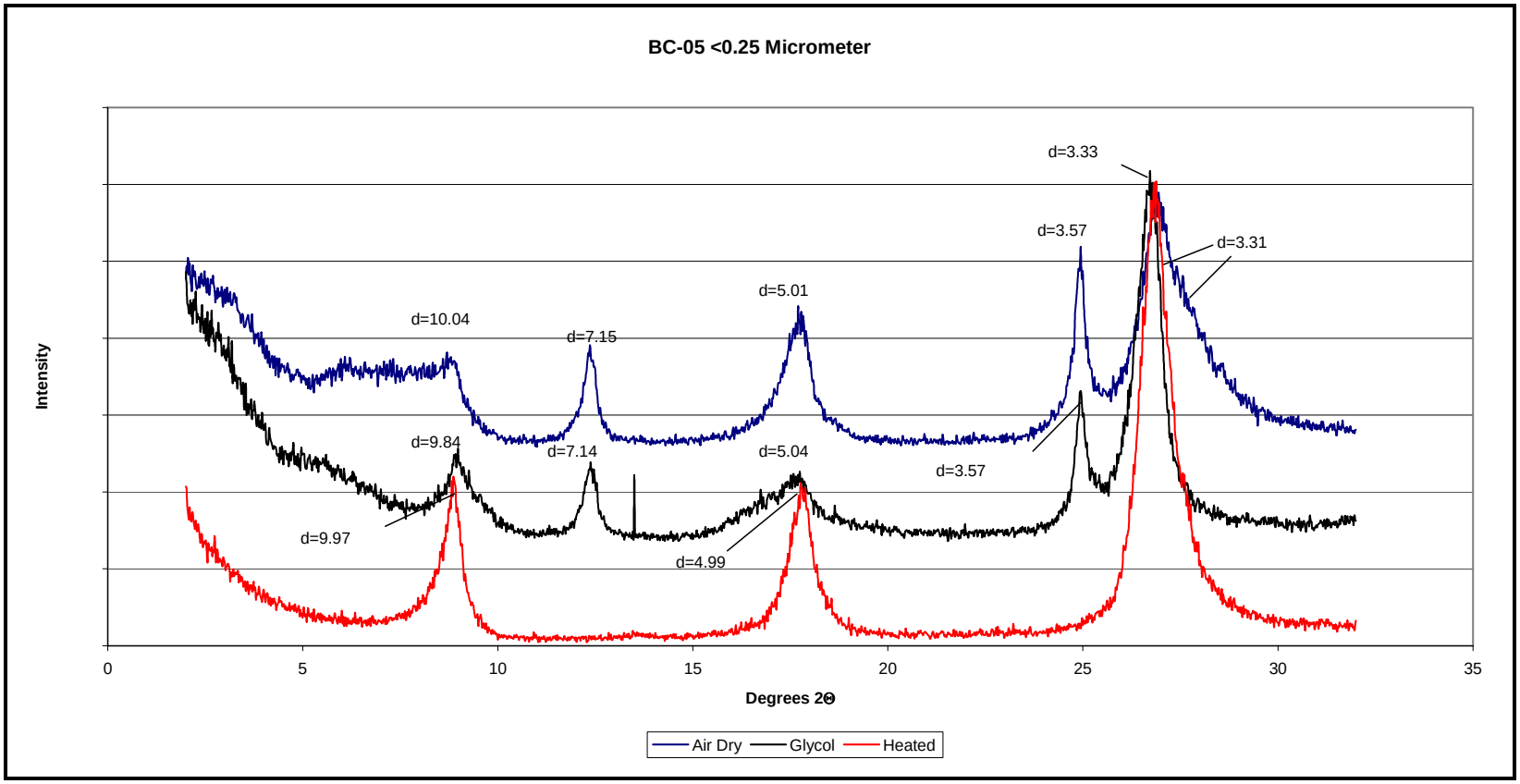
BC-05 <0.25 Micrometer
Intensity
d=10.04
d=7.15
d=5.01
d=3.57
d=3.33
d=3.31
d=9.84
d=7.14
d=5.04
d=3.57
d=9.97
d=4.99
0
5
10
15
20
25
30
35
Degrees 2Θ
Air Dry
Glycol
Heated

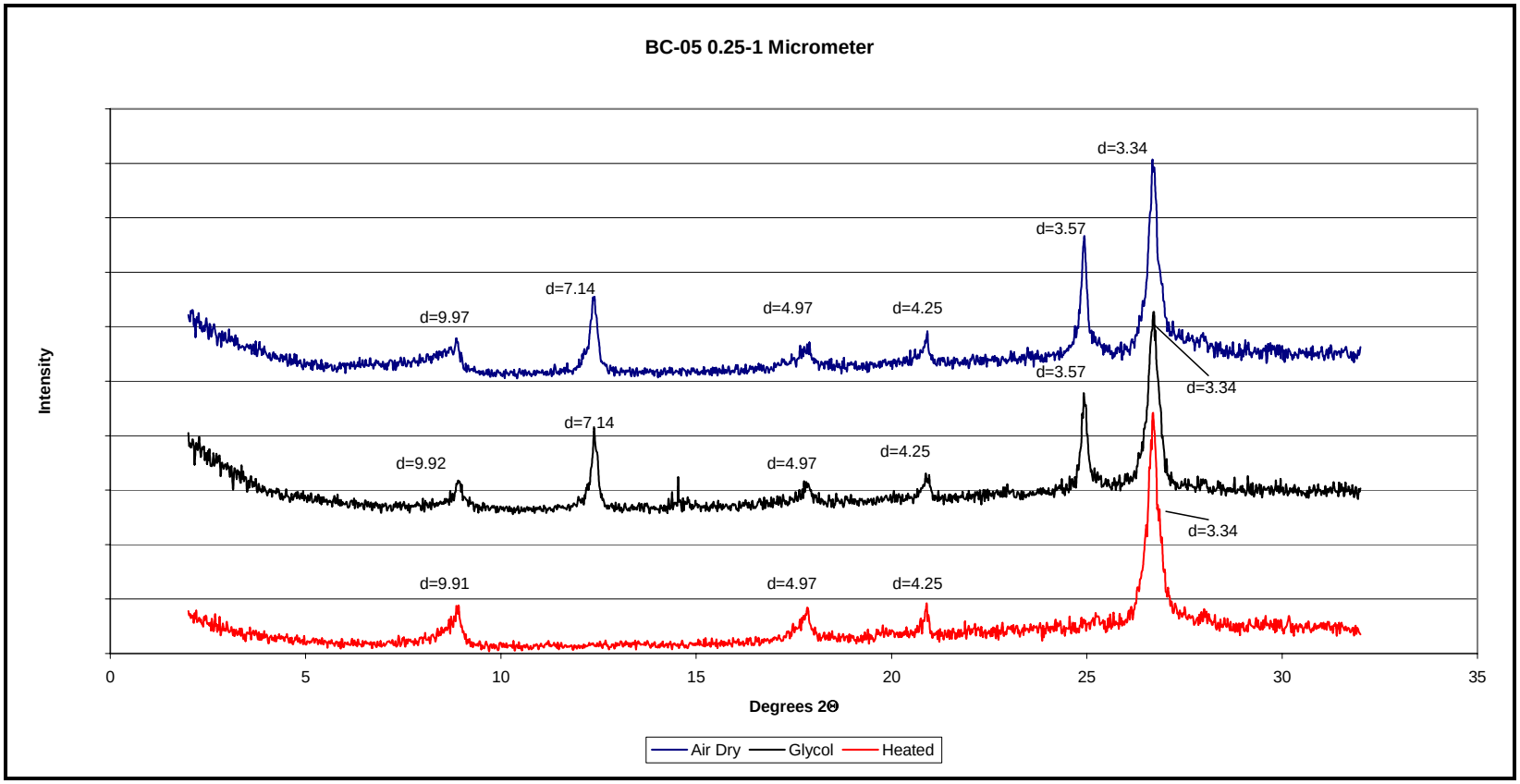
BC-05 0.25-1 Micrometer
Intensity
d=3.34
d=3.57
d=7.14
d=9.97
d=4.97
d=4.25
d=3.57
d=3.34
d=7.14
d=9.92
d=4.97
d=4.25
d=3.34
d=9.91
d=4.97
d=4.25
0
5
10
15
20
25
30
35
Degrees 2Θ
Air Dry
Glycol
Heated

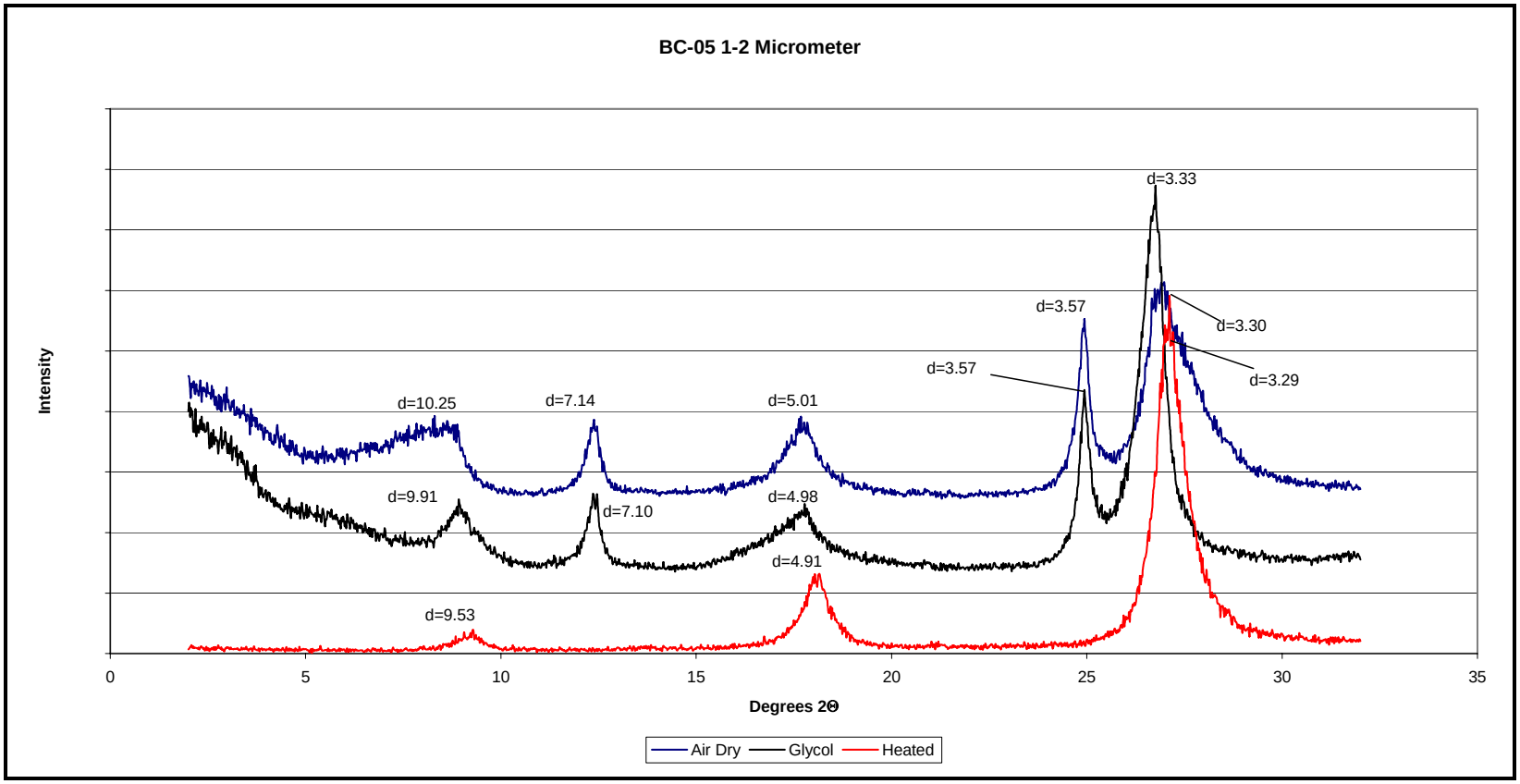
BC-05 1-2 Micrometer
Intensity
d=3.33
d=3.57
d=3.30
d=3.57
d=3.29
d=10.25
d=7.14
d=5.01
d=9.91
d=7.10
d=4.98
d=4.91
d=9.53
0
5
10
15
20
25
30
35
Degrees 2Θ
Air Dry
Glycol
Heated

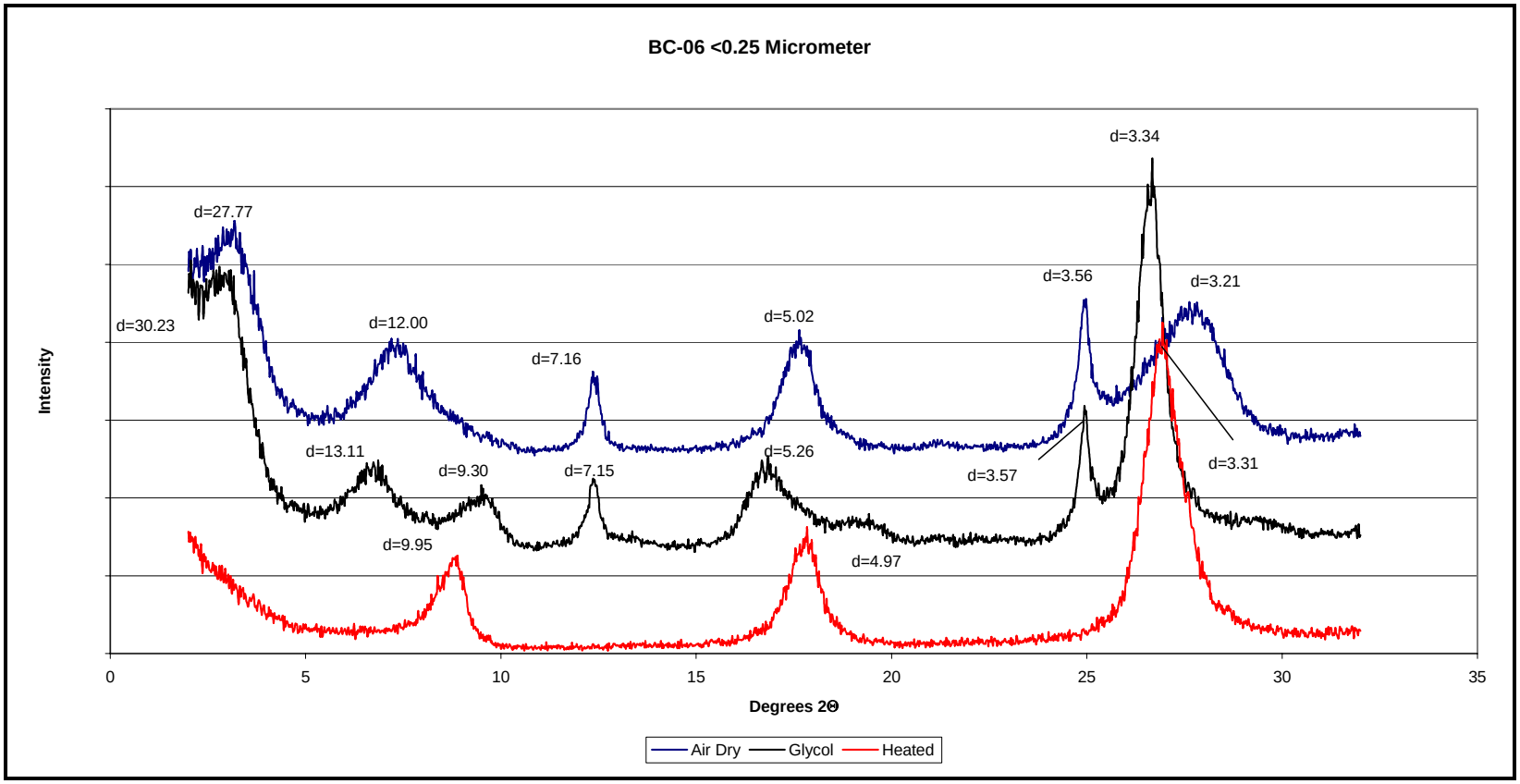
BC-06 <0.25 Micrometer
Intensity
d=27.77
d=30.23
d=12.00
d=7.16
d=5.02
d=3.56
d=3.34
d=3.21
d=13.11
d=9.30
d=7.15
d=5.26
d=3.57
d=3.31
d=9.95
d=4.97
0
5
10
15
20
25
30
35
Degrees 2Θ
Air Dry
Glycol
Heated

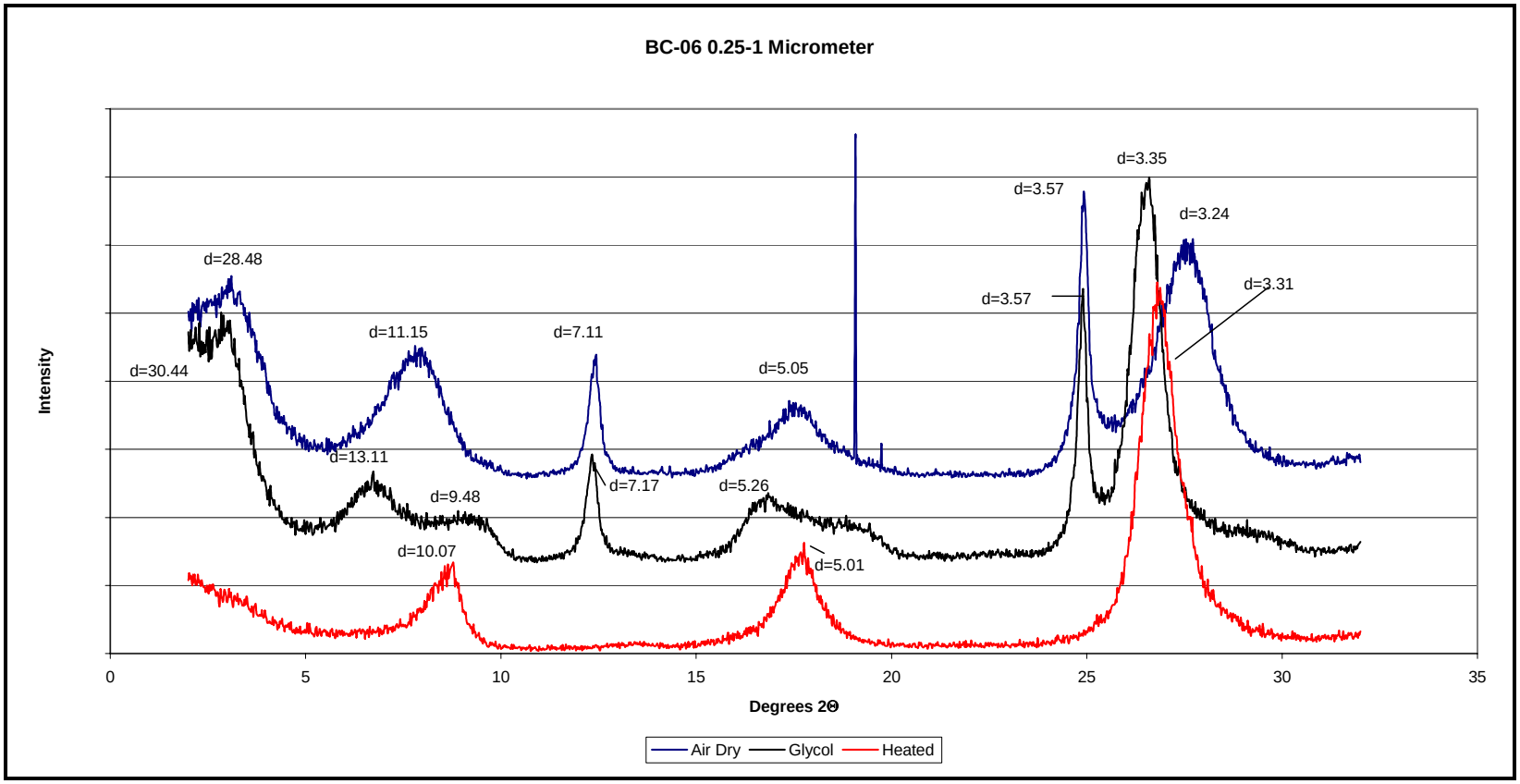
BC-06 0.25-1 Micrometer
Intensity
d=28.48
d=30.44
d=11.15
d=13.11
d=9.48
d=10.07
d=7.11
d=7.17
d=5.05
d=5.26
d=5.01
d=3.57
d=3.35
d=3.24
d=3.57
d=3.31
0
5
10
15
20
25
30
35
Degrees 2Θ
Air Dry
Glycol
Heated

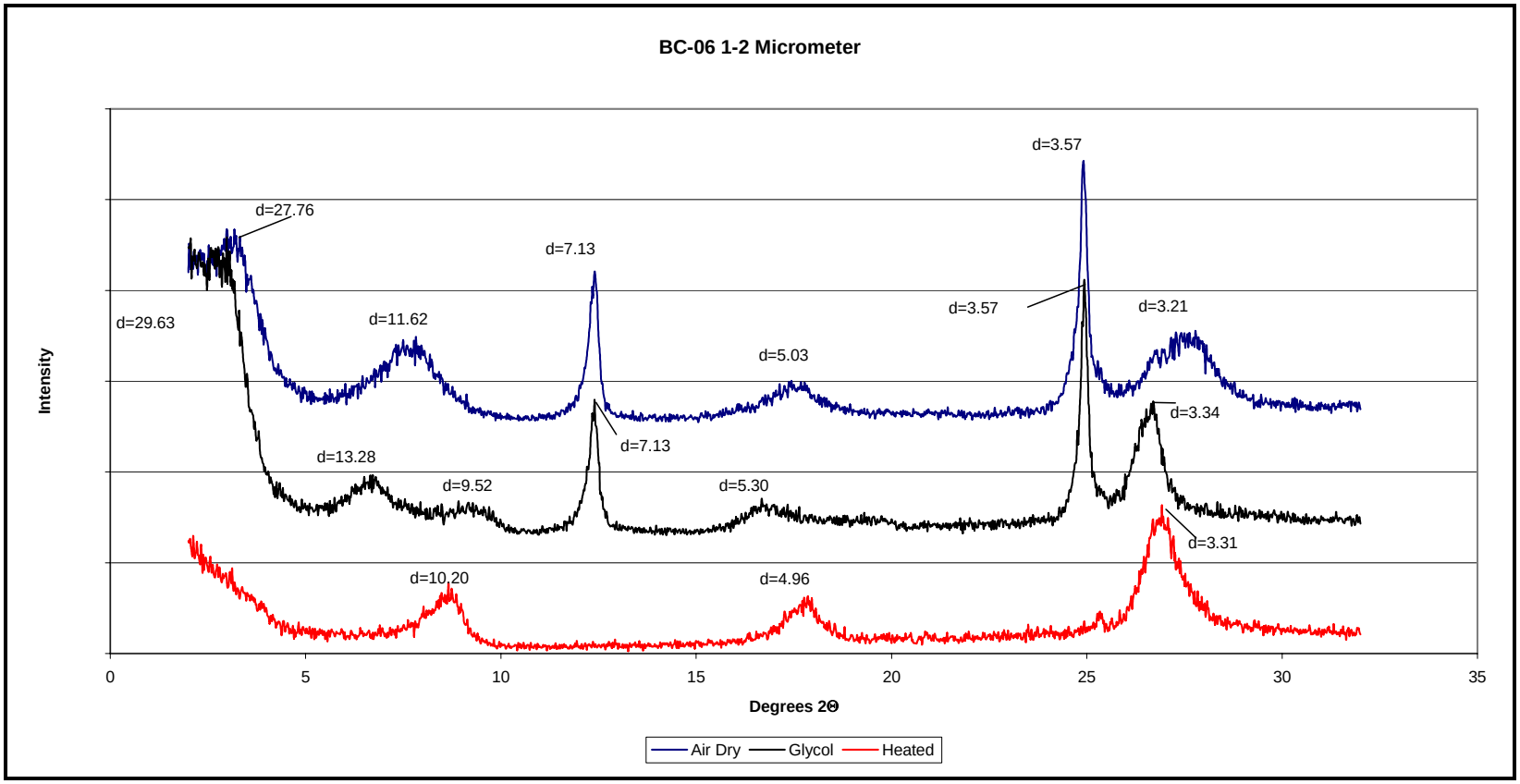
BC-06 1-2 Micrometer
Intensity
d=27.76
d=29.63
d=11.62
d=7.13
d=5.03
d=3.57
d=3.57
d=3.21
d=3.34
d=7.13
d=13.28
d=9.52
d=5.30
d=3.31
d=10.20
d=4.96
0
5
10
15
20
25
30
35
Degrees 2Θ
Air Dry
Glycol
Heated

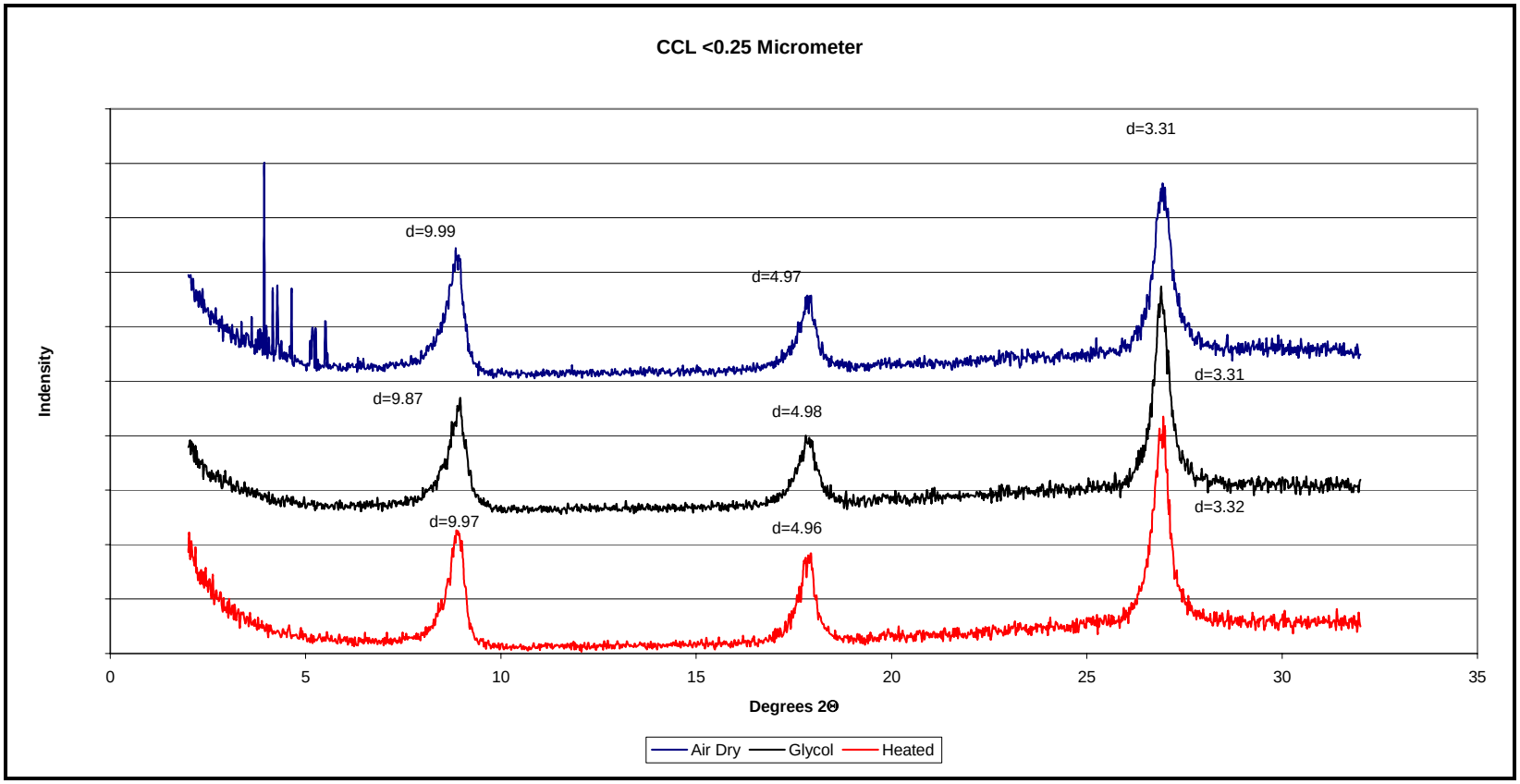
CCL <0.25 Micrometer
Indensity
d=3.31
d=9.99
d=4.97
d=3.31
d=9.87
d=4.98
d=3.32
d=9.97
d=4.96
0
5
10
15
20
25
30
35
Degrees 2Θ
Air Dry
Glycol
Heated

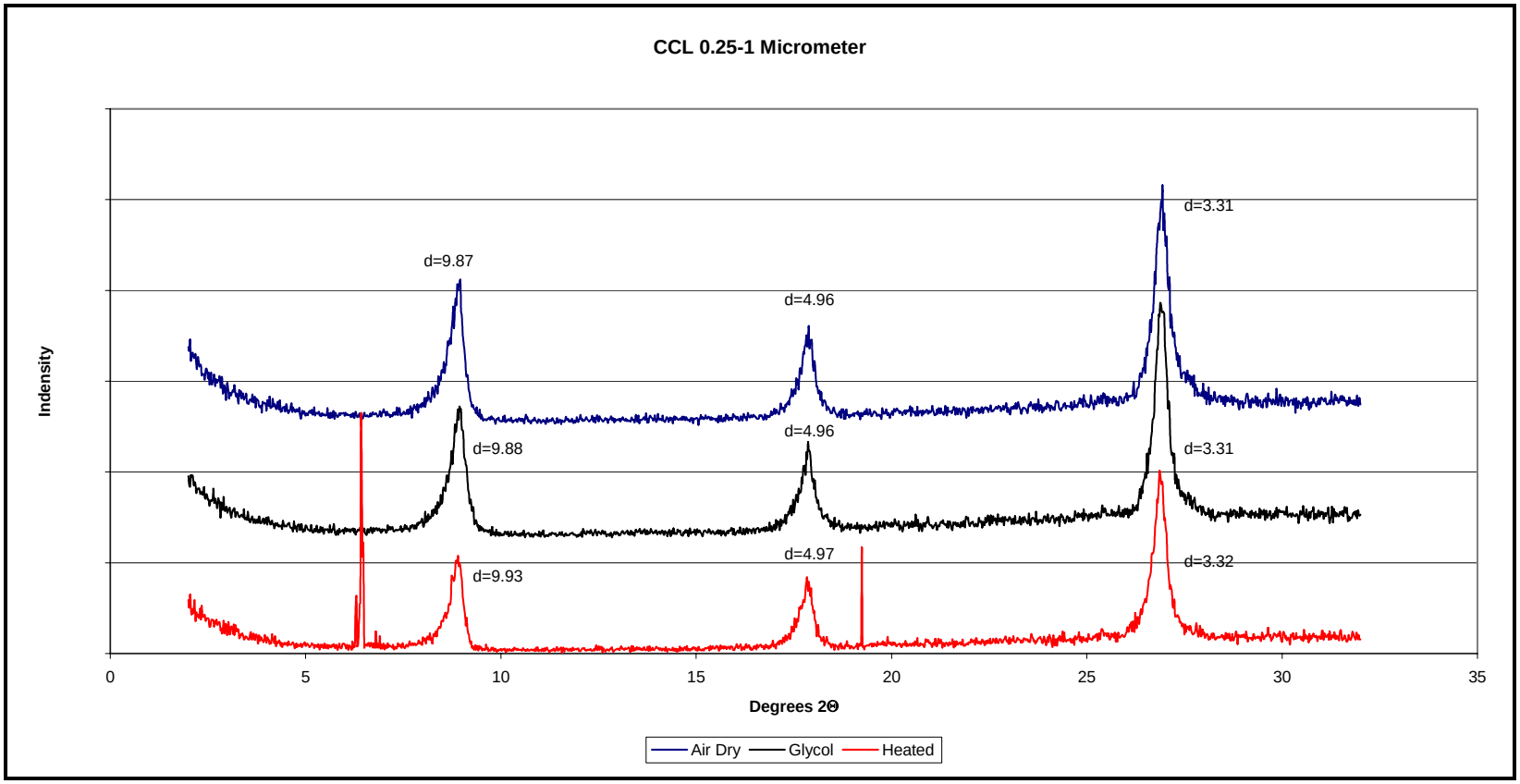
CCL 0.25-1 Micrometer
Indensity
d=9.87
d=4.96
d=3.31
d=9.88
d=4.96
d=3.31
d=9.93
d=4.97
d=3.32
0
5
10
15
20
25
30
35
Degrees 2Θ
Air Dry
Glycol
Heated

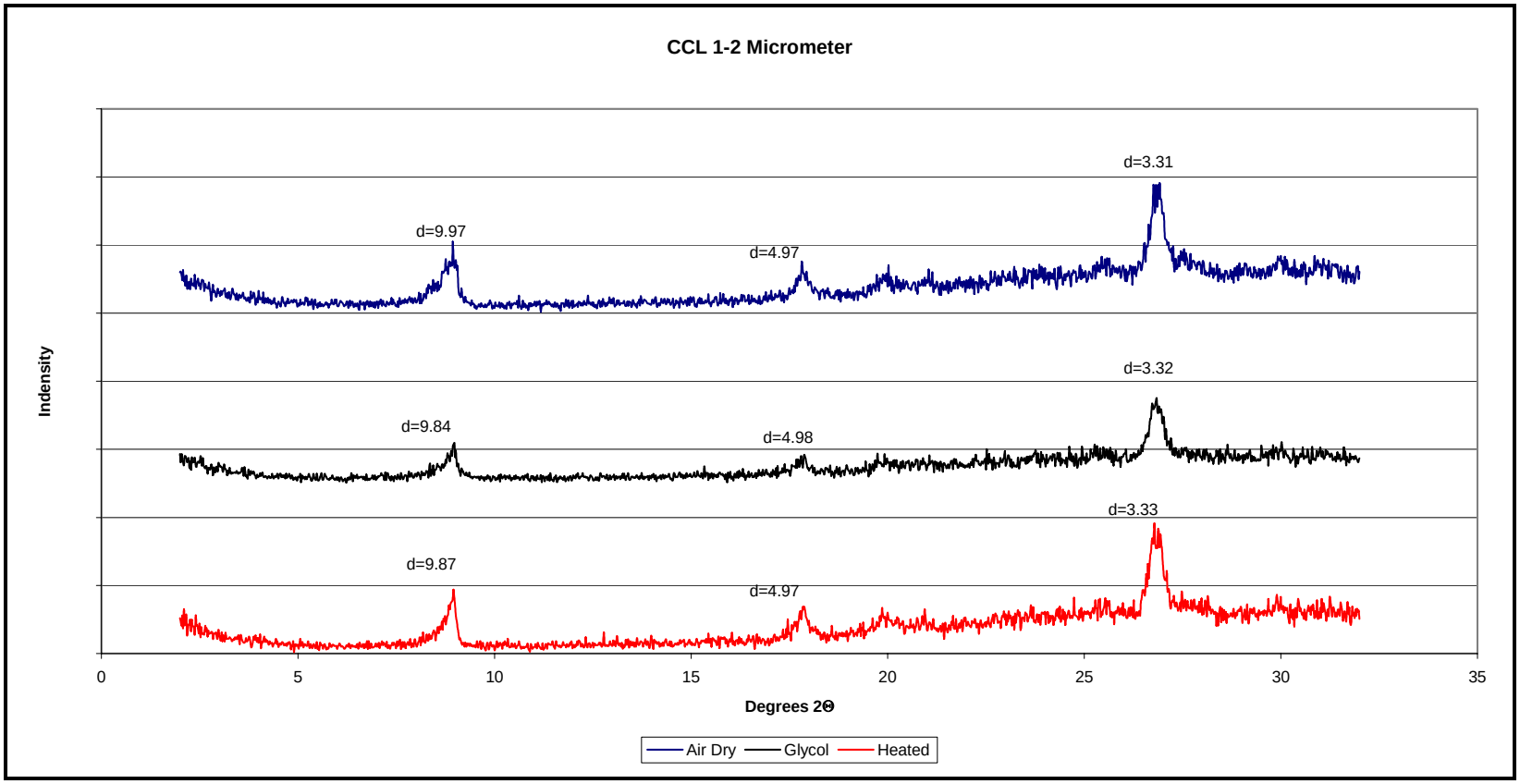
CCL 1-2 Micrometer
Indensity
d=3.31
d=9.97
d=4.97
d=3.32
d=9.84
d=4.98
d=3.33
d=9.87
d=4.97
0
5
10
15
20
25
30
35
Degrees 2Θ
Air Dry
Glycol
Heated

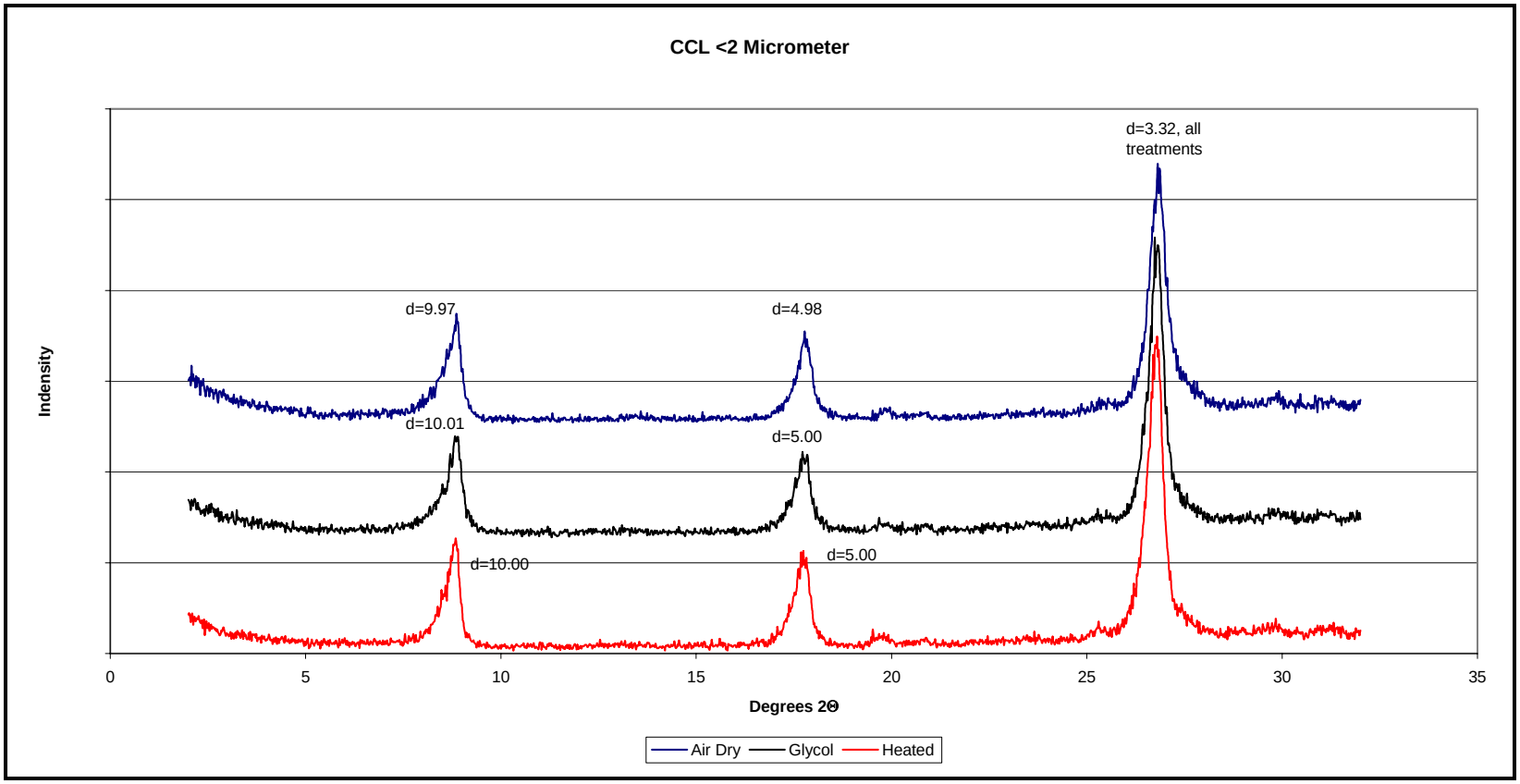
CCL <2 Micrometer
Indensity
d=3.32, all treatments
d=9.97
d=4.98
d=10.01
d=5.00
d=10.00
d=5.00
0
5
10
15
20
25
30
35
Degrees 2Θ
Air Dry
Glycol
Heated

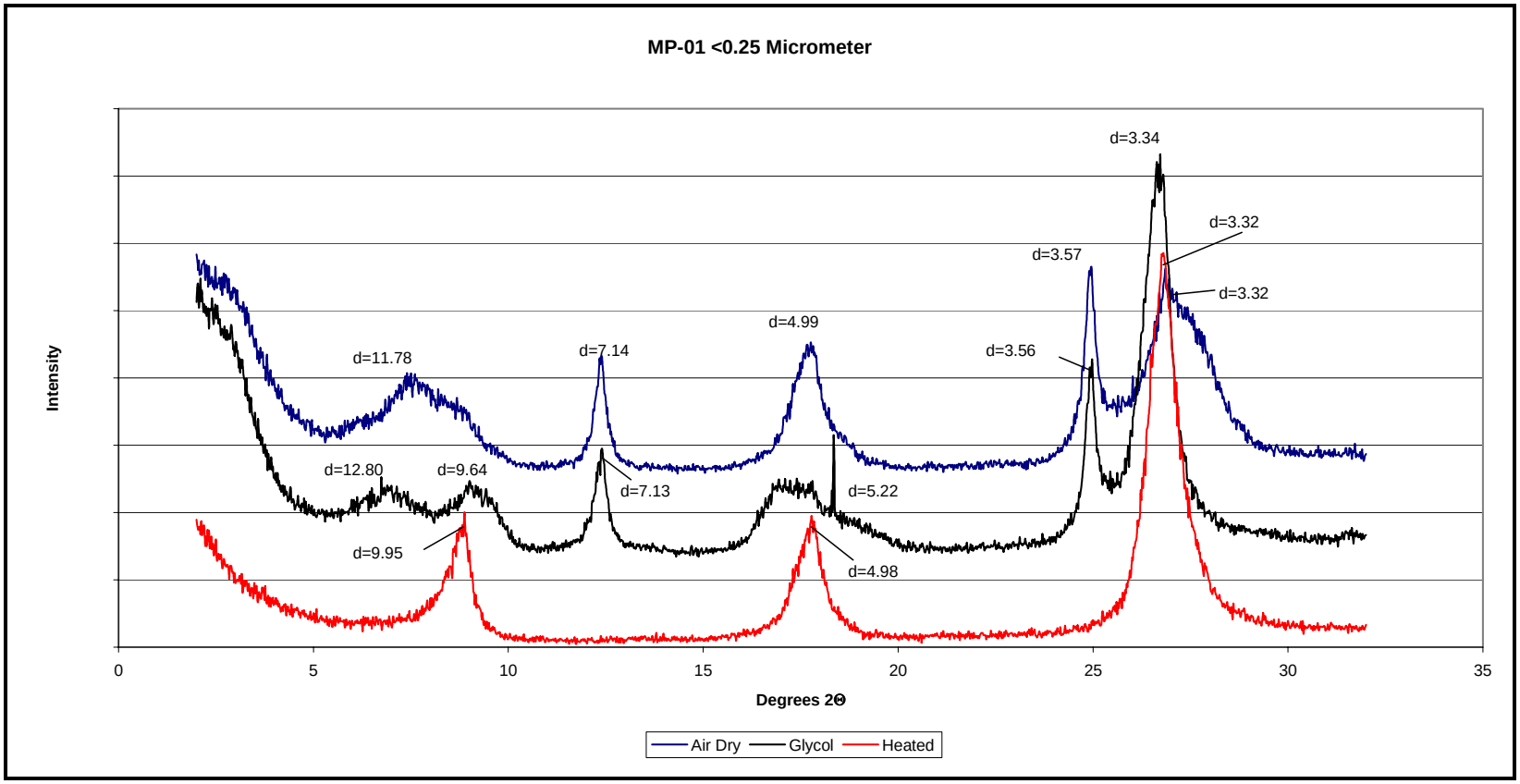
MP-01 <0.25 Micrometer
Intensity
d=3.34
d=3.32
d=3.57
d=3.32
d=4.99
d=11.78
d=7.14
d=3.56
d=12.80
d=9.64
d=7.13
d=5.22
d=9.95
d=4.98
0
5
10
15
20
25
30
35
Degrees 2Θ
Air Dry
Glycol
Heated

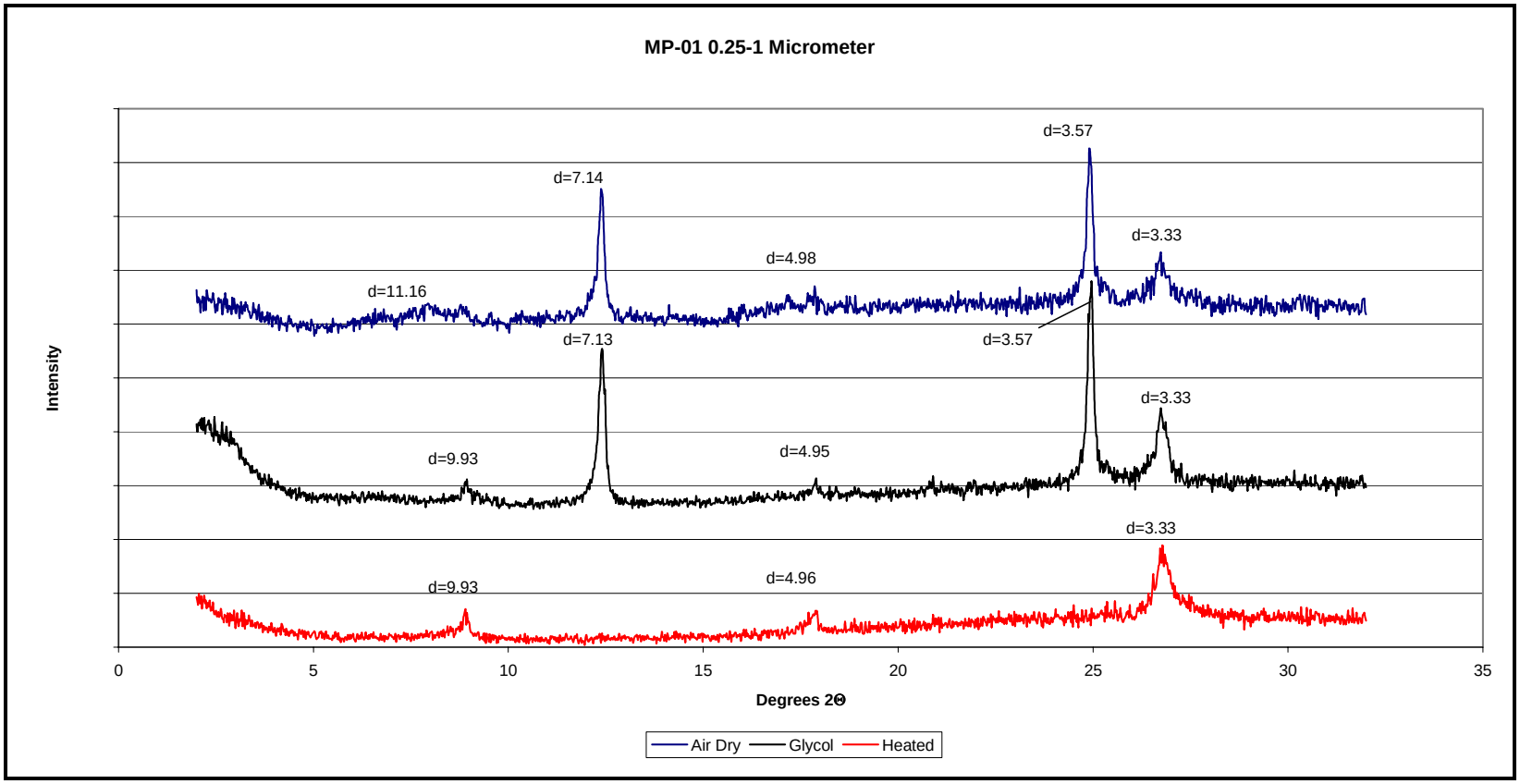
MP-01 0.25-1 Micrometer
Intensity
d=3.57
d=7.14
d=3.33
d=4.98
d=11.16
d=7.13
d=3.57
d=3.33
d=9.93
d=4.95
d=3.33
d=9.93
d=4.96
0
5
10
15
20
25
30
35
Degrees 2Θ
Air Dry
Glycol
Heated

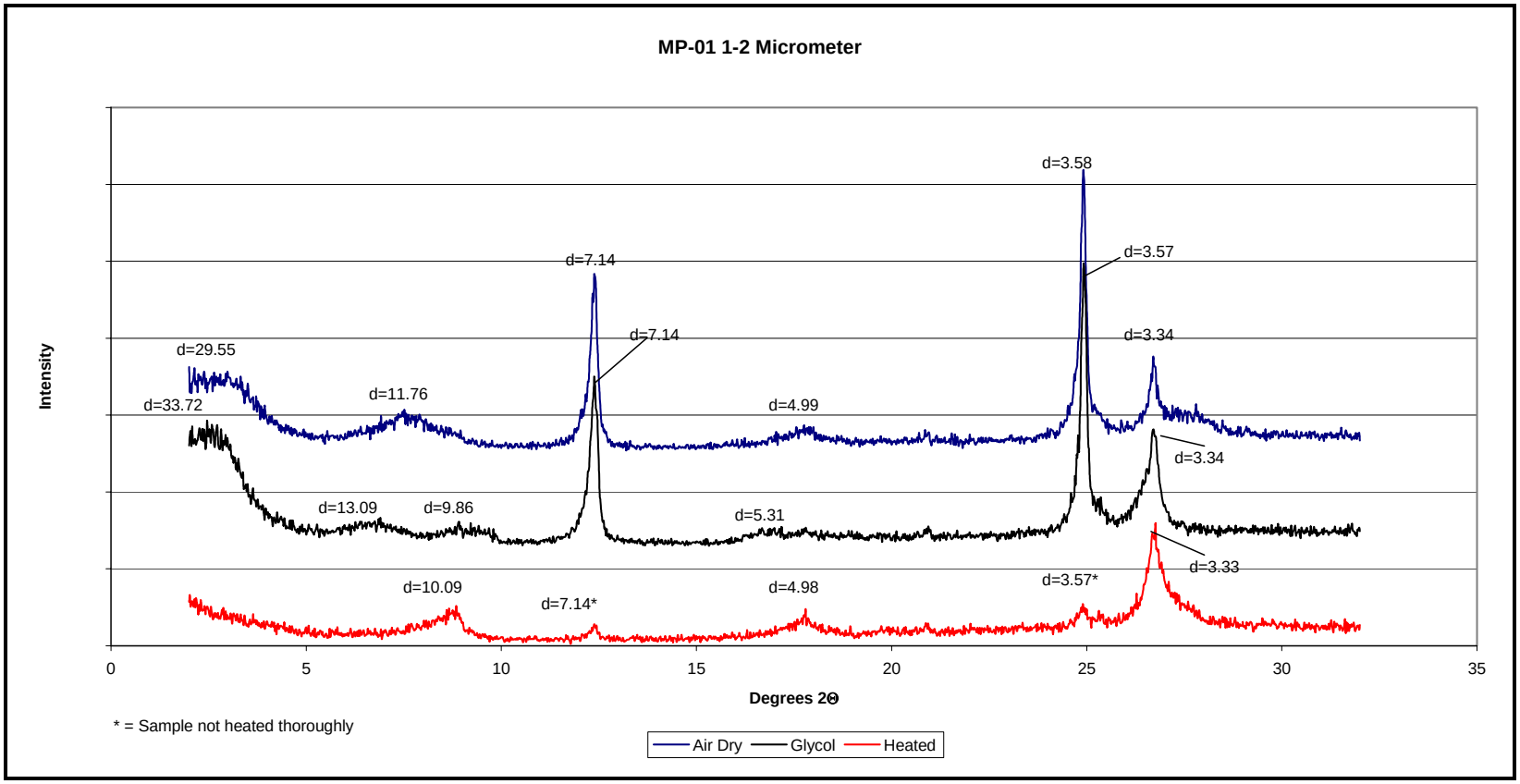
MP-01 1-2 Micrometer
Intensity
d=3.58
d=7.14
d=3.57
d=7.14
d=3.34
d=29.55
d=11.76
d=33.72
d=4.99
d=3.34
d=13.09
d=9.86
d=5.31
d=3.33
d=10.09
d=7.14*
d=4.98
d=3.57*
0
5
10
15
20
25
30
35
Degrees 2Θ
* = Sample not heated thoroughly
Air Dry
Glycol
Heated

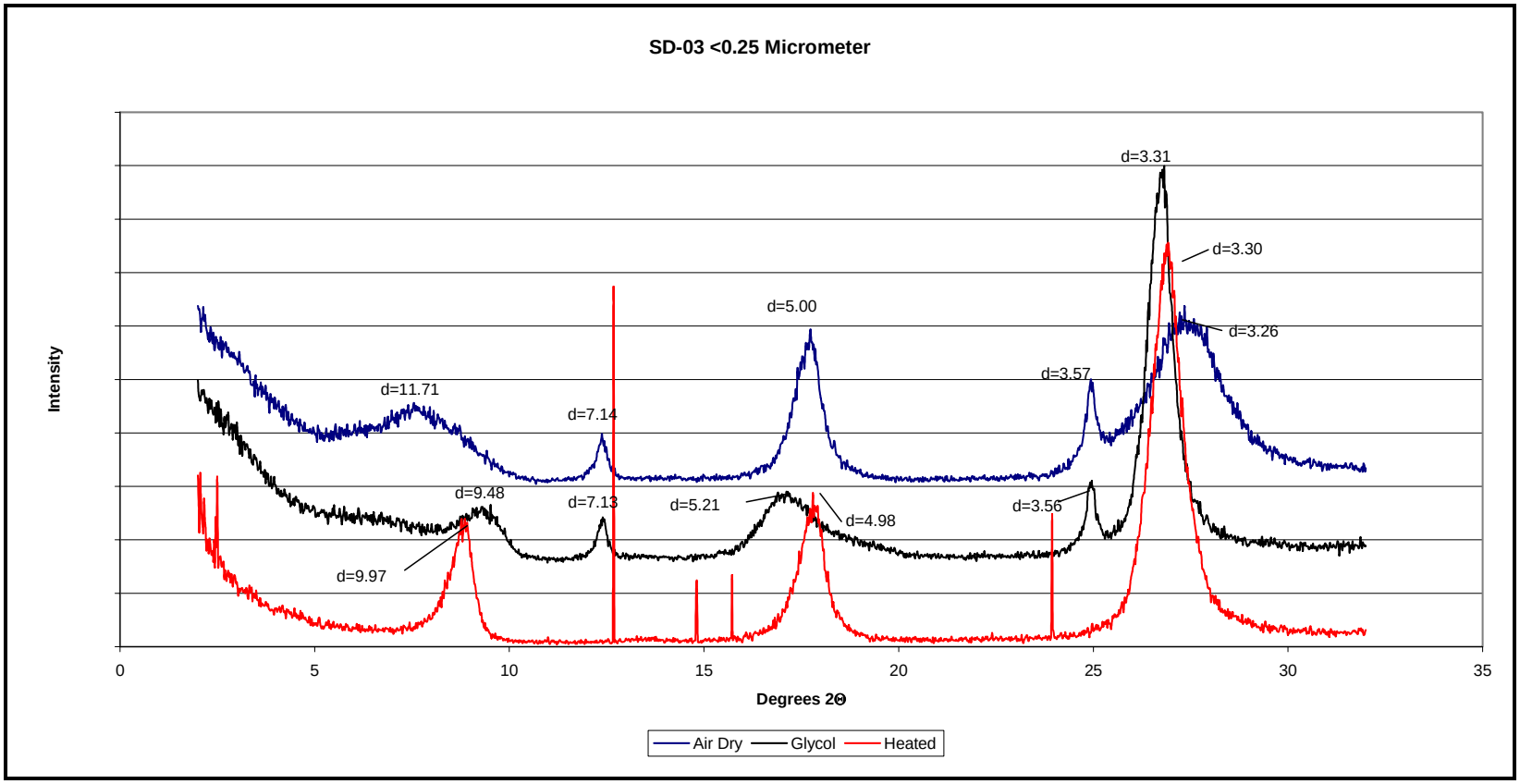
SD-03 <0.25 Micrometer
Intensity
d=3.31
d=3.30
d=3.26
d=5.00
d=3.57
d=11.71
d=7.14
d=9.48
d=7.13
d=5.21
d=4.98
d=3.56
d=9.97
0
5
10
15
20
25
30
35
Degrees 2Θ
Air Dry
Glycol
Heated

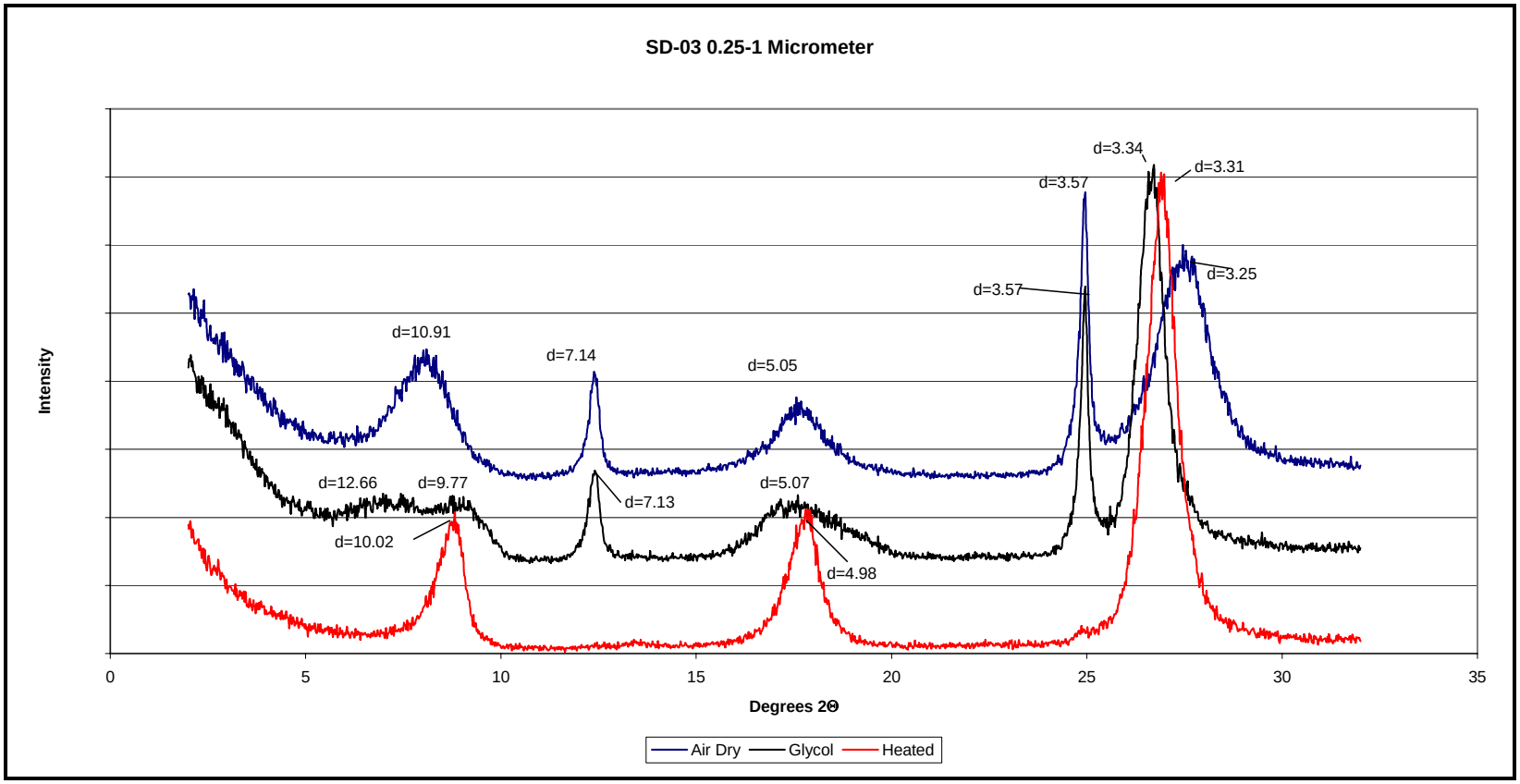
SD-03 0.25-1 Micrometer
Intensity
d=10.91
d=7.14
d=5.05
d=3.57
d=3.34
d=3.31
d=3.25
d=12.66
d=9.77
d=7.13
d=5.07
d=10.02
d=4.98
0
5
10
15
20
25
30
35
Degrees 2Θ
Air Dry
Glycol
Heated

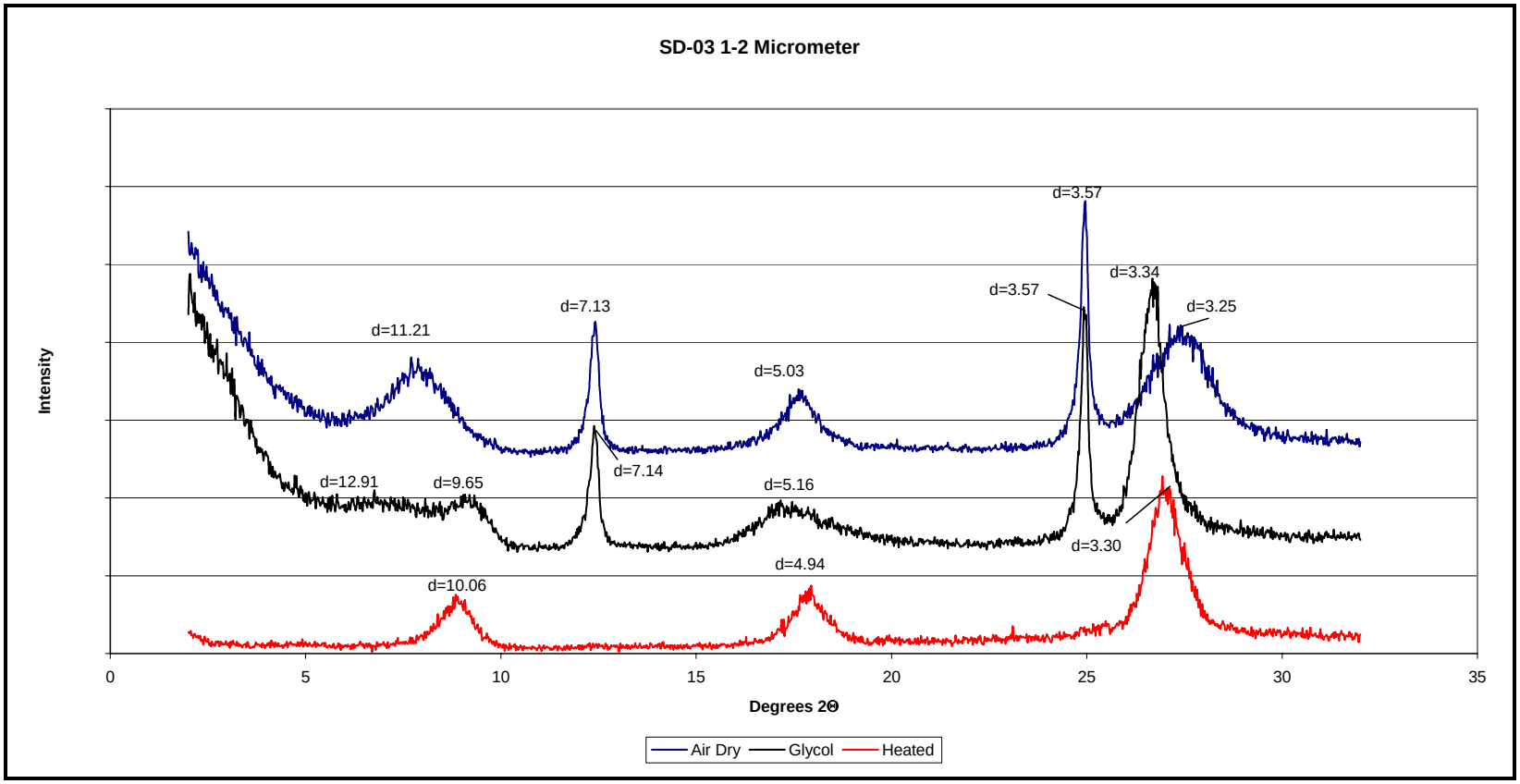
SD-03 1-2 Micrometer
Intensity
d=11.21
d=7.13
d=3.57
d=3.34
d=3.57
d=3.25
d=5.03
d=7.14
d=12.91
d=9.65
d=5.16
d=3.30
d=4.94
d=10.06
0
5
10
15
20
25
30
35
Degrees 2Θ
Air Dry
Glycol
Heated

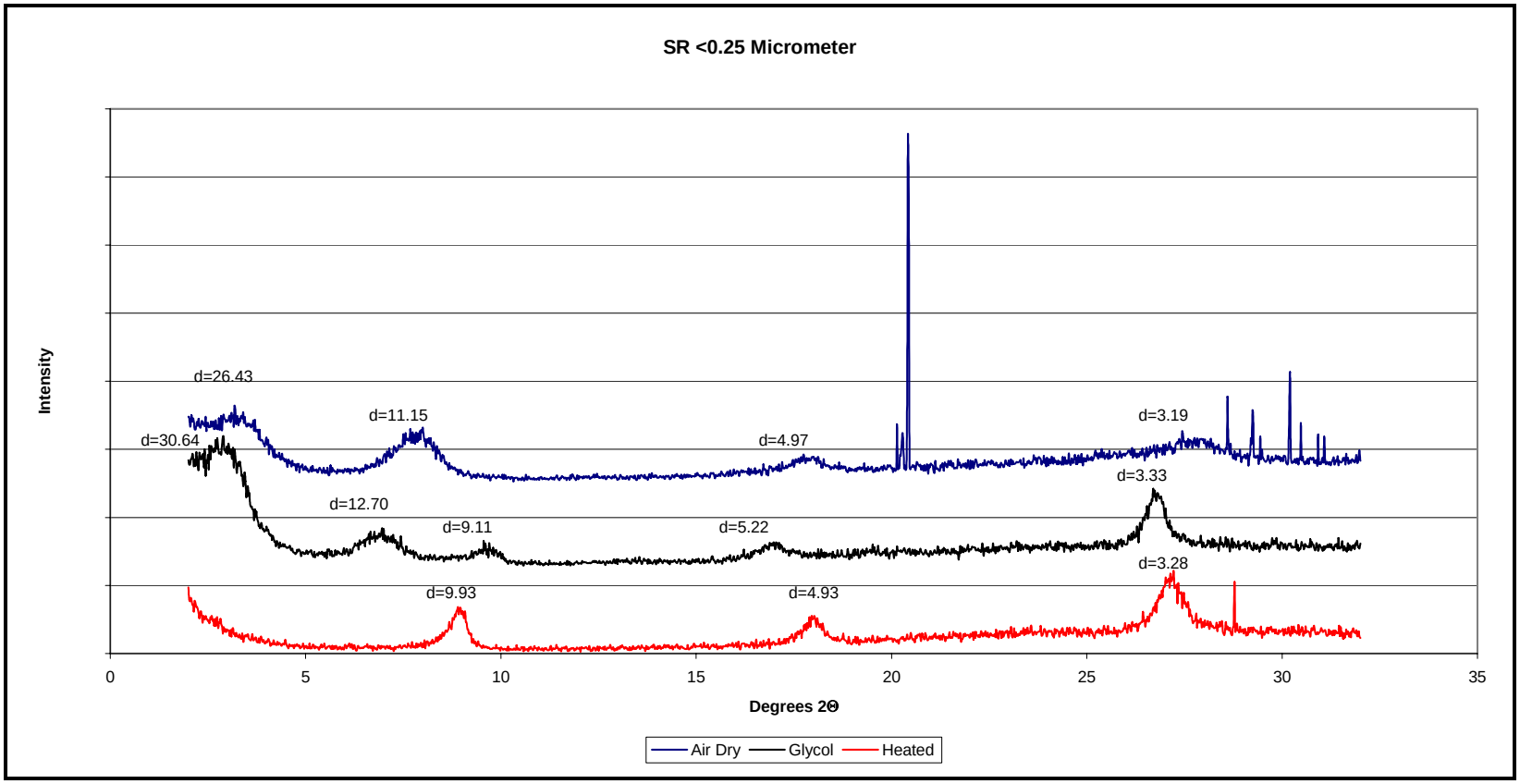
SR <0.25 Micrometer
Intensity
d=26.43
d=11.15
d=30.64
d=4.97
d=3.19
d=3.33
d=12.70
d=9.11
d=5.22
d=3.28
d=9.93
d=4.93
0
5
10
15
20
25
30
35
Degrees 2Θ
Air Dry
Glycol
Heated

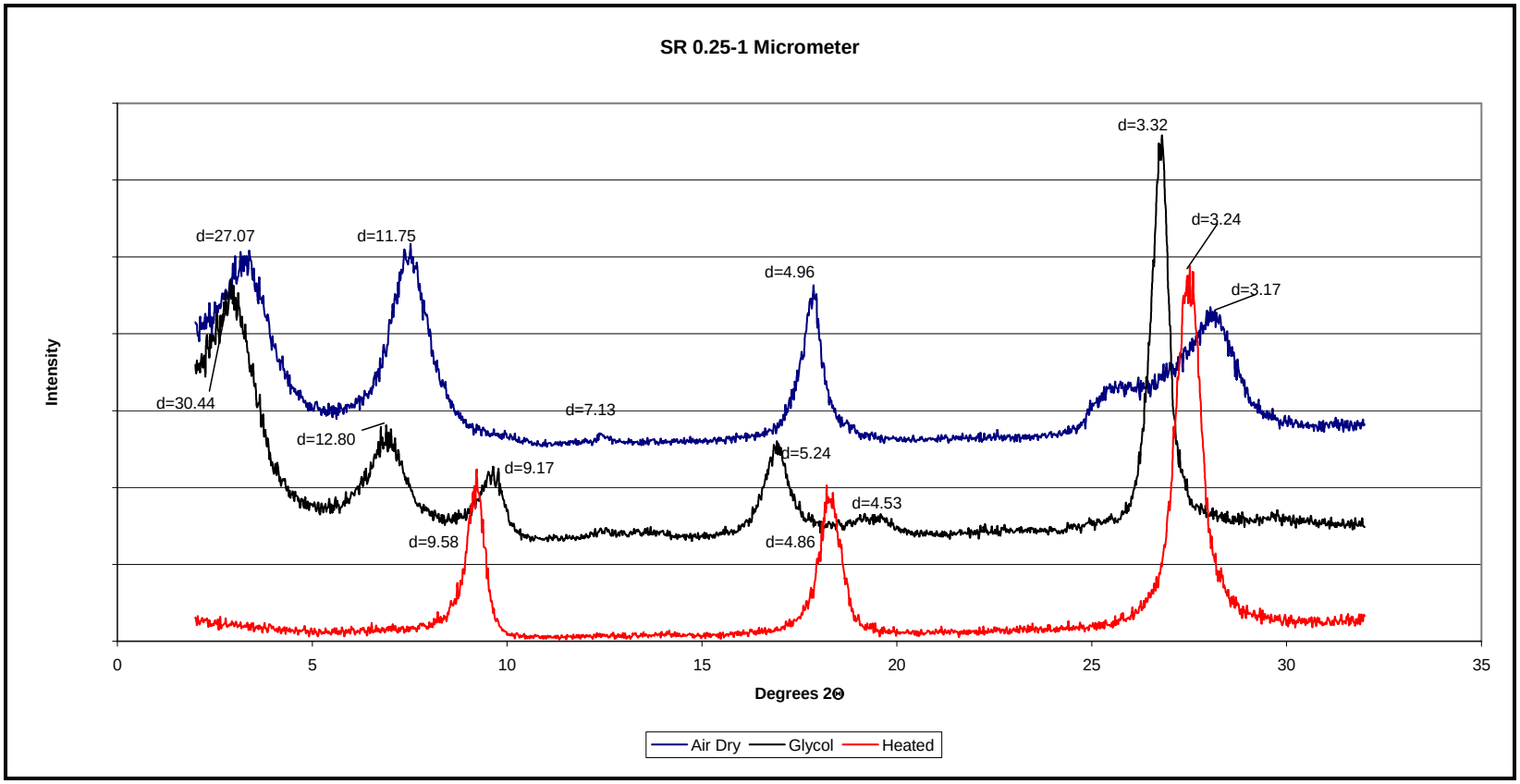
SR 0.25-1 Micrometer
Intensity
d=27.07
d=11.75
d=4.96
d=3.32
d=3.24
d=3.17
d=30.44
d=7.13
d=12.80
d=5.24
d=9.17
d=4.53
d=9.58
d=4.86
0
5
10
15
20
25
30
35
Degrees 2Θ
Air Dry
Glycol
Heated

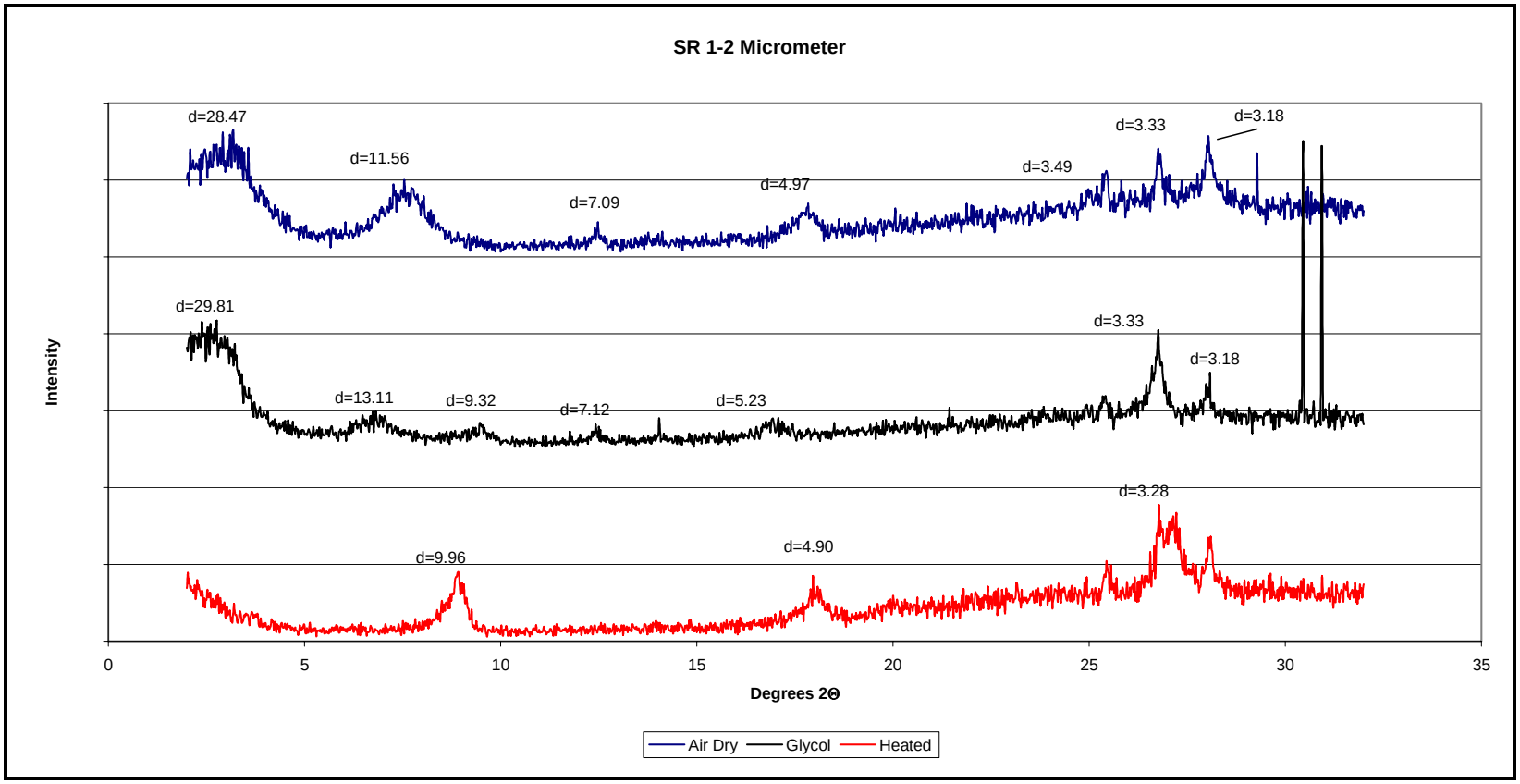
SR 1-2 Micrometer
d=28.47
d=11.56
d=7.09
d=4.97
d=3.49
d=3.33
d=3.18
d=29.81
d=13.11
d=9.32
d=7.12
d=5.23
d=3.33
d=3.18
d=9.96
d=4.90
d=3.28
Intensity
0
5
10
15
20
25
30
35
Degrees 2Θ
Air Dry
Glycol
Heated

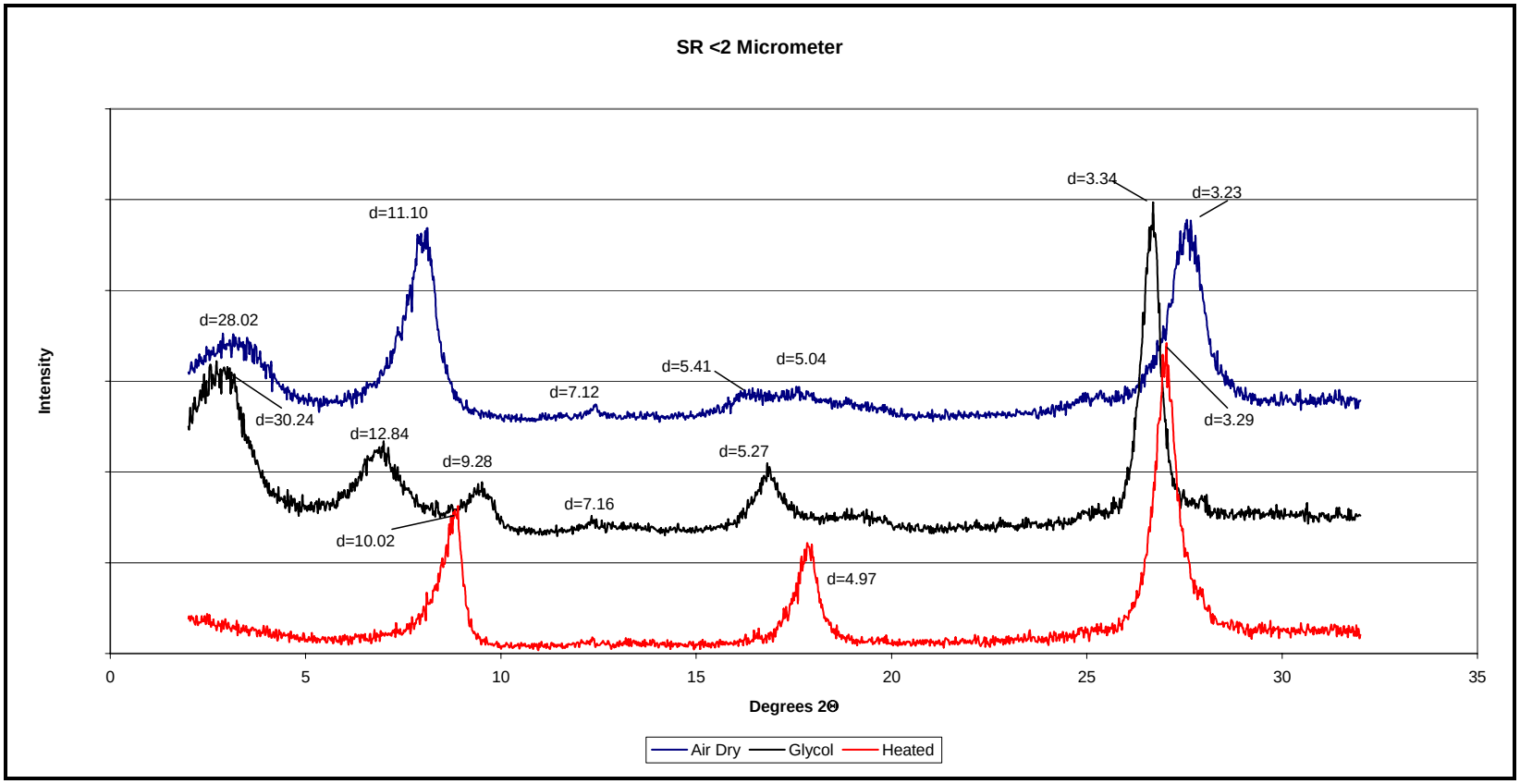
SR <2 Micrometer
Intensity
d=3.34
d=3.23
d=11.10
d=28.02
d=5.41
d=5.04
d=7.12
d=30.24
d=3.29
d=12.84
d=9.28
d=5.27
d=7.16
d=10.02
d=4.97
0
5
10
15
20
25
30
35
Degrees 2Θ
Air Dry
Glycol
Heated

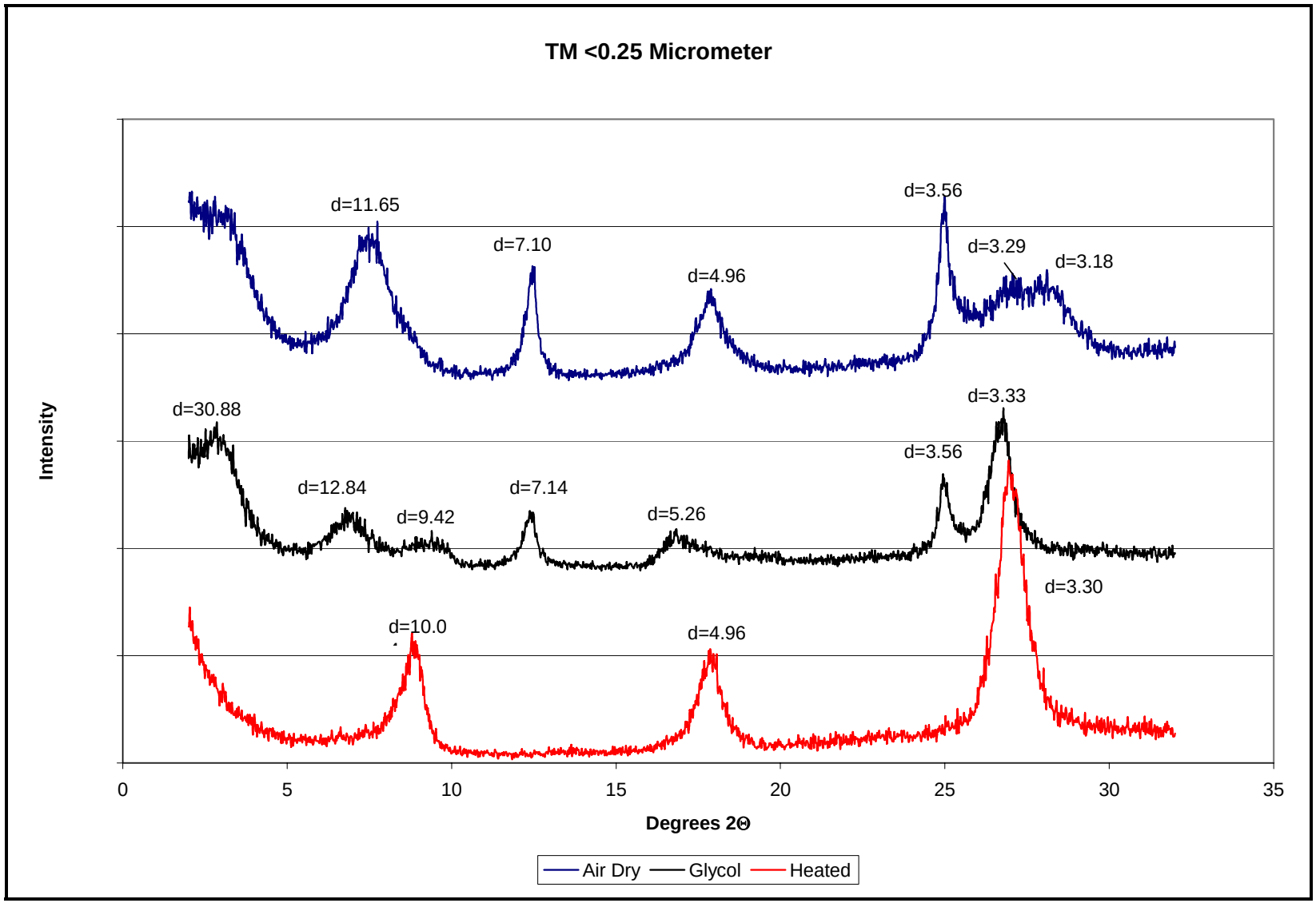
TM <0.25 Micrometer
Intensity
d=11.65
d=7.10
d=4.96
d=3.56
d=3.29
d=3.18
d=30.88
d=12.84
d=9.42
d=7.14
d=5.26
d=3.56
d=3.33
d=3.30
d=10.0
d=4.96
0
5
10
15
20
25
30
35
Degrees 2Θ
Air Dry
Glycol
Heated

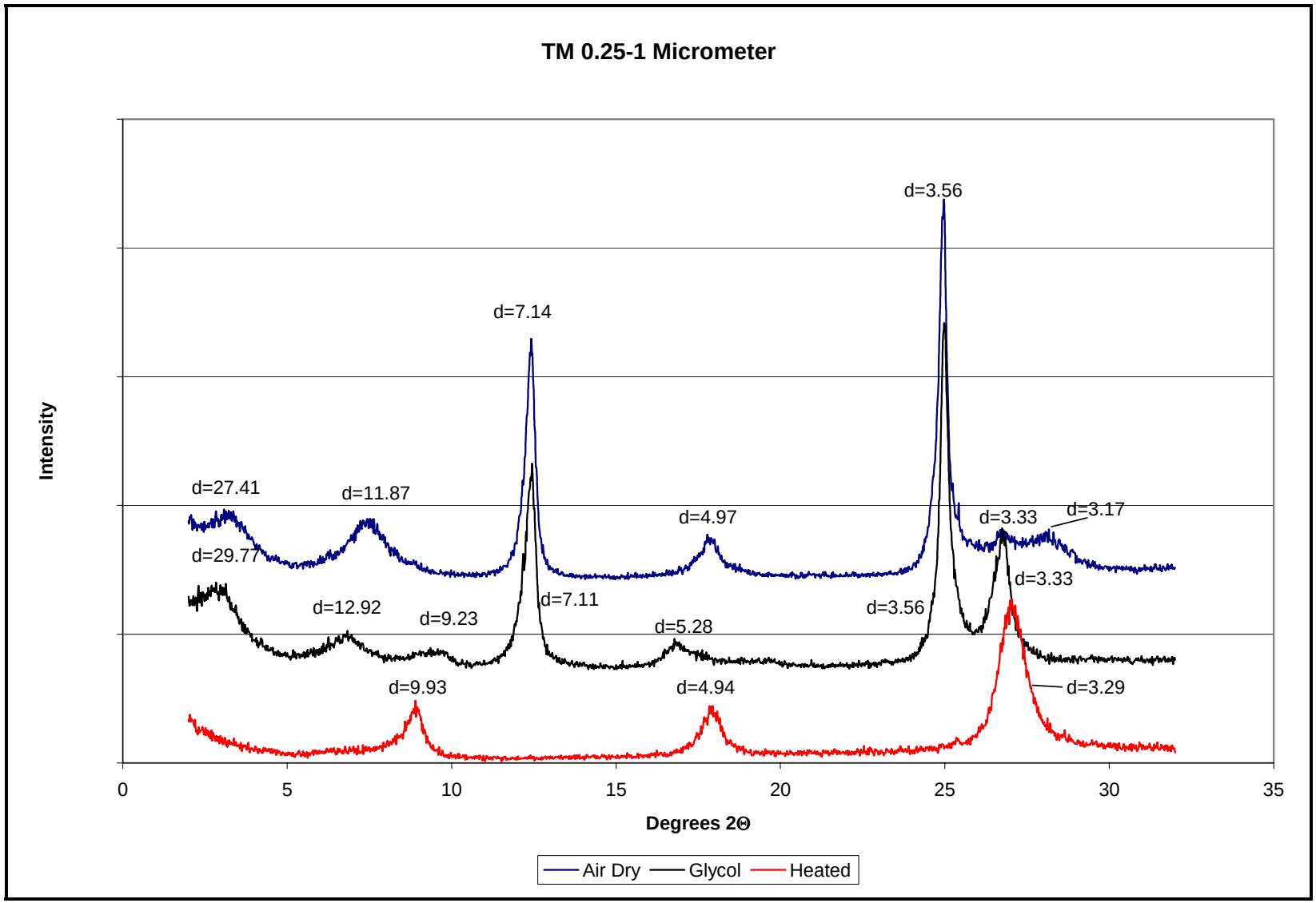
TM 0.25-1 Micrometer
Intensity
d=3.56
d=7.14
d=27.41
d=11.87
d=4.97
d=3.33
d=3.17
d=29.77
d=3.33
d=12.92
d=9.23
d=7.11
d=5.28
d=3.56
d=9.93
d=4.94
d=3.29
0
5
10
15
20
25
30
35
Degrees 2Θ
Air Dry
Glycol
Heated

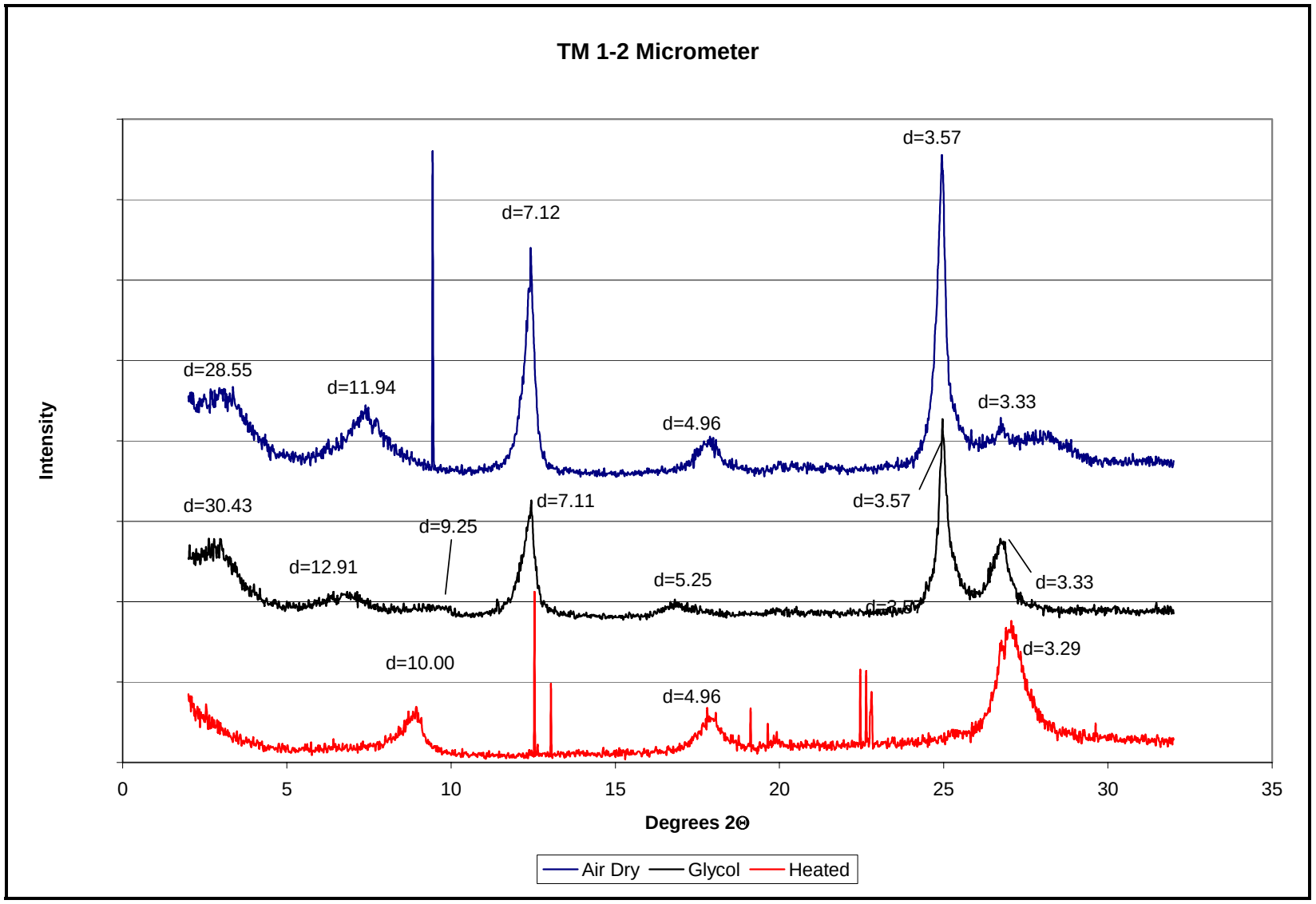
TM 1-2 Micrometer
Intensity
d=3.57
d=7.12
d=28.55
d=11.94
d=4.96
d=3.33
d=30.43
d=7.11
d=9.25
d=3.57
d=12.91
d=5.25
d=3.33
d=3.29
d=10.00
d=4.96
0
5
10
15
20
25
30
35
Degrees 2Θ
Air Dry
Glycol
Heated

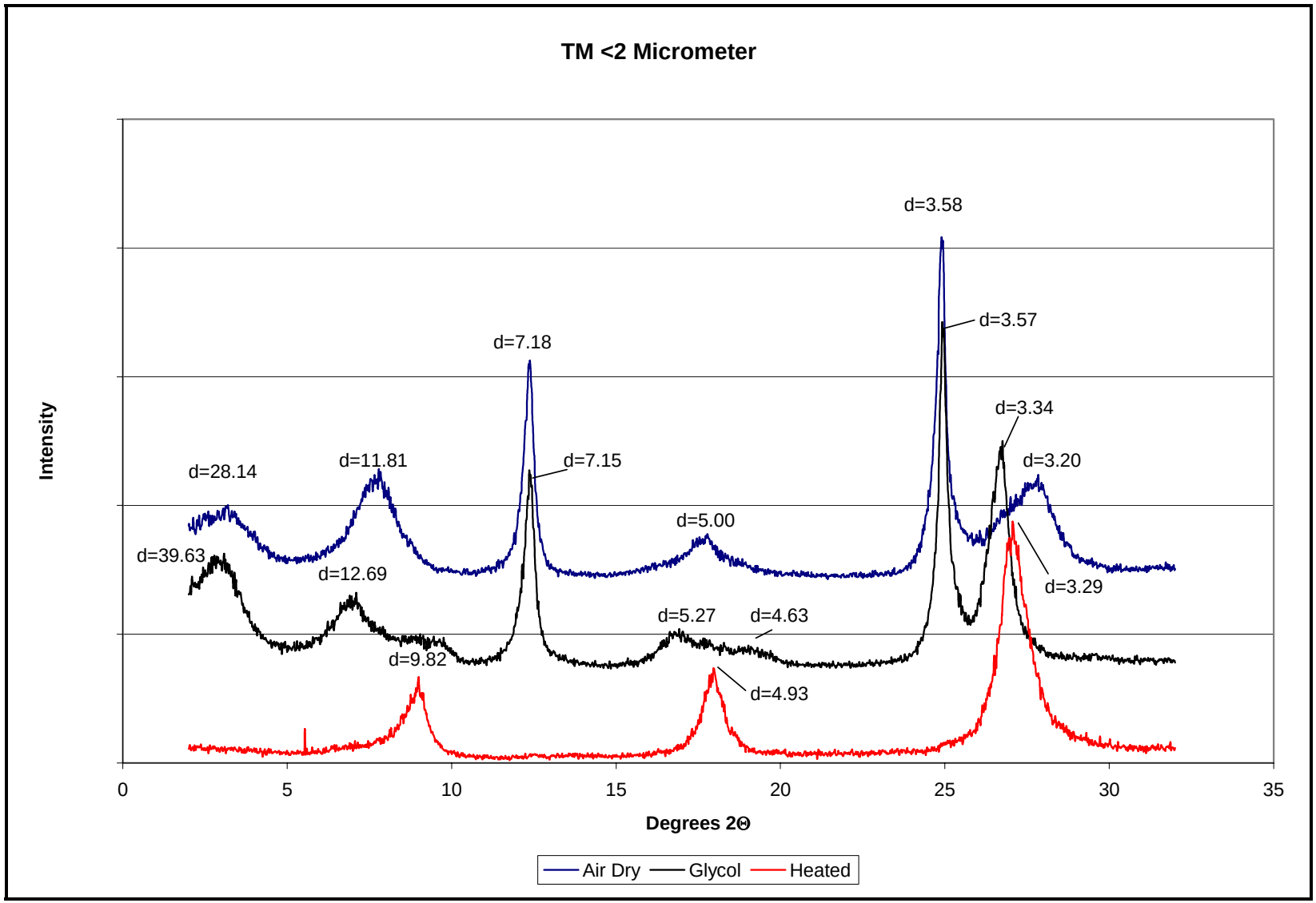
TM <2 Micrometer
Intensity
d=3.58
d=3.57
d=7.18
d=3.34
d=28.14
d=11.81
d=7.15
d=3.20
d=5.00
d=39.63
d=12.69
d=3.29
d=5.27
d=4.63
d=9.82
d=4.93
0
5
10
15
20
25
30
35
Degrees 2Θ
Air Dry
Glycol
Heated

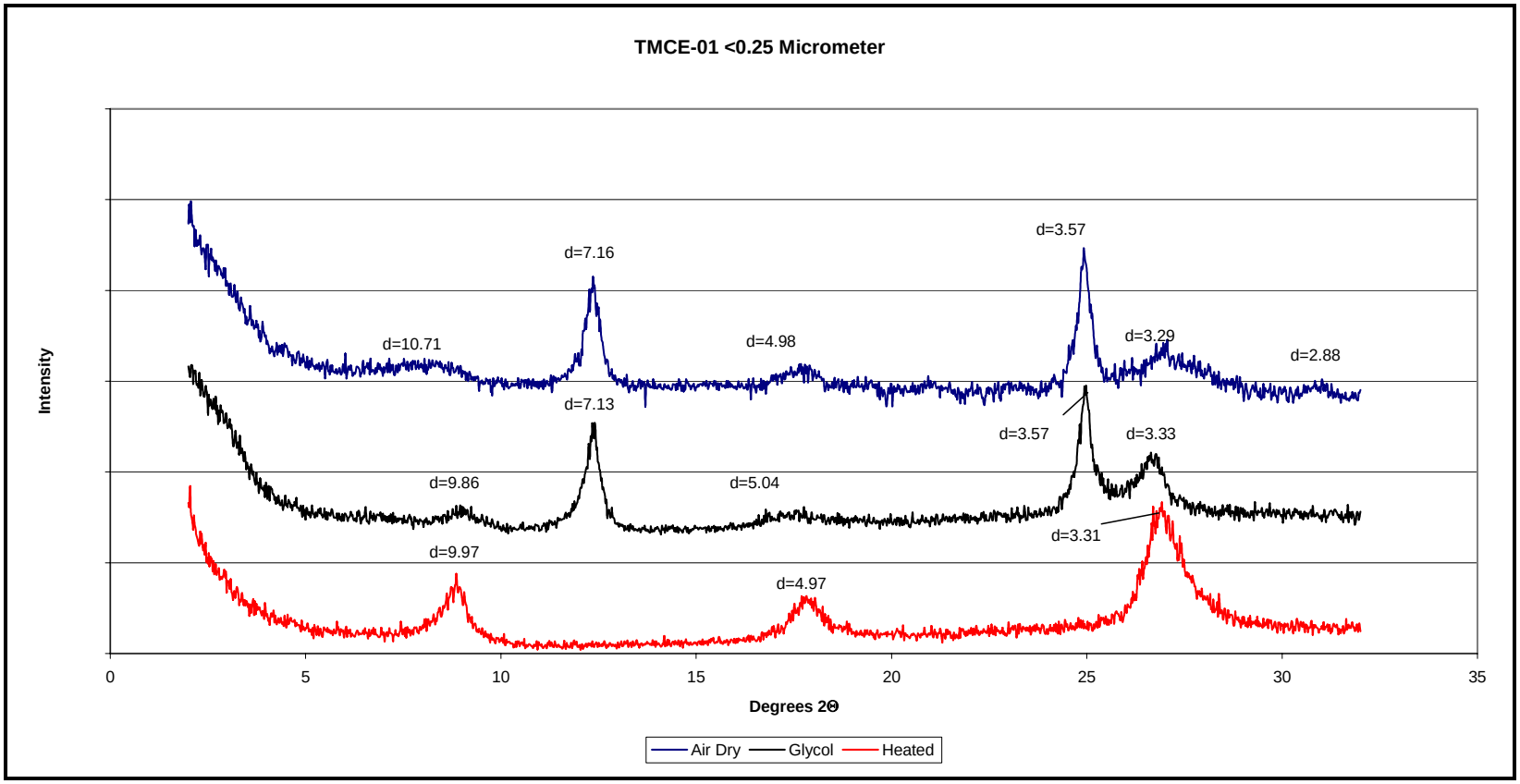
TMCE-01 <0.25 Micrometer
Intensity
d=7.16
d=3.57
d=10.71
d=4.98
d=3.29
d=2.88
d=7.13
d=3.57
d=3.33
d=9.86
d=5.04
d=3.31
d=9.97
d=4.97
0
5
10
15
20
25
30
35
Degrees 2Θ
Air Dry
Glycol
Heated

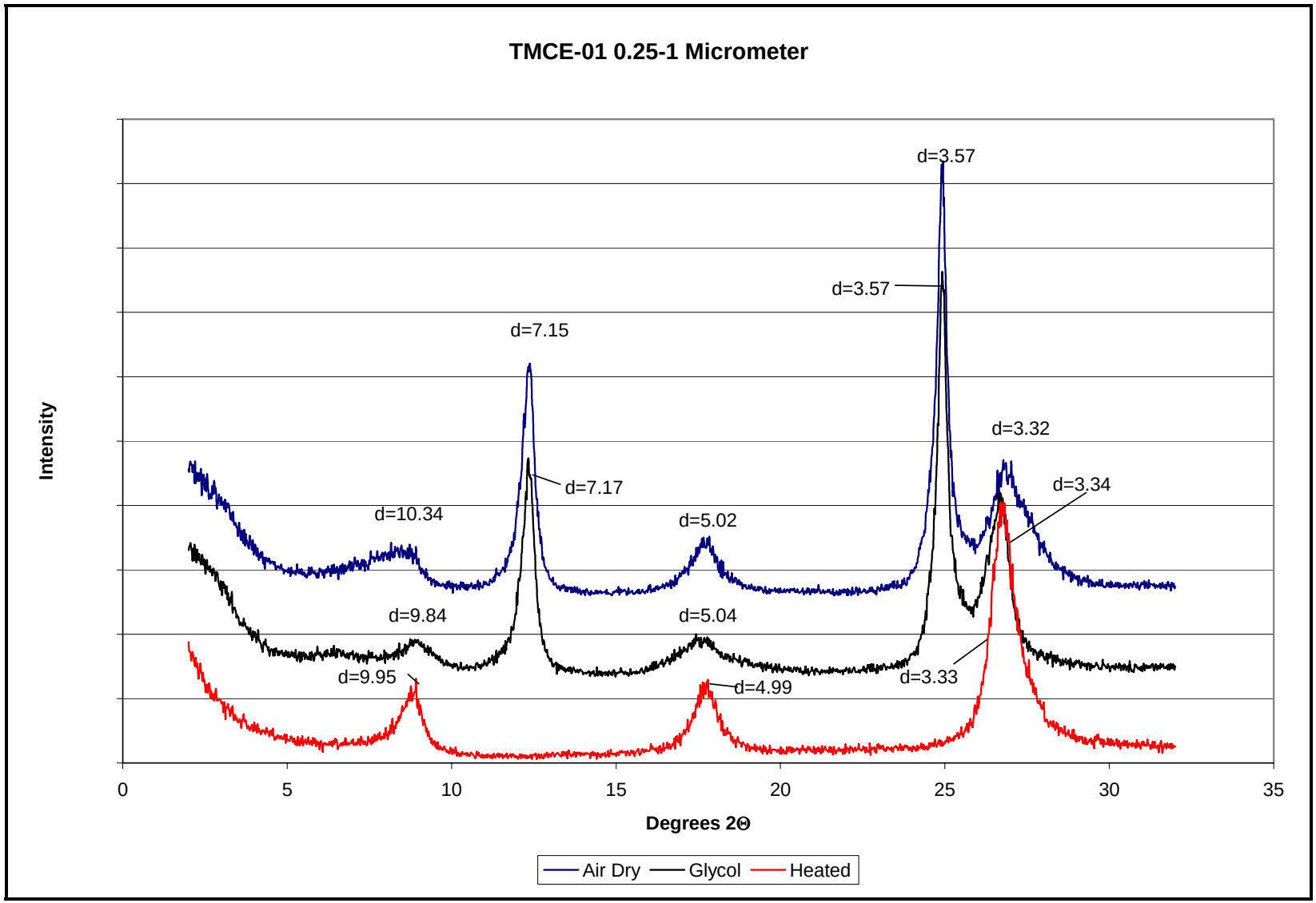
TMCE-01 0.25-1 Micrometer
Intensity
d=3.57
d=3.57
d=7.15
d=3.32
d=7.17
d=3.34
d=10.34
d=5.02
d=9.84
d=5.04
d=9.95
d=4.99
d=3.33
0
5
10
15
20
25
30
35
Degrees 2Θ
Air Dry
Glycol
Heated

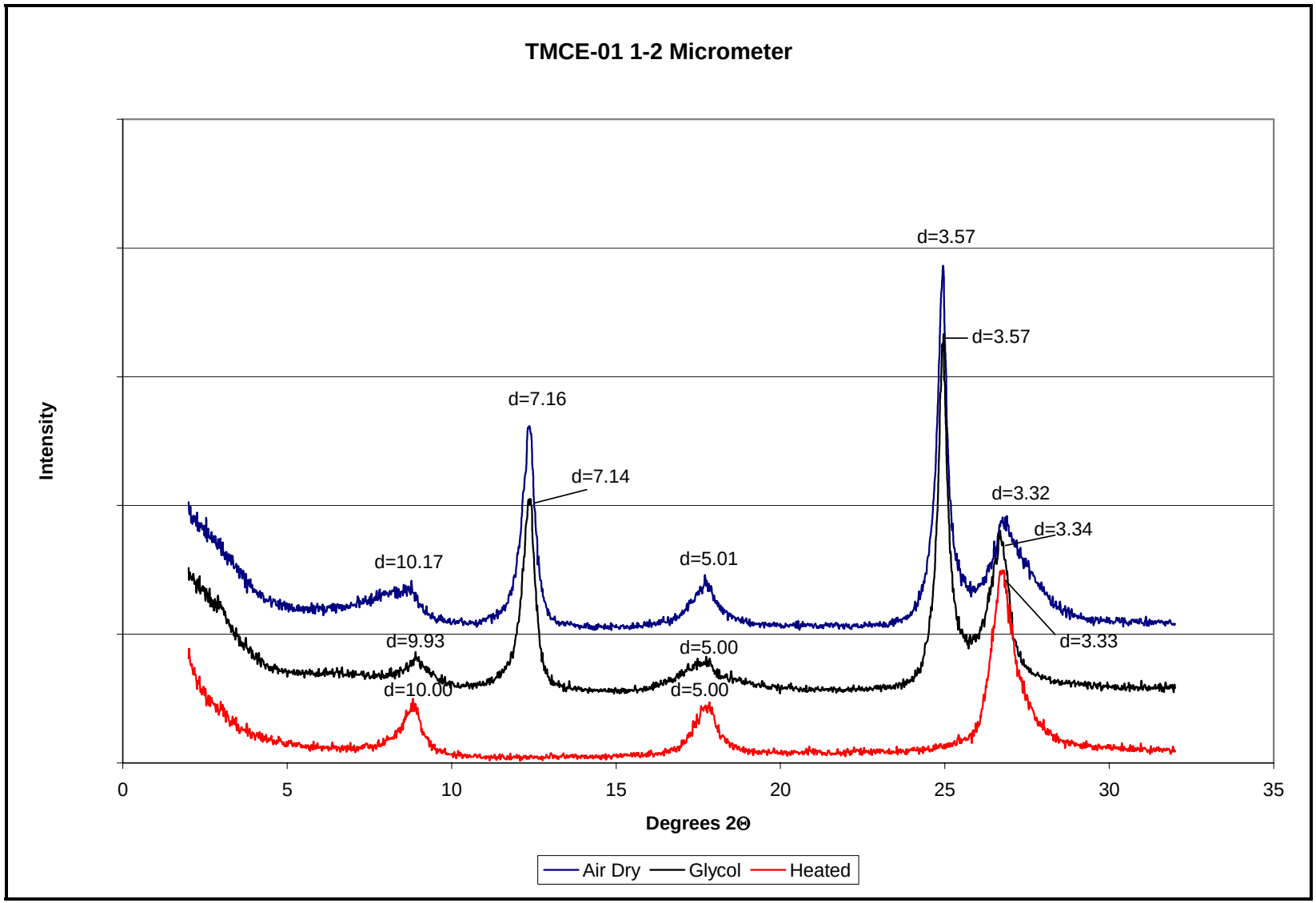
TMCE-01 1-2 Micrometer
Intensity
d=3.57
d=3.57
d=7.16
d=7.14
d=3.32
d=3.34
d=10.17
d=5.01
d=9.93
d=5.00
d=3.33
d=10.00
d=5.00
0
5
10
15
20
25
30
35
Degrees 2Θ
Air Dry
Glycol
Heated

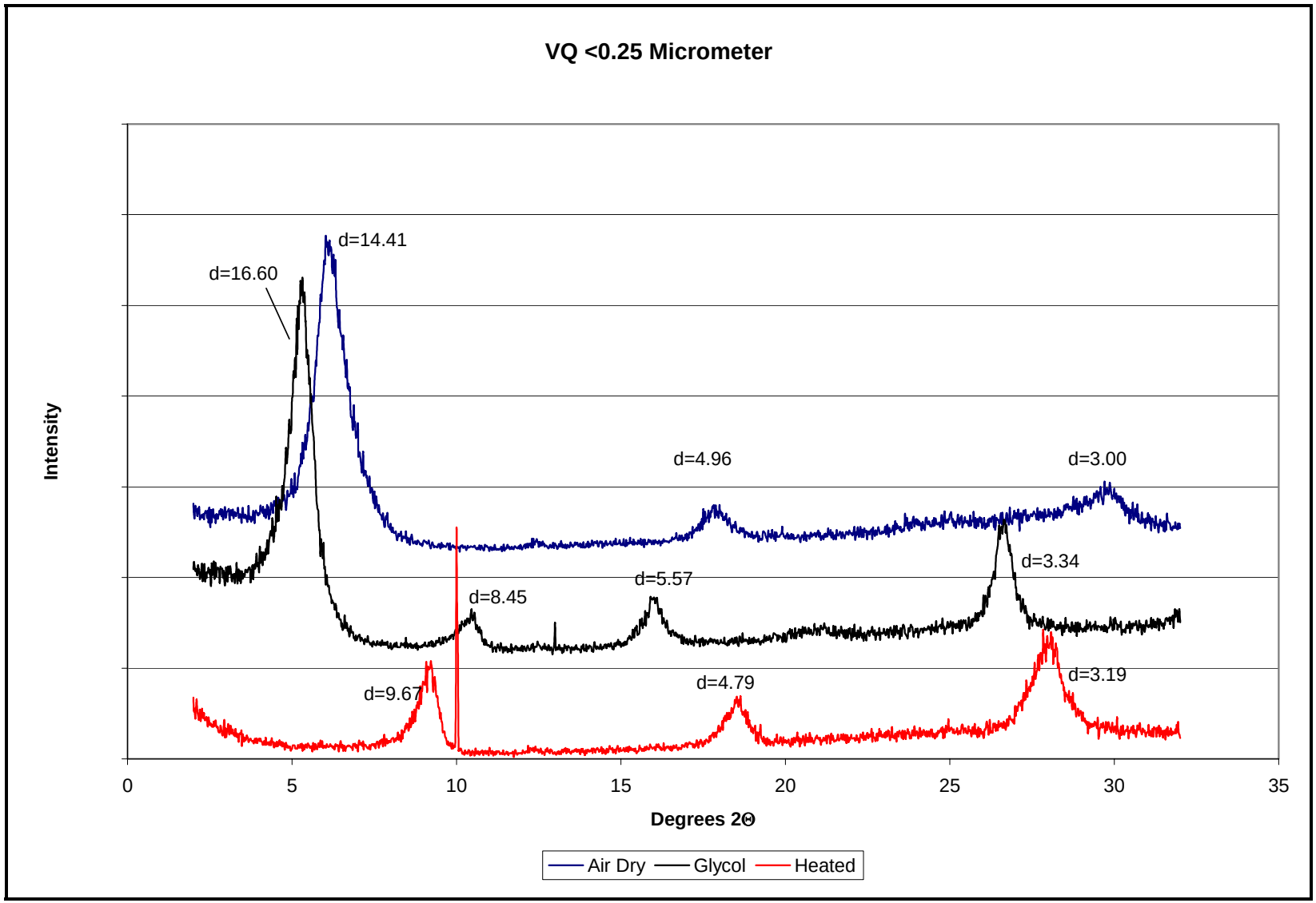
VQ <0.25 Micrometer
Intensity
d=16.60
d=14.41
d=4.96
d=3.00
d=3.34
d=5.57
d=8.45
d=9.67
d=4.79
d=3.19
0
5
10
15
20
25
30
35
Degrees 2Θ
Air Dry
Glycol
Heated

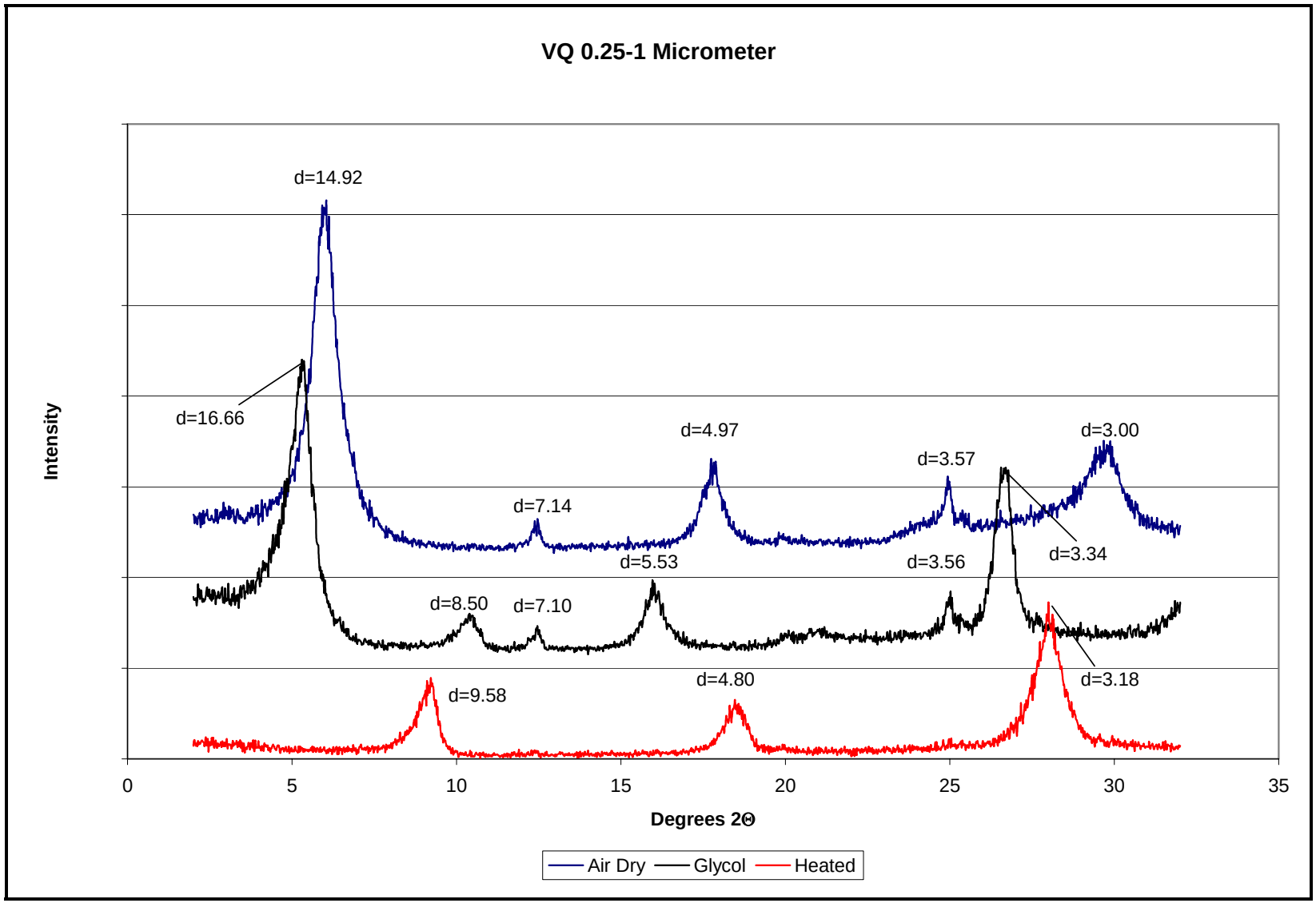
VQ 0.25-1 Micrometer
Intensity
d=14.92
d=16.66
d=4.97
d=3.57
d=3.00
d=7.14
d=5.53
d=3.56
d=3.34
d=8.50
d=7.10
d=4.80
d=9.58
d=3.18
0
5
10
15
20
25
30
35
Degrees 2Θ
Air Dry
Glycol
Heated

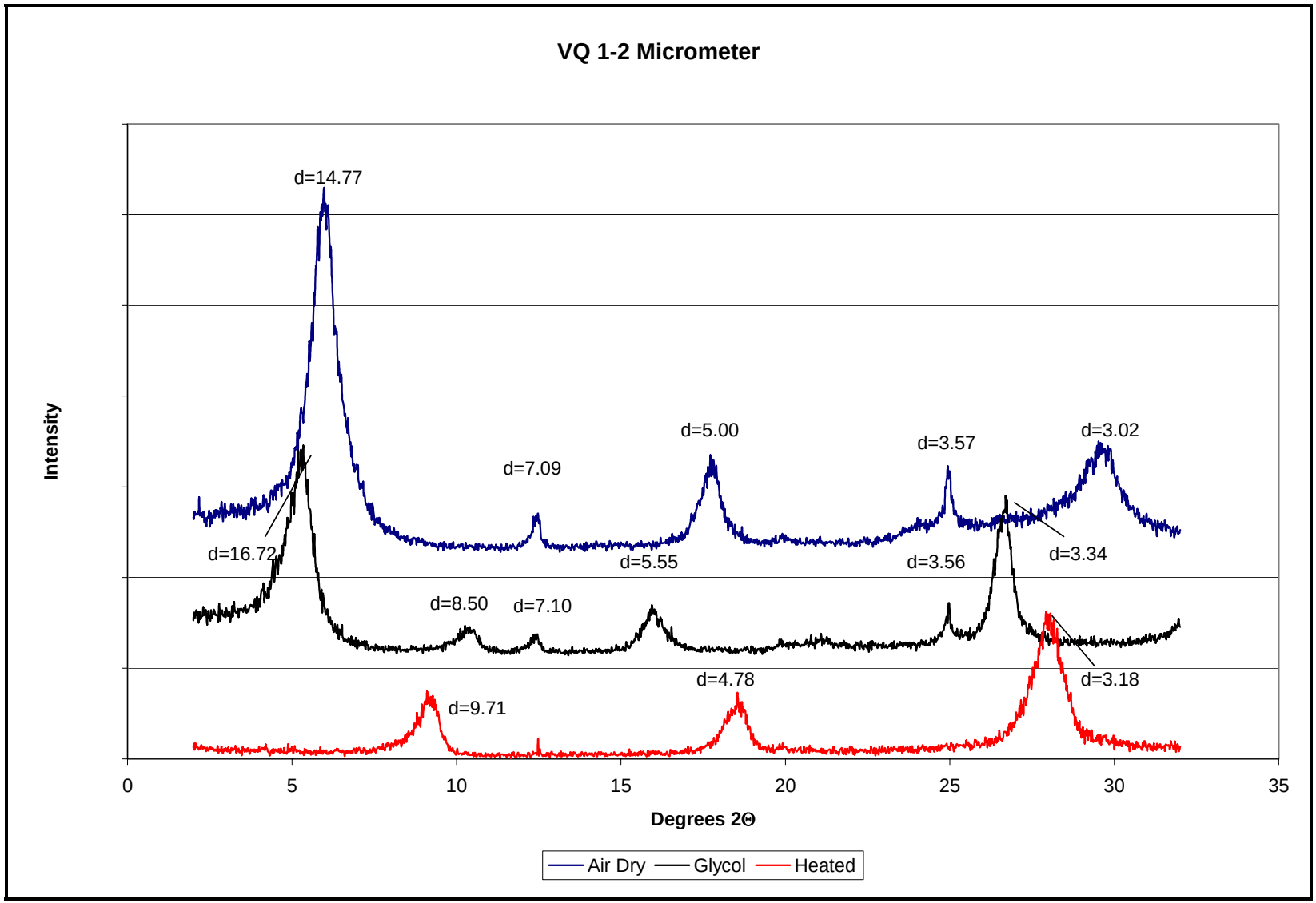
VQ 1-2 Micrometer
Intensity
d=14.77
d=7.09
d=5.00
d=3.57
d=3.02
d=16.72
d=5.55
d=3.56
d=3.34
d=8.50
d=7.10
d=4.78
d=3.18
d=9.71
0
5
10
15
20
25
30
35
Degrees 2Θ
Air Dry
Glycol
Heated

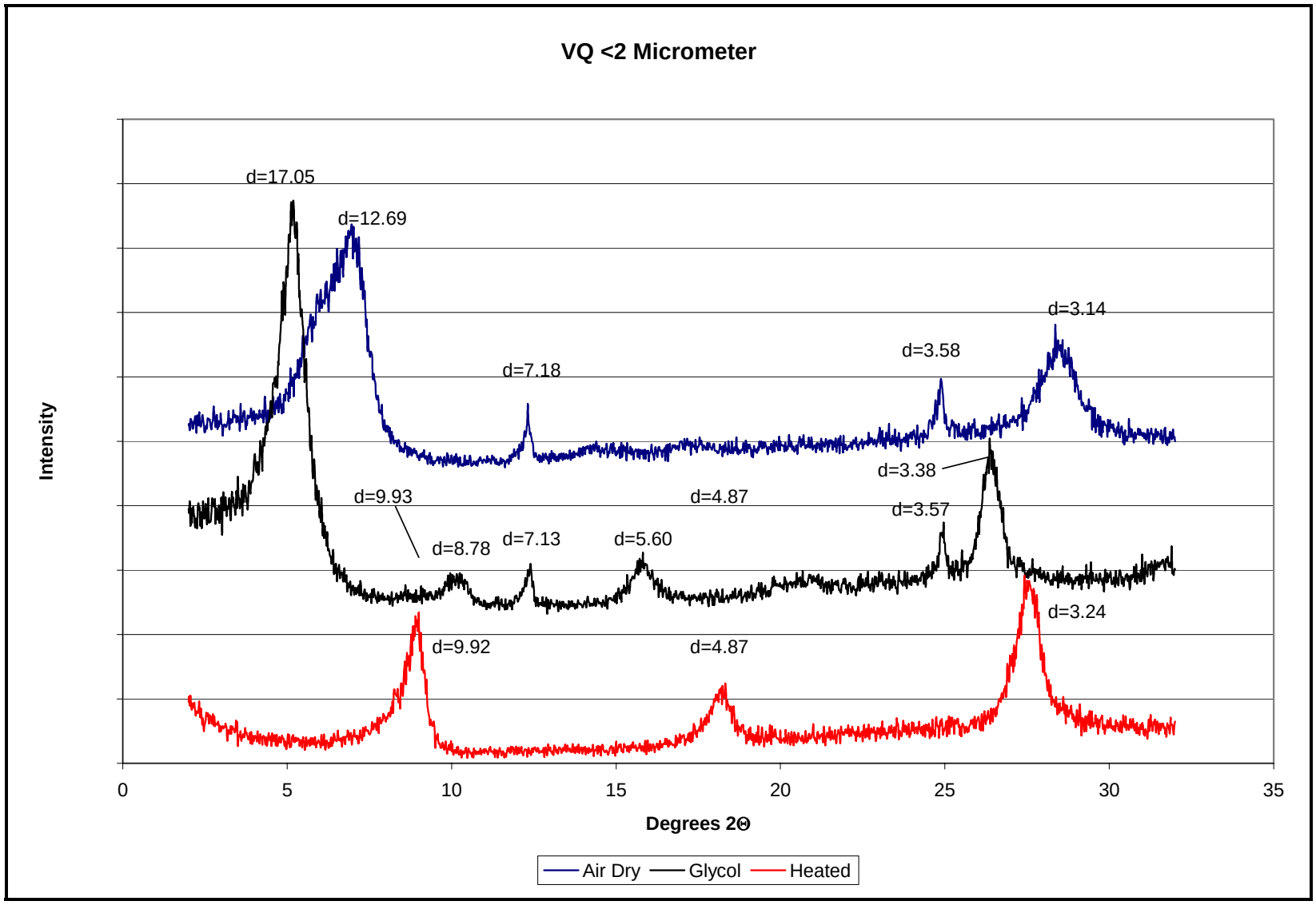
VQ <2 Micrometer
Intensity
d=17.05
d=12.69
d=7.18
d=3.58
d=3.14
d=3.38
d=9.93
d=4.87
d=3.57
d=8.78
d=7.13
d=5.60
d=3.24
d=9.92
d=4.87
0
5
10
15
20
25
30
35
Degrees 2Θ
Air Dry
Glycol
Heated

APPENDIX C: ILLITE POLYTYPE XRD PATTERS

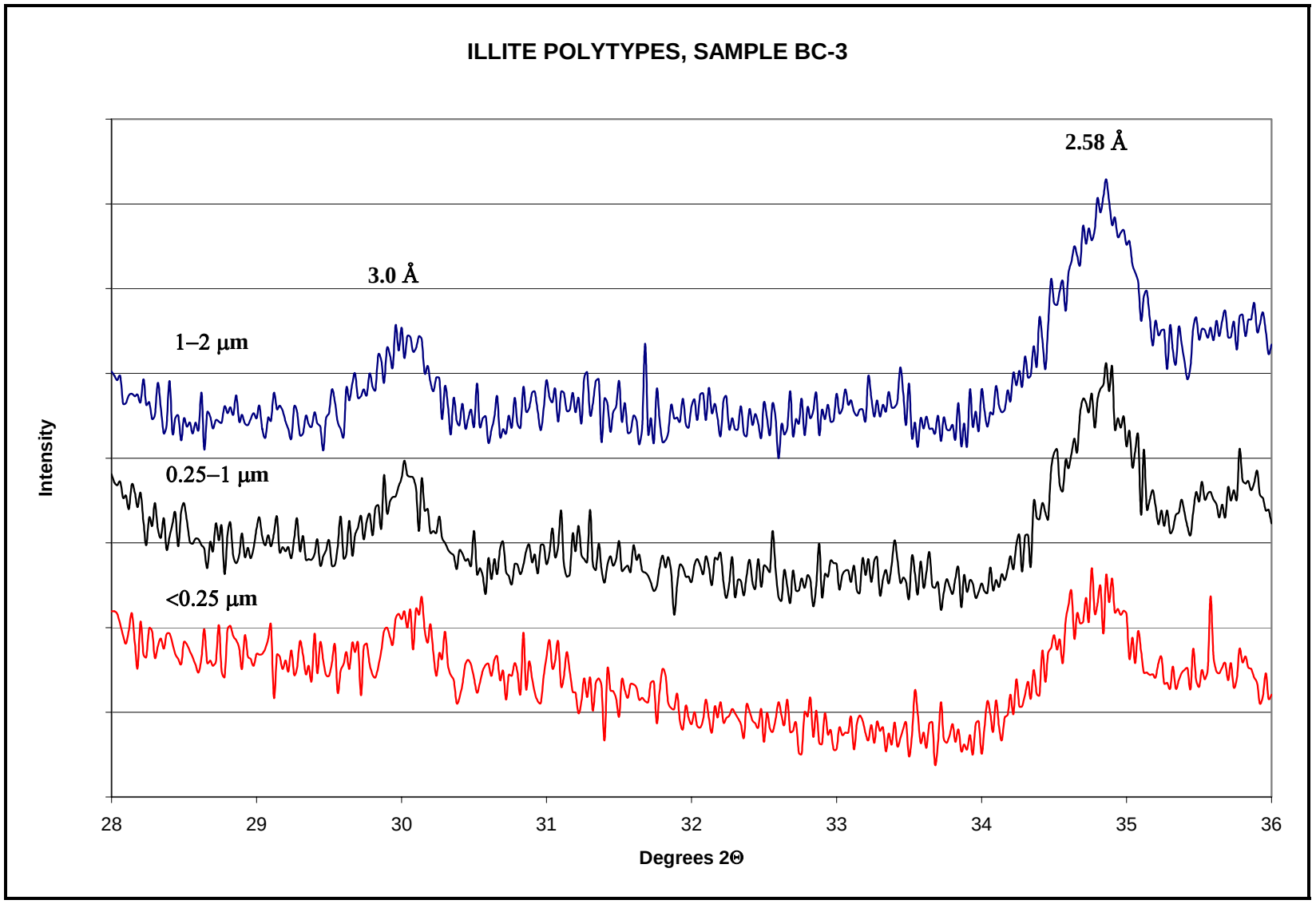
ILLITE POLYTYPES, SAMPLE BC-3
2.58 Å
3.0 Å
1–2 μm
0.25–1 μm
<0.25 μm
Intensity
28
29
30
31
32
33
34
35
36
Degrees 2Θ

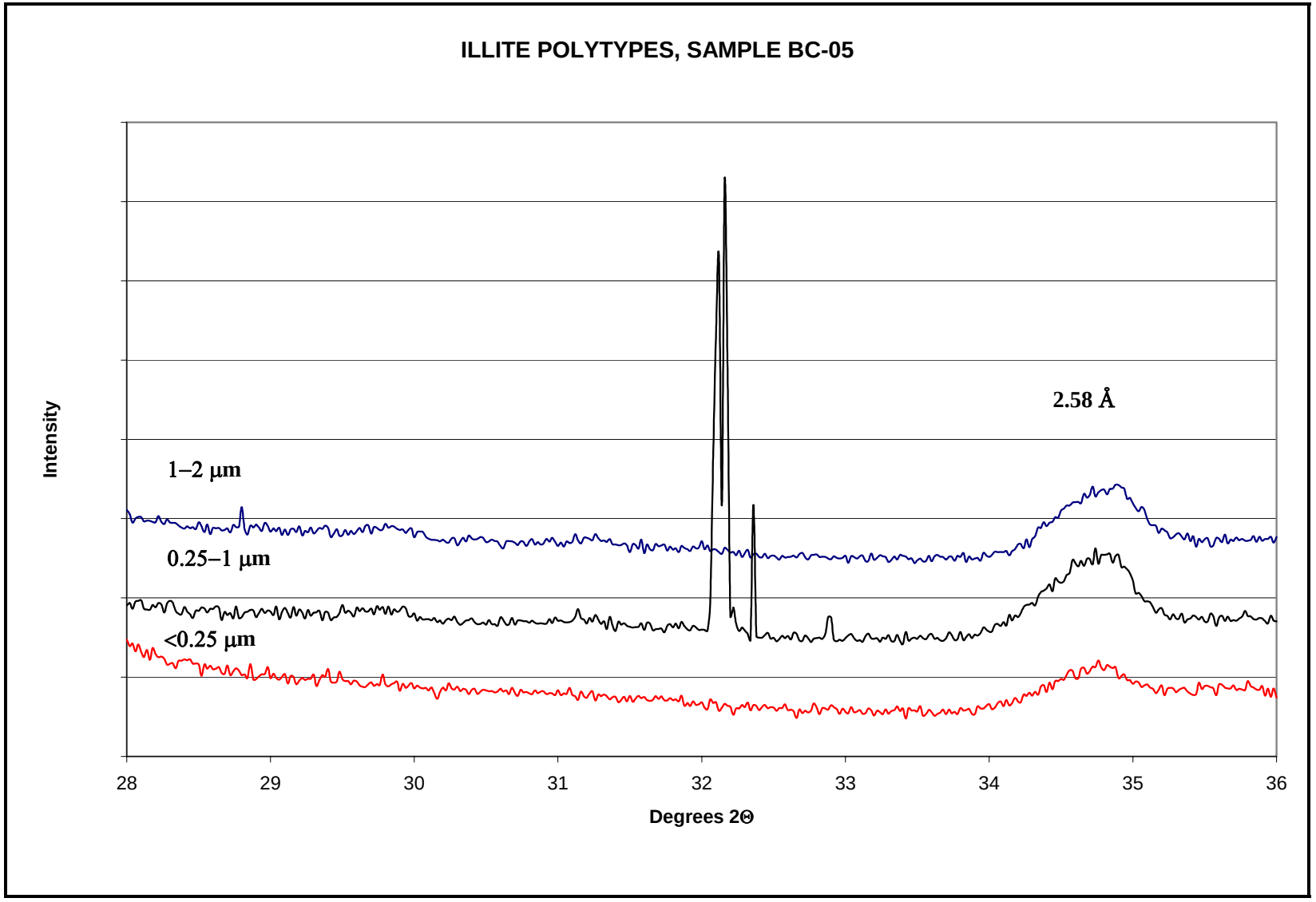
ILLITE POLYTYPES, SAMPLE BC-05
Intensity
2.58 Å
1–2 μm
0.25–1 μm
<0.25 μm
28
29
30
31
32
33
34
35
36
Degrees 2Θ

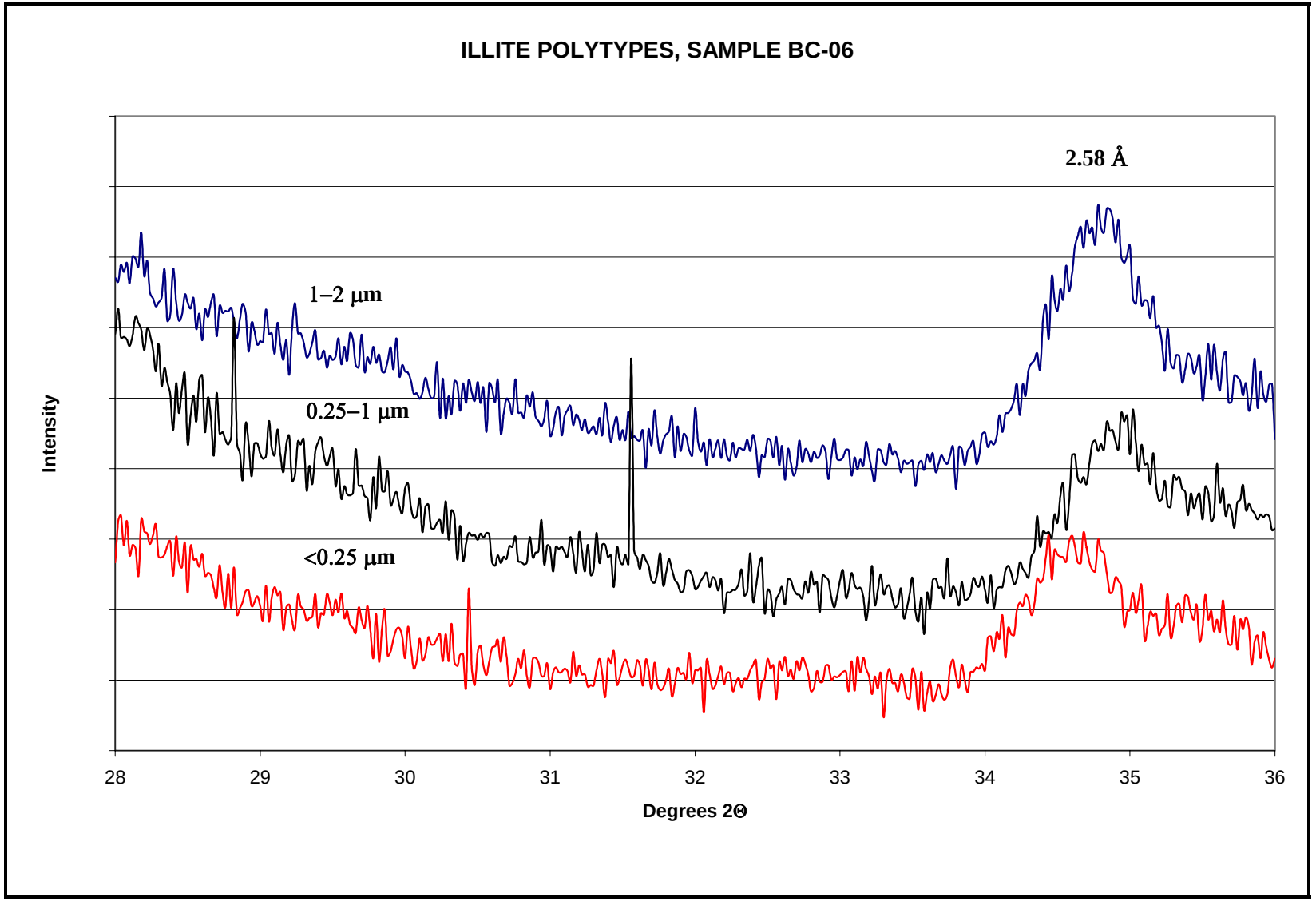
ILLITE POLYTYPES, SAMPLE BC-06
2.58 Å
1–2 μm
0.25–1 μm
<0.25 μm
Intensity
28
29
30
31
32
33
34
35
36
Degrees 2Θ

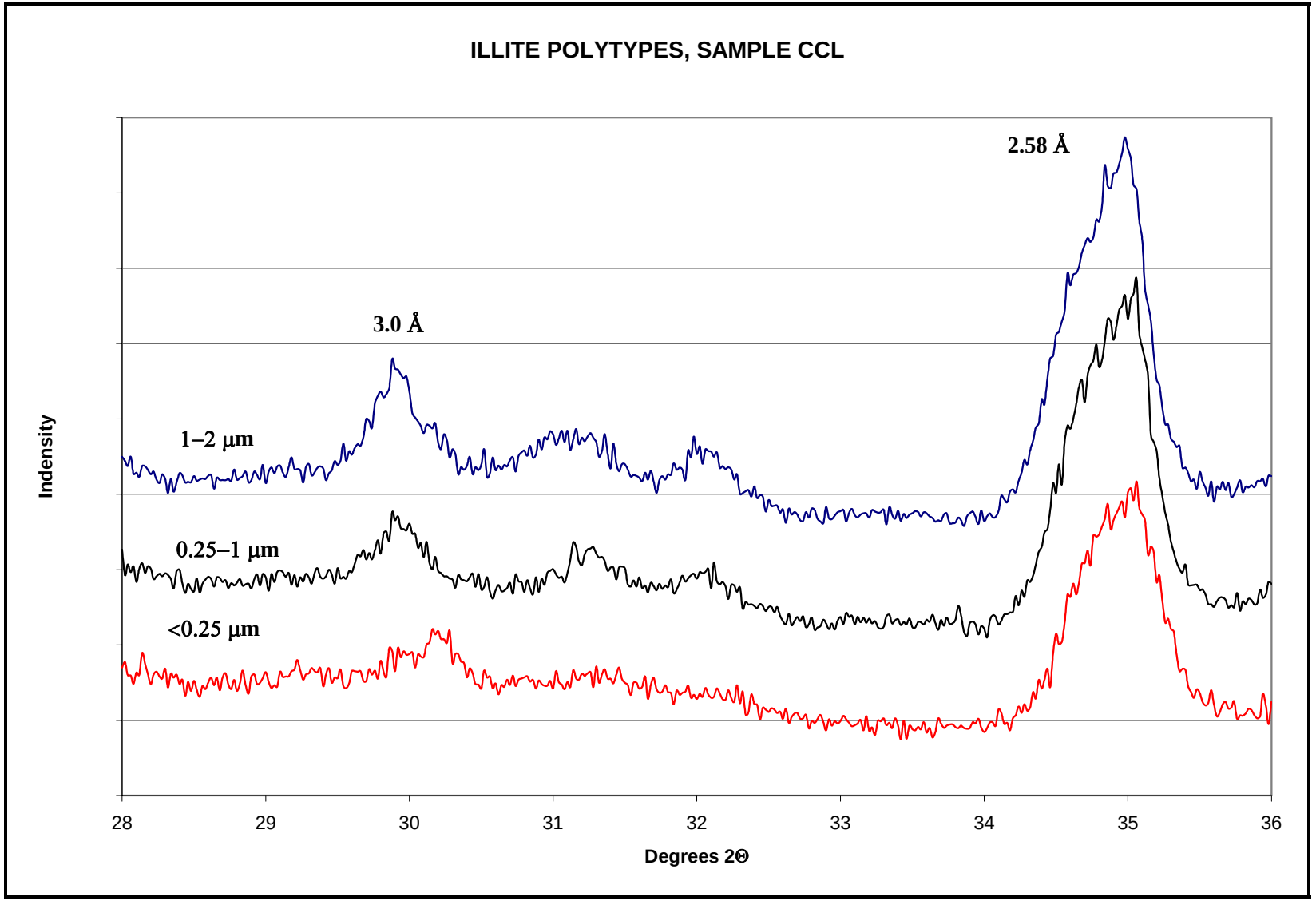
ILLITE POLYTYPES, SAMPLE CCL
2.58 Å
3.0 Å
1–2 μm
0.25–1 μm
<0.25 μm
Indensity
28
29
30
31
32
33
34
35
36
Degrees 2Θ

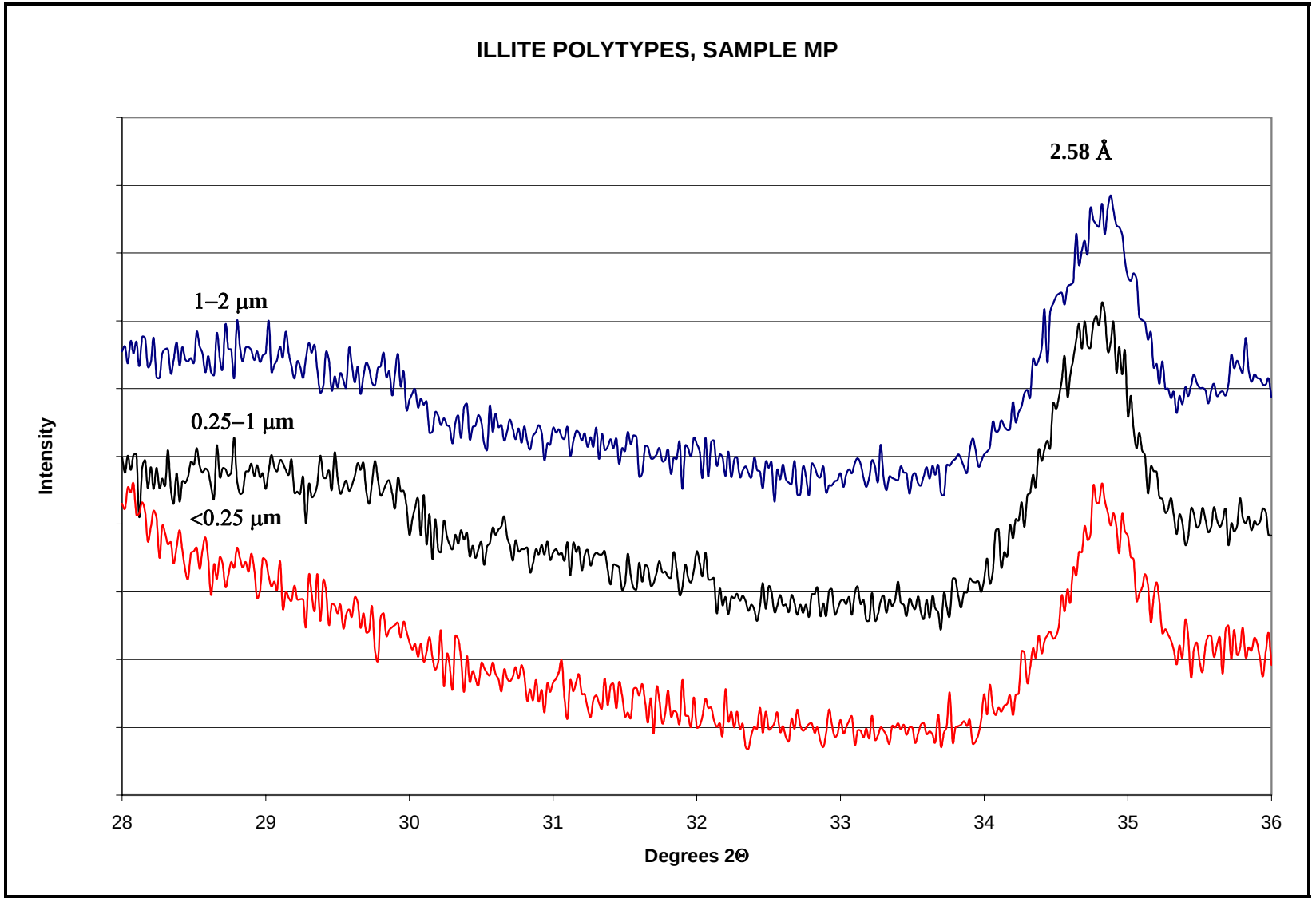
ILLITE POLYTYPES, SAMPLE MP
2.58 Å
1–2 μm
0.25–1 μm
<0.25 μm
Intensity
28
29
30
31
32
33
34
35
36
Degrees 2Θ

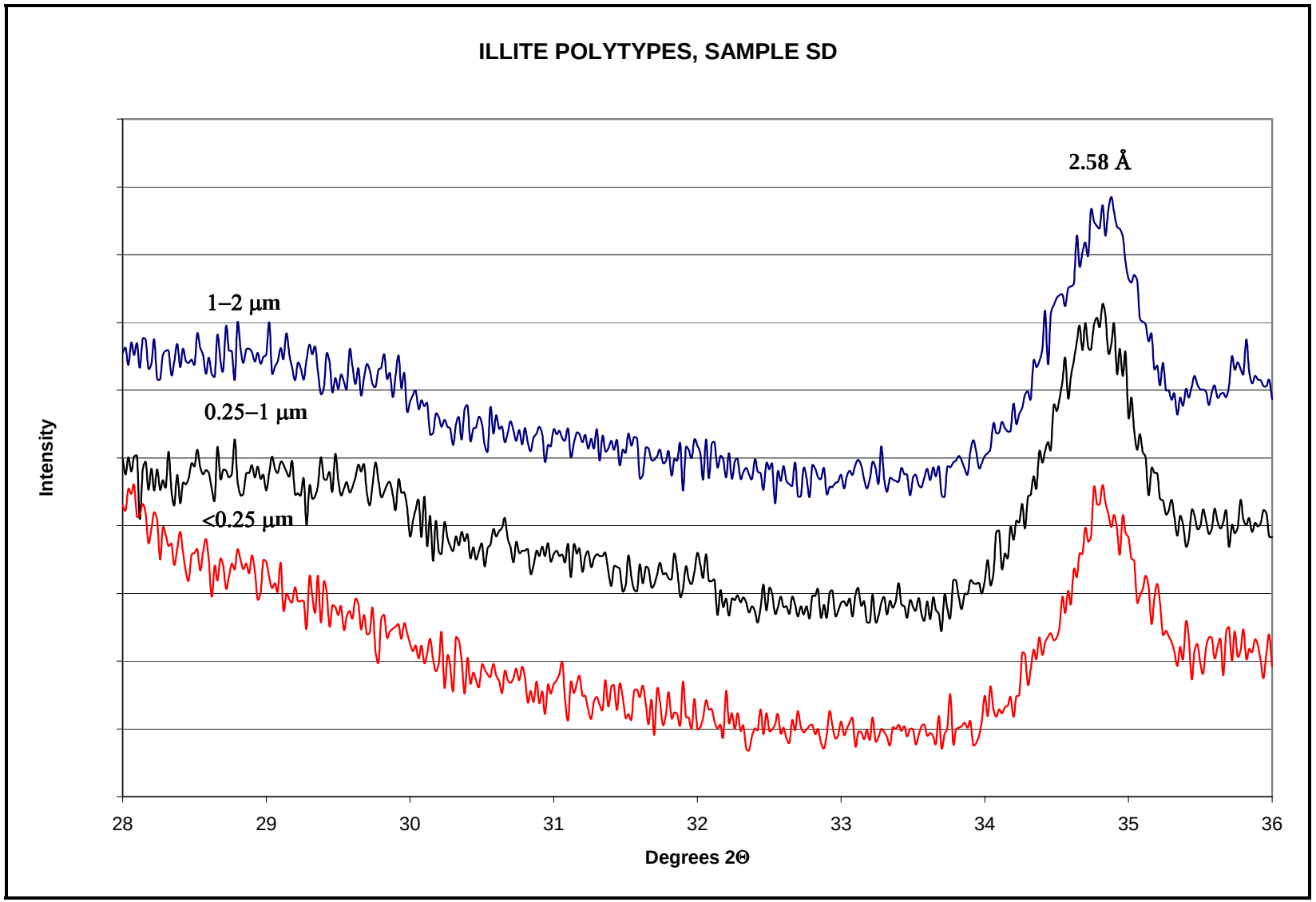
ILLITE POLYTYPES, SAMPLE SD
2.58 Å
1–2 μm
0.25–1 μm
<0.25 μm
Intensity
28
29
30
31
32
33
34
35
36
Degrees 2Θ